PHYSIOLOGICALLY BASED PHARMACOKINETIC MODELING OF CYP3A4, CYP1A2 AND TRANSPORTER SUBSTRATES, INHIBITORS AND INDUCERS FOR THE PREDICTION OF DRUG-DRUG INTERACTIONS

DISSERTATION

zur Erlangung des Grades des Doktors der Naturwissenschaften
der Naturwissenschaftlich-Technischen Fakultät
der Universität des Saarlandes

von
Hannah Esther Britz
Diplom-Pharmazeutin / Apothekerin

Saarbrücken
2024

Tag des Kolloqiums:	22. November 2024
Dekan:	Prof. Dr.-Ing. Dirk Bähre
Berichterstatter:	Prof. Dr. Thorsten Lehr Prof. Dr. Claus Jacob
Akad. Mitglied:	Dr. Jessica Hoppstädter
Vorsitz:	Prof. Dr. Andriy Luzhetskyy

Die vorliegende Arbeit wurde von Januar 2018 bis September 2024 unter der Anleitung von Herrn Professor Dr. Thorsten Lehr in der Fachrichtung Klinische Pharmazie der Naturwissenschatlich-Technischen Fakultät der Universität des Saarlandes angefertigt.

ABSTRACT

Adverse drug reactions, often caused by drug-drug interactions (DDIs), are a tremendous risk for multimorbid patients requiring polypharmacy. As a result, potential DDIs are an important area of investigation during drug development. New techniques, such as physiologically based pharmacokinetic (PBPK) modeling, are being applied and are recommended by both, the European Medicines Agency and the U.S. Food and Drug Administration. Consequently, there is a strong interest in the development of models for index substrates, inhibitors and inducers of important cytochrome P450 (CYP) enzymes and transporters involved in the absorption, distribution, metabolism and excretion of drugs.
In this thesis, whole-body PBPK models of index drugs were developed: midazolam, alfentanil (CYP3A4 substrates), theophylline (CYP1A2 substrate), digoxin (P-glycoprotein (Pgp) substrate), furosemide (organic anion transporter (OAT) substrate), clarithromycin, itraconazole (CYP3A4 and Pgp inhibitors), fluvoxamine (CYP1A2 inhibitor), probenecid (OAT inhibitor) and rifampicin (CYP3A4 and Pgp inducer). Two DDI networks were established, covering a total of 14 unique DDI combinations. All models are published open-source and accompanied by transparent documentation. In combination with previously developed models and models currently under development, they allow the prediction of highly complex and realistic scenarios and can provide dose recommendations for clinical drug interaction studies.

ZUSAMMENFASSUNG

Multimorbide Patienten benötigen häufig Therapien mit mehreren Arzneimitteln und sind somit besonders anfällig für das Auftreten unerwünschter Arzneimittelwirkungen, die häufig durch Arzneimittelwechselwirkungen verursacht werden. Potenzielle Arzneimittelwechselwirkungen sind daher wichtiger Untersuchungsgegenstand während der Arzneimittelentwicklung. Neue Techniken, wie die Physiologie-basierte Pharmakokinetik (PBPK) Modellierung werden dabei eingesetzt und von den Arzneimittelzulassungsbehörden empfohlen. Folglich besteht ein starkes Interesse an der Entwicklung von PBPK Modellen von Indexsubstraten, -inhibitoren und -induktoren wichtiger Cytochrom P450 (CYP) Enzyme und Transporter, die an der Absorption, Verteilung, Metabolisierung und der Ausscheidung von Arzneistoffen beteiligt sind. In dieser Arbeit wurden PBPK Modelle für Midazolam, Alfentanil (CYP3A4 Substrate), Theophyllin (CYP1A2 Substrat), Digoxin (P-Glykoprotein (Pgp) Substrat), Furosemid (Organo-Anion-Transporter (OAT) Substrat), Clarithromycin, Itraconazol (CYP3A4 und Pgp Inhibitoren), Fluvoxamin (CYP1A2 Inhibitor), Probenecid (OAT Inhibitor) und Rifampicin (CYP3A4 und Pgp Induktor) entwickelt und evaluiert, zwei Interaktionsnetzwerke erstellt und 14 verschiedene Arzneimittelinteraktionen vorhergesagt. Zusammen mit anderen bereits entwickelten Modellen bieten sie die Möglichkeit, sehr komplexe und realitätsnahe Szenarien vorherzusagen und können die Dosisfindung für klinische Interaktionsstudien unterstützen.

GRAPHICAL ABSTRACT

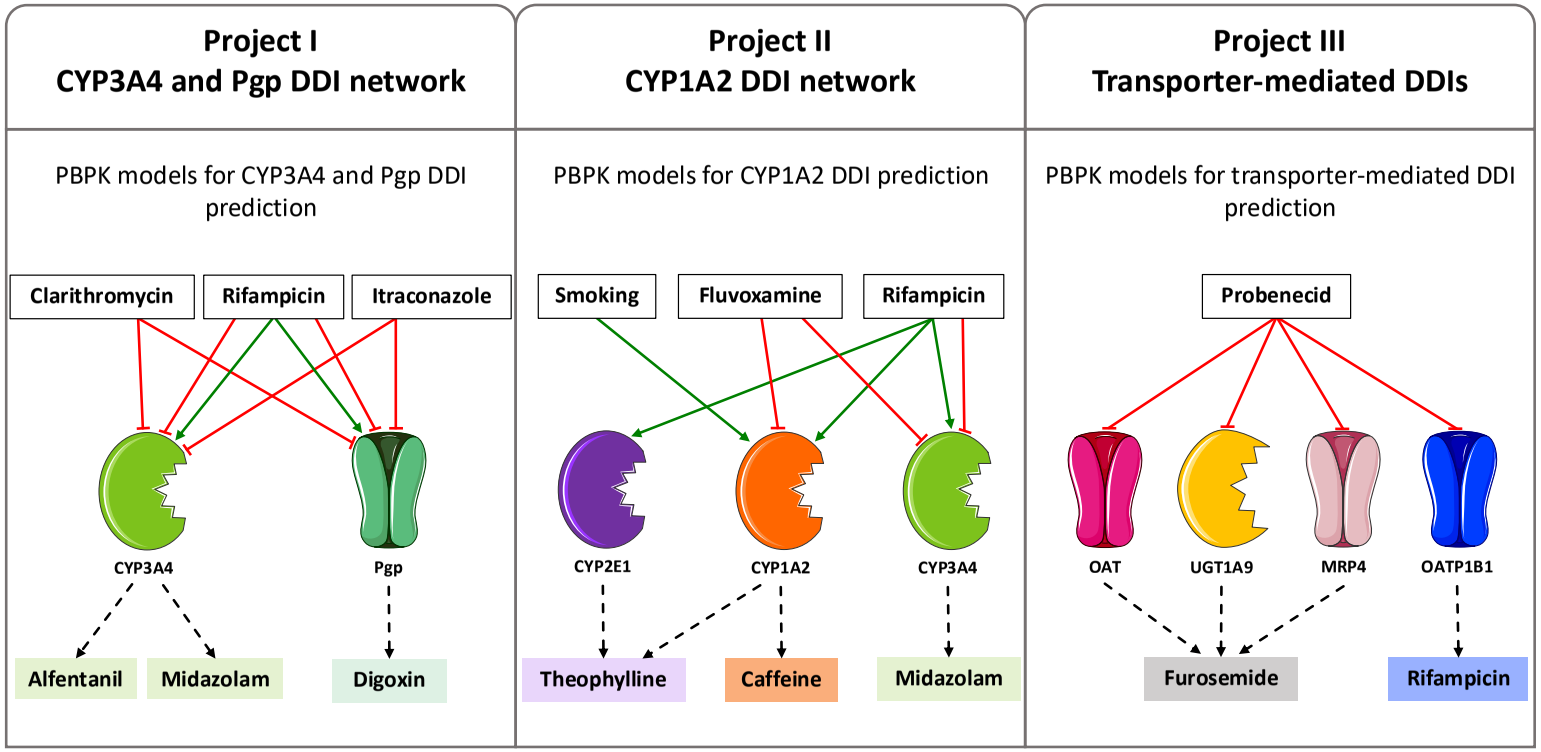

Graphical abstract. CYP: cytochrome P450, DDI: drug-drug interaction, MRP4: multidrug resistance-associated protein 4, OAT: organic anion transporter, OATP1B1: organic anion transporting polypeptide 1B1, PBPK: physiologically based pharmacokinetic, Pgp: P-glycoprotein, UGT1A9: uridine 5′-diphosphoglucuronosyltransferase 1A9. Red solid lines indicate inhibition and green solid lines indicate induction by perpetrator drugs. Dashed black lines indicate metabolism or transport of victim drugs. Parts of the figure were illustrated using pictures from Servier Medical Art. Servier Medical Art by Servier is licensed under a Creative Commons Attribution 3.0 Unported License (https://creativecommons.org/licenses/by/3.0/).

INCLUDED PUBLICATIONS

LIST OF PUBLICATIONS INCLUDED IN THIS THESIS

The following three papers are related to projects I-III in this thesis and were published in peer-reviewed scientific journals.

I. CYP3A4 and Pgp DDI network

Nina Hanke, Sebastian Frechen, Daniel Moj, **Hannah Britz**, Thomas Eissing, Thomas Wendl, Thorsten Lehr. PBPK Models for CYP3A4 and P-gp DDI prediction: A modeling network of rifampicin, itraconazole, clarithromycin, midazolam, alfentanil, and digoxin. CPT Pharmacometrics Syst Pharmacol. 2018;7(10): 647-659. doi: 10.1002/psp4.12343

II. CYP1A2 DDI network

Hannah Britz, Nina Hanke, Anke-Katrin Volz, Olav Spigset, Matthias Schwab, Thomas Eissing, Thomas Wendl, Sebastian Frechen, Thorsten Lehr. Physiologically-based pharmacokinetic models for CYP1A2 drug-drug interaction prediction: A modeling network of fluvoxamine, theophylline, caffeine, rifampicin, and midazolam. CPT Pharmacometrics Syst Pharmacol. 2019;8(5):296-307. doi: 10.1002/psp4.12397

III. Transporter-mediated DDIs

Hannah Britz, Nina Hanke, Mitchell E Taub, Ting Wang, Bhagwat Prasad, Éric Fernandez, Peter Stopfer, Valerie Nock, Thorsten Lehr. Physiologically based pharmacokinetic models of probenecid and furosemide to predict transporter mediated drug-drug interactions. Pharm Res. 2020;37(12):250. The final publication is available at Springer via doi: 10.1007/s11095-020-02964-z

CONTRIBUTION REPORT

The author Hannah Britz declares her contributions to the publications related to projects I-III included in this thesis according to the contributor roles taxonomy (CRediT) [1].

CYP3A4 and Pgp DDI network: Investigation, Writing - Review & Editing

CYP1A2 DDI network: Conceptualization, Data Curation, Investigation, Visualization, Writing - Original Draft, Writing - Review & Editing

Transporter-mediated DDIs: Conceptualization, Data Curation, Investigation, Visualization, Writing - Original Draft, Writing - Review & Editing

ACKNOWLEDGEMENTS

An dieser Stelle möchte ich meine Dankbarkeit gegenüber all jenen ausdrücken, die mich während der Erstellung dieser Dissertation unterstützt haben.
Mein besonderer Dank gilt zunächst Prof. Dr. Thorsten Lehr, der mir nicht nur die Möglichkeit gegeben hat, meine Diplomarbeit in seinem Arbeitskreis anzufertigen, sondern mich auch ermutigt und tatkräftig unterstützt hat, dort meine Promotion zu absolvieren. Seine wertvolle Anleitung, ermutigenden Worte und fachliche Expertise haben wesentlich zum Gelingen dieser Arbeit beigetragen.
Ein herzliches Dankeschön geht auch an Herrn Prof. Dr. Claus Jacob für die Übernahme des Zweitgutachtens.
Ebenso möchte ich meinen Kolleginnen und Kollegen im Arbeitskreis Klinische Pharmazie danken, mit denen ich während meiner Zeit zusammenarbeiten durfte. Ein besonderer Dank geht an das gesamte Team PBPK für die hilfreichen Diskussionen und den produktiven Austausch. Dr. Nina Hanke danke ich für ihre unermüdliche Geduld und die großartige Unterstützung. Dr. Simeon Rüdesheim und Dr. Denise Feick, danke ich herzlich für das Korrekturlesen meiner Arbeit und das konstruktive Feedback. Ein großes Dankeschön auch an „die Dinos“, die mir stets mit Ablenkung, Spaß und ermutigenden Worten zur Seite standen.
Meiner Familie und meinen Freunden gilt mein tiefster Dank. Ihre Unterstützung und Geduld haben mir die Kraft gegeben, die Höhen und Tiefen dieser Reise zu meistern. Besonders meinen Eltern, Josef und Gabriele, möchte ich dafür danken, dass sie mir so vieles mit auf den Weg gegeben haben und mir diese berufliche Laufbahn ermöglicht haben. Auch meinen Geschwistern Andreas und Lea danke ich von Herzen dafür, dass sie immer an meiner Seite stehen.

CONTENTS

LIST OF FIGURES

LIST OF TABLES

ABBREVIATIONS

ABC Adenosine triphosphate (ATP)-binding cassette

ADME Absorption, distribution, metabolism and excretion

ADR Adverse drug reaction

AUC Area under the plasma concentration-time curve

AUC_{last} Area under the plasma concentration-time curve from the time of drug administration to the time of the last concentration measurement

CKD Chronic kidney disease

C_{max} Peak plasma concentration

CRediT Contributor roles taxonomy

CYP Cytochrome P450

DDGI Drug-drug-gene interaction

DDI Drug-drug interaction

DGI Drug-gene interaction

EMA European Medicines Agency

FDA U.S. Food and Drug Administration

GFR Glomerular filtration rate

GMFE	Geometric mean fold error
$\mathbf{k_{deg}}$	Protein degradation rate constant
$\mathbf{k_{deg,app}}$	Apparent protein degradation rate constant in the presence of an irreversible inhibitor
$\mathbf{K_i}$	Inhibition constant
$\mathbf{K_M}$	Michaelis-Menten constant
$\mathbf{K_{M,app}}$	Apparent Michaelis-Menten constant in the presence of an inhibitor
MIDD	Model-informed drug development
MRD	Mean relative deviation
MRP	Multidrug resistance-associated protein
M&S	Modeling and simulation
OAT	Organic anion transporter
OATP	Organic anion transporting polypeptide
OSP	Open Systems Pharmacology
PBPK	Physiologically based pharmacokinetic
PD	Pharmacodynamics
Pgp	P-glycoprotein
PK	Pharmacokinetics
PopPK	Population pharmacokinetics
$\mathbf{R_{syn}}$	Protein synthesis rate
$\mathbf{R_{syn,app}}$	Apparent protein synthesis rate in the presence of an inducer
SLC	Solute carrier
UGT	Uridine 5'-diphospho-glucuronosyltransferase
$\mathbf{v}$	Reaction velocity
$\mathbf{v_{max}}$	Maximum reaction velocity
$\mathbf{v_{max,app}}$	Apparent maximum reaction velocity in the presence of an inhibitor

1 INTRODUCTION

1.1 MOTIVATION

On average, individuals covered by statutory health insurance in Germany take two different drugs per day and the number of daily drug doses increases with age (see figure 1.1) [2]. For instance, elderly people ≥ 65 years of age take an average of four drugs per day. This observed trend of increasing daily drug doses with age is closely related to the increasing prevalence of multimorbidity among the elderly in comparison to younger individuals [3]. Multimorbidity is also associated with treatment by multiple physicians and a higher frequency of medical consultations per year [4]. The combination of advanced age, a high number of concomitant drugs and multiple prescribers increases the potential for drug interactions and adverse drug reactions (ADRs) [5, 6].

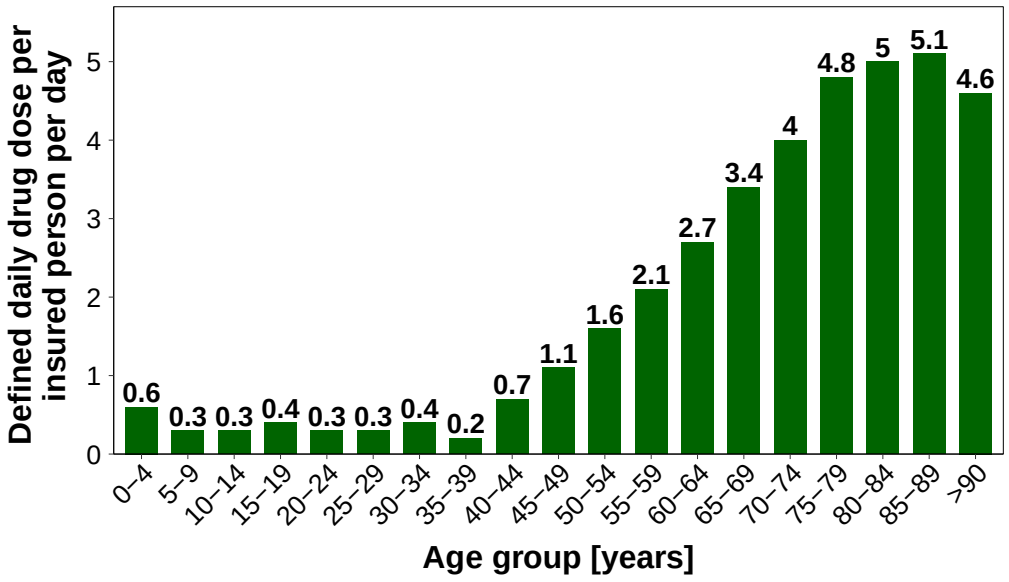

Figure 1.1: Defined daily drug doses. Defined daily drug doses per day for different age groups of persons covered by statutory health insurance in Germany in 2021 [2].

ADVERSE DRUG REACTIONS

According to Aronson et al., an ADR is defined as "an appreciably harmful or unpleasant reaction resulting from an intervention related to the use of a medicinal product; adverse effects usually predict hazard from future administration and warrant prevention, or specific treatment, or alteration of the dosage regimen or withdrawal of the product" [7].
ADRs can be categorized based on their cause, including:

1. Type of disease (e.g. hypokalemia associated with the intake of thiazide to treat hypertension [8])
2. Drug interactions (e.g. co-administration of theophylline and fluvoxamine can lead to toxic theophylline plasma concentrations [9])
3. Patient characteristics such as age, gender or altered physiology (e.g. altered drug pharmacokinetics (PK) of dabigatran etexilate in renal-impaired patients [10])
4. Problems with drug handling (e.g. dividing tablets with altered drug release).

Schurig et al. reported that 6.5% of emergency department visits were attributed to suspected ADRs [11]. In these cases, the probability of hospitalization was 89%. Particularly, elderly patients $\geq$ 65 years of age taking more than three medications exhibited a high susceptibility to ADRs [11]. Patients with suspected ADRs spend nine days in the hospital on average resulting in treatment costs of about $2250 per patient [12]. Enhancing awareness of drug-related symptoms among both healthcare professionals and patients could potentially prevent hospital admissions related to ADRs by up to 20% [11, 12]. Implementing this preventative measure would reduce health insurance costs by about $87 million per year [11, 12].

DRUG INTERACTIONS

When two or more drugs are taken concurrently, drug interactions must always be considered as potential causes of ADRs. Drug interactions occur when the effects of a drug are altered by the presence of another drug (drug-drug interaction (DDI)), genetic polymorphisms (drug-gene interaction (DGI)) or by food intake (drug-food interaction) [13, 14]. DDIs have been estimated to be associated with 20% of ADRs and the risk of a potentially clinically relevant DDI increases with the number of drugs taken [15, 16].
DDIs can be categorized into pharmacodynamic (PD) and PK interactions [17]. PD describes the association between drug concentration and the corresponding drug response. PK, on the other hand, describes the concentration changes of a drug in different regions of the body [18].
In the case of PD DDIs, the pharmacological effect of a drug (victim drug) is directly influenced during co-administration of another drug (perpetrator drug) [19]. This can result in additive, synergistic or antagonistic drug response effects [19, 20]. For example, co-administration of phenprocoumon with non-steroidal anti-inflammatory drugs can increase the risk of bleeding events [21]. In the case of PK DDIs, absorption, distribution, metabolism and excretion (ADME) parameters of a victim drug are influenced by a perpetrator drug, leading to altered plasma concentrations of the victim drug during co-administration of the perpetrator drug [18, 19]. The absorption of drugs may be affected by pH value changes in the gastrointestinal tract or complex formation during co-administration. For instance, the absorption of levothyroxine is reduced when administered with proton pump inhibitors, as proton pump inhibitors increase gastric pH, leading to reduced solubility and absorption of levothyroxine [22, 23]. The metabolism and excretion of victim drugs may be affected by inhibition or induction of metabolizing enzymes by perpetrator drugs. The metabolizing cytochrome P450 (CYP) enzyme

family plays a prominent role in PK DDIs. A subset of ten enzymes, including CYP3A4, CYP1A2 and CYP2E1, participate in the metabolism of more than 90% of all known therapeutic drugs [24]. To give an example, the elimination half-life of pioglitazone (CYP2C8 substrate) is prolonged during co-administration with gemfibrozil due to CYP2C8 inhibition by gemfibrozil [25]. The absorption, distribution and excretion of victim drugs may be affected by inhibition or induction of transporters by perpetrator drugs [26]. P-glycoprotein (Pgp) and organic anion transporter (OAT) are prominent examples of drug transporters affected by PK DDIs [27]. The induction of Pgp by rifampicin, for example, leads to reduced plasma concentrations of the Pgp substrate digoxin [28].

Clinically relevant DDIs are primarily caused by induction or inhibition of metabolizing enzymes and transporters [17]. The induction of drug-metabolizing enzymes and transporters is characterized by an increased level of activity after repeated perpetrator exposure. This results in a more rapid (metabolic) elimination of co-administered drugs by the induced enzyme [29]. Inhibition can be classified as either reversible or irreversible (see figure 1.2).

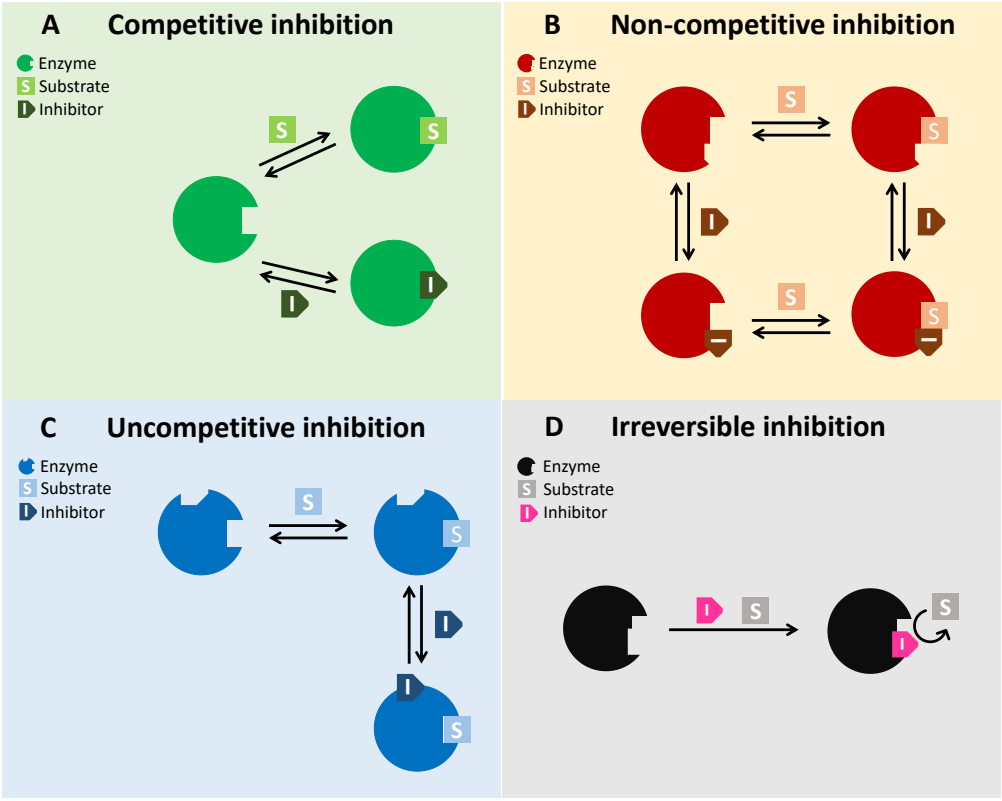

Figure 1.2: Inhibition types. Inhibition of metabolizing enzymes can be either reversible (A-C) or irreversible (D). Reversible inhibition includes competitive (A), non-competitive (B) and uncompetitive (C) inhibition [30]. Adapted from Zhao et al. [31].

Reversible inhibitions include competitive, non-competitive and uncompetitive inhibition [30]. During competitive inhibition, the substrate and inhibitor compete for the same binding site on the enzyme. The inhibitor binds exclusively to the free enzyme, preventing the substrate from binding to it. This inhibition

can be overcome by high substrate concentrations [17, 32, 33] (see figure 1.2 A). During non-competitive inhibition, the inhibitor binds to either the enzyme or the enzyme-substrate complex but not at the active site [32, 33] (see figure 1.2 B). For instance, the strong OAT inhibitor probenecid inhibits OAT and uridine 5'-diphospho-glucuronosyltransferase 1A9 (UGT1A9) in a non-competitive manner [34, 35]. In the rare occurrence of uncompetitive inhibition, the inhibitor binds to the enzyme-substrate complex in a reversible manner [32, 33, 36] (see figure 1.2 C). Irreversible inhibition is caused by the covalent binding of the inhibitor to the enzyme, resulting in the inactivation of the enzyme [32]. As a result, the amount of free enzymes is reduced and they are no longer available for substrate binding (see figure 1.2 D). To give an example, clarithromycin inhibits CYP3A4 through irreversible inhibition [37].

During drug development, drug regulatory agencies such as the U.S. Food and Drug Administration (FDA) and the European Medicines Agency (EMA) mandate the investigation of the PK of drugs under development. They also require an assessment of the potential impact of PK DDIs on ADME parameters [38–40]. To support the pharmaceutical industry in meeting these requirements, drug regulatory agencies issue guidance documents. These documents provide recommendations for conducting both *in vitro* and *in vivo* drug interaction studies with investigational drugs [40–42]. The FDA guidance documents and associated tables entitled "Table of Substrates, Inhibitors, and Inducers" and "FDA's Examples of Drugs that Interact with CYP Enzymes and Transporter Systems" provide drugs to be used as substrates, inhibitors or inducers for the evaluation of suspected DDI pathways [40–44]. For *in vitro* DDI studies, the tables provide examples of substrates, selective inhibitors and inducers for CYP-mediated metabolism, as well as substrates and inhibitors for transporters [43, 44]. In the context of clinical DDI studies drugs are proposed that are characterized as clinical index substrates, inhibitors and inducers for CYP-mediated metabolism and substrates and inhibitors of transporter systems [43, 44]. Substrates for CYP-mediated metabolism are further categorized into sensitive substrates, which show an increase in area under the plasma concentration-time curve (AUC) $\geq$ 5-fold when co-administered with a strong inhibitor and moderate sensitive substrates, which show an AUC increase of $\geq$ 2-fold to $<$ 5-fold when co-administered with a strong inhibitor. Strong CYP inhibitors are drugs that increase the AUC of sensitive substrates by $\geq$ 5-fold when co-administered. Moderate CYP inhibitors increase the AUC of sensitive substrates by $\geq$ 2-fold to $<$ 5-fold during co-administration, whereas weak CYP inhibitors result in an AUC increase of $\geq$ 1.25-fold to $<$ 2-fold [44]. Drugs are classified as strong CYP inducers when the AUC of a sensitive substrate decreases by $\geq$ 80% during co-administration. Moderate and weak CYP inducers reduce the AUC of sensitive substrates by $\geq$ 50% to $<$ 80% and by $\geq$ 20% to $<$ 50%, respectively, during co-administration [44]. This categorization is not applied to transporter system substrates and inhibitors. Instead, a separate specification is used for each transporter system [44].

NEED FOR PREDICTIVE MODELS

The increasing complexity of pharmacotherapy, especially among the elderly, is a central issue in clinical practice and requires a deeper understanding of the underlying mechanisms and potential risks associated with ADRs and drug interactions. To ensure patient safety and optimize therapeutic outcome, solutions must be developed that enable the identification and assessment of potential drug interactions. Mathematical and statistical model-based approaches are essential for understanding and predicting these complex drug interactions. They assist in analyzing the effects of PK and PD, provide valuable insights into potential drug interactions [45], enhance decision-making processes [40] and offer a quantitative and mechanistic framework to address these challenges. Particularly, the development and combination of models for index substrates, inhibitors and inducers proposed by the FDA and EMA advances the investigation of potential drug interactions.

1.2 MODEL-INFORMED DRUG DEVELOPMENT

Model-informed drug development (MIDD) describes the development and application of mathematical and statistical models to characterize the PK and PD of a drug using available preclinical and clinical data [46]. MIDD is applied to support drug development and decision-making and encompasses the entire drug development process [45, 47]. This typically involves the use of modeling and simulation (M&S) techniques, including pharmacometrics, systems pharmacology and other mathematical and statistical approaches [48]. Table 1.1 shows the drug development process and lists potential applications of different M&S techniques. Among these techniques, physiologically based pharmacokinetic (PBPK) modeling has emerged as a powerful tool to investigate drug interactions in a mechanistic and quantitative manner [45].

Table 1.1: Modeling and Simulation techniques. Drug development phases and potential for M&S techniques adapted from Kim et al. [47].

Drug development phases	Model types
Discovery	
• Identification and validation of targets • Characterization of target mechanism	• Systems pharmacology • PK model • PK/PD model
Preclinical development	
• Optimization of therapeutic drug candidates, dosage form and dosage regimen • Identification of surrogate markers and animal models for toxicity • Evaluation of *in vivo* potency and intrinsic activity • Extrapolation of preclinical data to humans • Dose selection for first-in-human studies • Evaluation of *in vivo* drug interactions	• PK model • PK/PD model • PBPK model • Allometric scaling

NDA: new drug approval, PBPK: physiologically based pharmacokinetic, PD: pharmacodynamic, PK: pharmacokinetic

Table 1.1: Modeling and Simulation techniques. Drug development phases and potential for M&S techniques adapted from Kim et al. [47]. (*continued*)

Drug development phases	Model types
Clinical development	
• Characterization of dose-effect relationship • Design of subsequent clinical trials • Evaluation of – Dosage forms – Administration pathways – Special populations (dose recommendations) – Food and gender effects • Efficient analysis of data for label recommendations • Identification and confirmation of predictive covariates • Characterization of – Active metabolites – Drug-drug interactions – Drug-disease interactions	• PK model • PK/PD model • PBPK model • Population scaling
Post-marketing	
• Facilitation of the NDA review process and resolving regulatory issues • Detection of – Drug-drug interactions – Drug-disease interactions – Other covariates (demographics or genetics) • Design and development of extended release formulation	• PK model • PK/PD model

NDA: new drug approval, PBPK: physiologically based pharmacokinetic, PD: pharmacodynamic, PK: pharmacokinetic

1.2.1 *Pharmacometrics*

Williams et al. define pharmacometrics as "the science of developing and applying mathematical and statistical methods to characterize, understand, and predict a drug's pharmacokinetic and pharmacodynamic behavior, quantify the uncertainty of information about that behavior and rationalize knowledge-driven decision-making in the process" [49]. In drug development, pharmacometrics includes the development of PK, PD, PK/PD, population PK (PopPK), PBPK and disease progression models [49, 50]. Those models are based on a large amount of data generated during the drug development process and can improve drug development and drug therapy [51]. The choice of technique depends on the research question and the data availability [47, 50].

1.2.1.1 *Pharmacokinetic models*

PK models are mathematical models used to describe drug and/or metabolite concentration-time courses. Compartments are the fundamental building blocks of PK models and, depending on the model type, are used to represent the body with its physiological spaces or abstract concepts that do not obligatorily have physiological or anatomical relevance [47, 49]. Drug distribution between the compartments can be parameterized with volumes and rate constants. The connection between compartments is a major factor that distinguishes different PK models [49, 52]. An exemplary structure of a PK model is presented in figure 1.3.

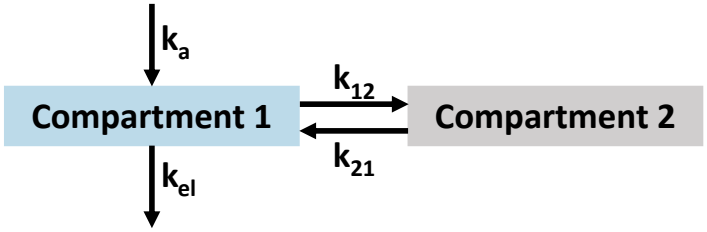

Figure 1.3: PK model structure. In the PK model, the compartments are connected via rate constants (k_a, k_{el},k_{12}, k_{21}). Adapted from Williams et al. [49].

POPULATION PHARMACOKINETIC MODELS

PopPK models are empirical compartment-based models [47]. They are developed based on observed clinical data and aim to understand system characteristics by extrapolating from these data ("top-down" approach) [53, 54]. The concentration-time profile of a drug is described using population PK parameters and the variability in a population [55]. PopPK models integrate structural, stochastic and covariate models [52]. The structural model describes the population median drug concentration-time profile, while the stochastic model accounts for random effects within the observed data. The covariate model considers variability based on subject characteristics such as demographics [52, 55].

PHYSIOLOGICALLY BASED PHARMACOKINETIC MODELS

PBPK models are more complex and consist of various compartments, with each compartment assigned to a specific organ or tissue and connected through blood flow [47, 56]. The arrangement of these compartments defines the structural model [57]. The structural model generally remains consistent across mammalian species and is drug-independent [57]. It is combined with system-specific (anatomical and physiological properties, e.g. organ volume) and drug properties (e.g. plasma-protein binding affinity) to a framework [57]. In this framework, the physiological and biochemical processes are described by differential equations [56]. This allows the quantitative prediction of the PK of a drug [56]. Whole-body PBPK models use a structural model that includes compartments for all organs and tissues thought to be generally relevant to the processes of a drug [53]. Figure 1.4 illustrates the structure of a whole-body PBPK model. PBPK models developed within the same framework can be combined, enabling the development of PBPK DDI networks and the simultaneous assessment of DDIs, while accounting for the

complexities of polypharmacy and multiple interacting pathways within the body. PBPK modeling provides a "bottom-up" approach [53, 54]. They combine prior information on system characteristics and relevant variables to predict outcomes. Insights into the underlying mechanisms can be gained from any discrepancies between predictions and observations.

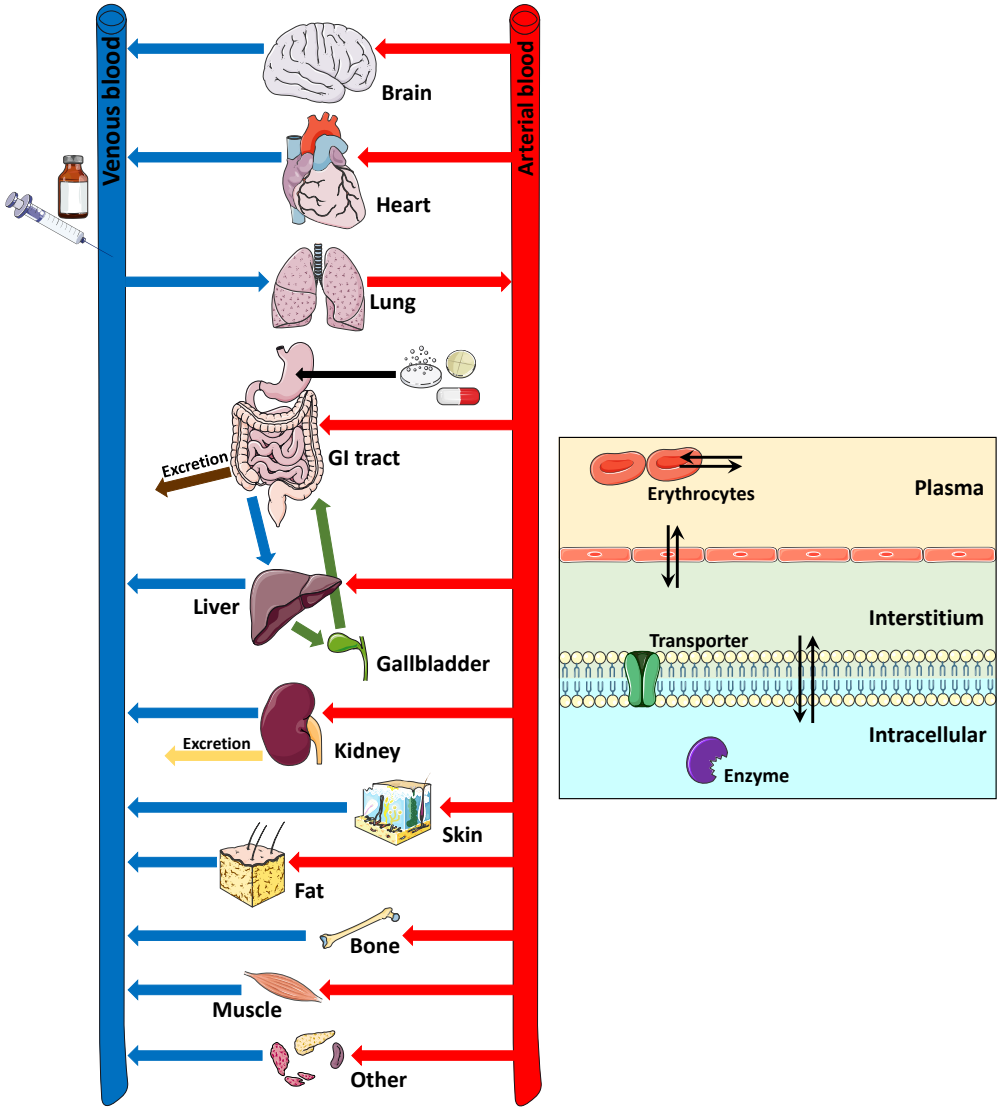

Figure 1.4: PBPK model structure. In a PBPK model, a network of compartments represents various organs within the body. These compartments are connected via arterial and venous blood flow. Each compartment can be further divided into four subcompartments: erythrocytes, plasma, interstitial space and intracellular space. Adapted from Rowland et al. [57] and Kuepfer et al. [58]. Parts of the figure were illustrated using pictures from Servier Medical Art. Servier Medical Art by Servier is licensed under a Creative Commons Attribution 3.0 Unported License (https://creativecommons.org/licenses/by/3.0/).

PBPK modeling gives support for further information about ADME of a drug or its metabolites and the application during drug development is recognized by the FDA and EMA [59–61]. Guidelines for the format and content of PBPK analyses have been published by both agencies [62, 63]. The manifold applications of PBPK modeling include the prediction of metabolizing enzyme-mediated DDIs,

transporter-mediated DDIs, PK for special populations (e.g. pediatrics), PK in renal-impaired patients and support in oral drug product development [42, 63–65]. PBPK models to investigate drug interactions can be developed *de novo* using *in vitro* parameters and already established DDI networks or utilizing clinical DDI studies.

2

AIMS

The aim of this thesis is to develop whole-body PBPK models of clinically relevant index enzyme and transporter substrates, inhibitors or inducers, as recommended by regulatory agencies such as the FDA and the EMA and their use in predicting DDIs [40, 43, 44]. The primary objective is to develop comprehensive whole-body PBPK models encompassing substrates, inhibitors and inducers of key drug metabolizing enzymes and transporters involved in ADME processes, including CYP3A4, CYP1A2, Pgp and OAT. PBPK models for midazolam, alfentanil, theophylline, digoxin, furosemide, clarithromycin, itraconazole, fluvoxamine, probenecid and rifampicin have been developed and evaluated for their ability to predict DDIs. These models have been made publicly accessible through the PBPK model library [66]. This work has been divided into three distinct projects, as described below:

Project I: CYP3A4 and Pgp DDI network
In project I, whole-body PBPK models for recommended CYP3A4 and Pgp substrates, inhibitors and inducers were developed. These compounds included midazolam and alfentanil as CYP3A4 substrates, digoxin as Pgp substrate, itraconazole and clarithromycin as CYP3A4 and Pgp inhibitor and rifampicin as CYP3A4 and Pgp inducer. The developed models were subsequently employed to predict DDIs in eight unique drug combinations, resulting in a comprehensive PBPK DDI network. This investigation provides insights into the complex interplay between metabolic enzymes and transporters in drug interactions.

Project II: CYP1A2 DDI network
This project aimed to establish a PBPK DDI model network for CYP1A2. Whole-body PBPK models of theophylline (CYP1A2 substrate) and fluvoxamine (CYP1A2 inhibitor) were developed, incorporating the current knowledge of relevant PK mechanisms. These models were then combined with previously developed models of caffeine (CYP1A2 substrate), rifampicin (CYP1A2 inducer) and midazolam. A total of four distinct DDI combinations were predicted and a comprehensive CYP1A2 DDI network was established. Furthermore, the PBPK model was used to investigate how variations in CYP1A2 activity, possibly due to genetic polymorphisms or lifestyle factors such as smoking, may affect the PK of CYP1A2 substrates supported by a PopPK analysis.

Project III: Transporter-mediated DDIs
The objective of project III was to develop and evaluate whole-body PBPK models for transporter-mediated DDIs focusing on OAT. To achieve this, whole-body PBPK models of furosemide (OAT index substrate) and probenecid (clinical OAT inhibitor) were developed and evaluated by predicting the probenecid-furosemide interaction. Moreover, since probenecid is also an organic anion transporting polypeptide 1B1 (OATP1B1) inhibitor and rifampicin is an OATP1B1 sub-

strate, the probenecid-rifampicin interaction was predicted. Project III highlights the importance of renal drug transporters in drug elimination and the potential for significant DDIs when transporter function is altered by co-administered drugs.

3

METHODS

3.1 PHYSIOLOGICALLY BASED PHARMACOKINETIC MODELING

Figure 3.1 shows the whole-body PBPK modeling workflow applied in projects I-III.

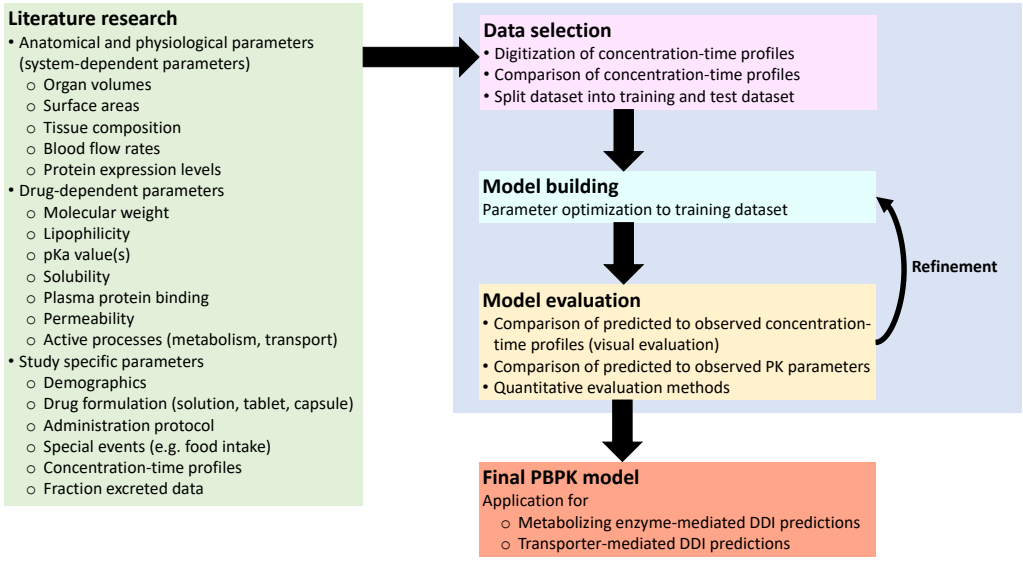

Figure 3.1: Whole-body PBPK modeling workflow. Whole-body PBPK model development included extensive literature research for parameters describing the anatomical and physiological characteristics (system-dependent parameters) of the individual as well as properties of the examined drug (drug-dependent parameters) and reports of clinical studies. In the next step, the collected data was analyzed and selected for the model building and evaluation process. The final whole-body PBPK models were applied for metabolizing enzyme- and transporter-mediated DDI predictions. DDI: drug-drug interaction

3.1.1 *PBPK model building*

PBPK model building started with the gathering of physicochemical parameters, information on drug ADME processes (drug-dependent parameters) as well as anatomical and physiological data (system-dependent parameters). Additionally, reported drug plasma concentration-time profiles, fractions excreted in urine or feces and information on drug formulation and administration protocols for different routes and doses were collected from clinical study reports. This data was then divided into two datasets: a training dataset for model building and a test dataset for model evaluation. To generate typical individuals for model simulations, ethnicity, sex and mean values of age, body weight and height were used as reported in the respective studies. Drug concentrations in various compart-

ments were then simulated based on these individuals. To ensure that the relative expression in different organs was adequately represented, relevant ADME transporters and metabolizing enzymes were implemented with protein expression data in accordance with parameters for Michaelis-Menten or first-order kinetic parameters, derived from the literature. The training dataset was used to optimize model input parameters that were not reported in experimental reports by simultaneously fitting all simulations of the training dataset to their observed data. The whole-body PBPK models incorporated the minimal number of parameters necessary for accurately and mechanistically characterizing drug PK and DDIs.

3.1.2 *PBPK model evaluation*

The performance evaluation of the whole-body PBPK models was performed by comparing the predicted plasma concentration-time profiles and fractions excreted unchanged in urine profiles to the observed clinical data. Predicted plasma concentrations, AUC and peak plasma concentration (C_{max}) values were compared to their respective observed data in goodness-of-fit plots. To quantitatively assess the model performance, the mean relative deviation (MRD) of all predicted plasma concentrations (equation 3.1) was calculated during model evaluation in projects II and III, while the geometric mean fold error (GMFE) of all predicted AUC and C_{max} values (equation 3.2) was calculated during model evaluation in projects I-III. Adequate model performance was defined as MRD and GMFE values ≤ 2.

$$MRD = 10^x \text{ with } x = \sqrt{\frac{\sum_{i=1}^{k} (\log_{10} c_{predicted,i} - \log_{10} c_{observed,i})^2}{k}} \tag{3.1}$$

where MRD = mean relative deviation, $c_{predicted,i}$ = predicted plasma concentration, $c_{observed,i}$ = corresponding observed plasma concentration, k = number of observed values.

$$GMFE = 10^x \text{ with } x = \frac{1}{m} \sum_{i=1}^{m} |\log_{10} \left(\frac{\text{PK parameter}_{predicted,i}}{\text{PK parameter}_{observed,i}} \right)| \tag{3.2}$$

where GMFE = geometric mean fold error, $\text{PK parameter}_{\text{predicted,i}}$ = predicted AUC or C_{max} value, $\text{PK parameter}_{\text{observed,i}}$ = corresponding observed AUC or C_{max} value, m = number of studies.

3.1.3 *PBPK model sensitivity analysis*

To investigate the impact of the relative change of model parameters on the predicted AUC from the time of drug administration to the time of the last concentration measurement (AUC_{last}), local sensitivity analyses were performed with simulations of the highest recommended doses using a relative perturbation of 1000. The parameters optimized during parameter identifications, as well as those associated with optimized parameters or those that might have a strong impact on model predictions were used. Sensitivity to a parameter was calculated according

to equation 3.3 and a threshold value of 0.5 was set, implying that a 100% change in the investigated parameter value causes a 50% change in the predicted AUC_{last}.

$$S = \frac{\Delta AUC}{AUC} \cdot \frac{p}{\Delta p} \tag{3.3}$$

where S = sensitivity of the AUC_{last} to the examined model parameter, ΔAUC = change of the simulated AUC_{last}, AUC = simulated AUC_{last} with the original parameter value, p = original parameter value, Δp = change of the examined parameter value.

3.1.4 *PBPK DDI modeling*

The whole-body PBPK models of the perpetrator drugs were coupled with the simultaneously developed victim drug models. Interaction parameter values obtained from *in vitro* experiment reports were used to model inhibition and induction processes. If the corresponding parameter was not available, the inhibition constant was optimized during compound model development using the clinical data from an interaction study. For auto-inhibition or auto-induction, the corresponding parameters were identified during the development of the perpetrator model without including additional DDI studies in the model training dataset. The mathematical implementation of the various interaction mechanisms is described in detail below.

3.1.4.1 *Competitive inhibition*

When competitive inhibitors are co-administered with a substrate, the inhibitor reversibly binds to the active site of an enzyme or transporter. High substrate concentrations can partially or completely reverse the inhibition. This competitive inhibition results in an increase in the Michaelis-Menten constant (K_M) (apparent Michaelis-Menten constant in the presence of an inhibitor ($K_{M,app}$), equation 3.4) while the maximum reaction velocity (v_{max}) remains unaffected. Equation 3.5 describes the reaction velocity (v) during co-administration of a competitive inhibitor [33].

$$K_{M,app} = K_M \cdot \left(1 + \frac{[I]}{K_{ic}}\right) \tag{3.4}$$

$$v = \frac{v_{max} \cdot [S]}{K_{M,app} + [S]} \tag{3.5}$$

where $K_{M,app}$ = apparent Michaelis-Menten constant in the presence of an inhibitor, K_M = Michaelis-Menten constant, $[I]$ = free inhibitor concentration, K_{ic} = dissociation constant of the competitive inhibitor-enzyme/transporter complex, v = reaction velocity, v_{max} = maximum reaction velocity, $[S]$ = free substrate concentration.

3.1.4.2 *Non-competitive inhibition*

When non-competitive inhibitors are co-administered with a substrate, the inhibitor binds reversibly with the same inhibition constant (K_i) to the free enzyme to a site different from the active site or to the enzyme-substrate complex. The substrate can still bind to either the free enzyme or the enzyme-inhibitor complex, resulting in unaffected substrate binding. However, in the presence of the inhibitor, v_{max} is reduced (apparent maximum reaction velocity in the presence of an inhibitor ($v_{max,app}$)), as described in equation 3.6. The reaction velocity is described by equation 3.7 [33].

$$v_{max,app} = \frac{v_{max}}{1 + \frac{[I]}{K_{in}}} \tag{3.6}$$

$$v = \frac{v_{max,app} \cdot [S]}{K_M + [S]} \tag{3.7}$$

where $v_{max,app}$ = apparent maximum reaction velocity in the presence of an inhibitor, v_{max} = maximum reaction velocity, $[I]$ = free inhibitor concentration, K_{in} = dissociation constant of the non-competitive inhibitor-enzyme-substrate complex, v = reaction velocity, $[S]$ = free substrate concentration, K_M = Michaelis-Menten constant.

3.1.4.3 *Mixed inhibition*

When mixed inhibitors are co-administered with a substrate, the inhibitor binds to the free enzyme in a competitive manner or to the enzyme-substrate complex in an uncompetitive manner with different affinities. As a result of mixed inhibition, K_M increases while v_{max} decreases in the presence of a mixed inhibitor as described by equations 3.8 ($K_{M,app}$) and 3.9 ($v_{max,app}$). The reaction velocity in a mixed inhibition is defined by equation 3.10 [33].

$$K_{M,app} = K_M \cdot \frac{\left(1 + \frac{[I]}{K_{ic}}\right)}{\left(1 + \frac{[I]}{K_{iu}}\right)} \tag{3.8}$$

$$v_{max,app} = \frac{v_{max}}{1 + \frac{[I]}{K_{iu}}} \tag{3.9}$$

$$v = \frac{v_{max,app} \cdot [S]}{K_{M,app} + [S]} \tag{3.10}$$

where $K_{M,app}$ = apparent Michaelis-Menten constant in the presence of an inhibitor, K_M = Michaelis-Menten constant, $[I]$ = free inhibitor concentration, K_{ic} = dissociation constant of the competitive inhibitor-enzyme complex, K_{iu} = dissociation constant of the uncompetitive inhibitor-(enzyme-substrate) complex, $v_{max,app}$ = apparent maximum reaction velocity in the presence of an inhibitor, v_{max} = maximum reaction velocity, v = reaction velocity, $[S]$ = free substrate concentration.

3.1.4.4 *Mechanism-based inhibition (irreversible inhibition)*

Mechanism-based inhibition is an irreversible form of enzyme inhibition. When mechanism-based inhibitors and substrates are co-administered, the inhibitor binds to the enzyme, modifying the active site and preventing substrate binding. To account for this, in the protein turnover equation, the protein degradation rate constant (k_{deg}) is substituted with the apparent protein degradation rate constant in the presence of an irreversible inhibitor ($k_{deg,app}$) (equations 3.11 and 3.12) [33]. Since mechanism-based inhibitors also act as competitive inhibitors, the reaction velocity equation during co-administration is described as shown in equations 3.4 and 3.5.

$$k_{deg,app} = k_{deg} + \frac{k_{inact} \cdot [I]}{K_I + [I]} \tag{3.11}$$

$$\frac{d[E]}{dt} = R_{syn} - k_{deg,app} \cdot [E] \tag{3.12}$$

with $k_{deg,app}$ = apparent protein degradation rate constant in the presence of an irreversible inhibitor, k_{deg} = protein degradation rate constant, k_{inact} = maximum inactivation rate constant, $[I]$ = free irreversible inhibitor concentration, K_I = concentration for half-maximal inactivation, $\frac{d[E]}{dt}$ = protein turnover, R_{syn} = rate of protein synthesis, $[E]$ = protein concentration.

3.1.4.5 *Induction*

During simultaneous administration of inducer and substrate, the protein synthesis is altered. Specifically, in the protein turnover equation, the protein synthesis rate (R_{syn}) is replaced by the apparent protein synthesis rate in the presence of an inducer ($R_{syn,app}$), which is described by equations 3.13 and 3.14 [33].

$$R_{syn,app} = R_{syn} \cdot (1 + \frac{E_{max} \cdot [I]}{EC_{50} + [I]}) \tag{3.13}$$

$$\frac{d[E]}{dt} = R_{syn,app} - k_{deg} \cdot [E] \tag{3.14}$$

where $R_{syn,app}$ = apparent rate of protein synthesis in the presence of an inducer, R_{syn} = rate of protein synthesis, E_{max} = maximal induction effect *in vivo*, $[I]$ = free inducer concentration, EC_{50} = concentration for half-maximal induction *in vivo*, $\frac{d[E]}{dt}$ = protein turnover, k_{deg} = degradation rate constant, $[E]$ = protein concentration.

3.1.5 *PBPK DDI performance evaluation*

For the evaluation of the DDI predictions, the predicted plasma concentration-time profiles of the victim drug were compared with the observed profiles, both

alone and during co-administration of the perpetrator drug. In addition, DDI AUC ratios and DDI C_{max} ratios (equation 3.15) were calculated and compared. To assess the accuracy of the DDI predictions, GMFE values for DDI AUC ratios and DDI C_{max} ratios were calculated according to equation 3.2.

$$\text{DDI PK parameter ratio} = \frac{\text{PK parameter}_{\text{DDI}}}{\text{PK parameter}_{\text{Control}}} \tag{3.15}$$

where PK parameter = AUC or C_{max}, PK $\text{parameter}_{\text{DDI}}$ = AUC or C_{max} of the victim drug during simultaneous perpetrator administration, PK $\text{parameter}_{\text{Control}}$ = AUC or C_{max} of the victim drug alone.

3.2 INVESTIGATED DRUG-METABOLIZING ENZYMES, DRUG TRANSPORTERS AND DRUGS

The PBPK models presented in this thesis were developed to comprehensively assess DDIs, focusing on key drug-metabolizing enzymes and transporters. Understanding these interactions is essential for predicting drug behavior in the body during DDIs and avoiding ADRs.

3.2.1 *Drug-metabolizing enzymes*

Among the CYP enzyme family, particularly CYP3A4 and CYP1A2, play pivotal roles in drug metabolism. CYP3A4 is the predominant CYP enzyme in the liver and intestinal epithelium, responsible for metabolizing more than half of all therapeutic drugs [24]. CYP1A2, exclusively expressed in the liver, contributes to approximately 13% of the total CYP content in liver microsomes and metabolizes approximately 15% of all known drugs [67, 68]. The broad and overlapping substrate specificity of both enzymes makes them central to the study of DDIs, as inhibition or induction can significantly alter the PK of co-administered drugs, leading to clinically relevant interactions [69].

3.2.2 *Drug transporters*

Beyond metabolizing enzymes, drug transporters are essential for the ADME processes of many drugs. These transporters, categorized into the adenosine triphosphate (ATP)-binding cassette (ABC) family and the solute carrier (SLC) family, regulate drug transport across cellular membranes and play a critical role in clinically relevant DDIs [26, 27]. Pgp from the ABC family and OAT from the SLC family are particularly important [27]. Pgp is mainly expressed in the intestine, liver, kidney and brain and influences the absorption, distribution and elimination of many therapeutic drugs [26, 70]. OAT, predominantly expressed in the kidney, is involved in the active secretion of drugs and endogenous organic anions into the urine [71, 72]. Inhibition or induction of these transporters by co-administered drugs can lead to significant changes in drug PK, resulting in DDIs.

3.2.3 *Drugs*

The selection of specific drugs for PBPK modeling in this thesis was guided by their established use as probe substrates, inhibitors or inducers in studies of CYP- and transporter-mediated DDIs.

3.2.3.1 *CYP3A4 and Pgp DDI network*

For the CYP3A4- and Pgp-mediated DDI network in project I, midazolam and alfentanil were selected as representative CYP3A4 substrates due to their predominant metabolism via CYP3A4 [73–75]. **Midazolam** is a benzodiazepine used for sedation prior to surgical procedures and for the treatment of epileptic seizures [76, 77]. After oral administration, midazolam undergoes extensive first-pass metabolism via CYP3A subfamily, resulting in hydroxylated metabolites [73, 78]. **Alfentanil** is a synthetic opioid used as an analgesic for the induction of anesthesia and is exclusively administered intravenously [74]. The metabolism is primarily mediated by CYP3A4 in the liver, with 99% of the administered dose excreted as metabolites [74, 75]. Clarithromycin and itraconazole were selected as strong CYP3A4 inhibitors that also inhibit Pgp [44]. **Clarithromycin** is a macrolide antibiotic prescribed for the treatment of bacterial infections of the respiratory tract, ear, nose, throat and skin [79]. Its main metabolic pathway includes hydroxylation via CYP3A4 [80]. Due to its irreversible CYP3A4 inhibition, clarithromycin exhibits a dose-dependent PK [37]. **Itraconazole** is a triazole antifungal agent used to treat superficial and systemic mycoses [81]. CYP3A4 is involved in its extensive metabolism to several metabolites [82]. Due to the inhibitory effects on CYP3A4 of itraconazole metabolites, the PBPK model of itraconazole incorporates three metabolites.
Digoxin was selected as a representative Pgp substrate due to its predominant intestinal absorption, renal tubular and biliary-intestinal secretion by Pgp [43, 44, 83, 84]. Rifampicin was selected as a Pgp inducer [43, 44, 84]. **Digoxin** is a cardiac glycoside employed in the management of atrial fibrillation, atrial flutter and heart failure [85]. It is minimally metabolized by hepatic enzymes and mostly excreted unchanged in urine, making it a valuable substrate for investigating Pgp-mediated DDIs [43, 44, 83]. **Rifampicin** is an antibiotic used to treat mycobacterium infections such as tuberculosis [86]. It affects multiple drug-metabolizing enzymes and transporters and the FDA recommends it as a strong inducer of CYP3A4, a moderate inducer of CYP1A2 and an inhibitor of OATP1B1, in addition to being an inducer of Pgp [43, 44, 84].

3.2.3.2 *CYP1A2 DDI network*

Project II focused on CYP1A2-mediated DDIs. Theophylline was selected as a moderate sensitive CYP1A2 substrate and fluvoxamine as a strong CYP1A2 and weak CYP3A4 inhibitor [40, 43, 44]. **Theophylline** is a methylxanthine used to treat asthma and obstructive pulmonary disease [87]. Its metabolism is primarily mediated by CYP1A2 and only to a small extent by CYP2E1 [88–90]. **Fluvoxamine** is a selective serotonin reuptake inhibitor used in treating major depressive disorder and obsessive-compulsive disorder [91]. Fluvoxamine undergoes metabolism

via CYP1A2 and CYP2D6 [92–94]. Smoking habits and polymorphisms in the *CYP2D6* gene can influence the PK of fluvoxamine [94, 95].

3.2.3.3 *Transporter-mediated DDIs*

Project III examined transporter-mediated DDIs, focusing on the interaction between the clinical OAT1/OAT3 substrate furosemide and the OAT1/OAT3 inhibitor probenecid [34, 43, 44, 96]. **Furosemide** is a loop diuretic agent and is used in the treatment of edema or hypertension [97]. Furosemide is glucuronidated by UGT1A9 and UGT1A1 and is transported via OAT1/OAT3 [96, 98]. **Probenecid** is a uricosuric agent employed in the management of gout or hyperuricemia [99]. It is primarily metabolized via glucuronidation and excreted in the urine, with only a small extent excreted unchanged [100, 101].

3.3 SOFTWARE

The whole-body PBPK models of the ten drugs presented in this thesis were built using the open-source PK-Sim® and MoBi® modeling software tools (Open Systems Pharmacology-Suite®, Open Systems Pharmacology) [33, 102]. Published plasma concentration-time and fractions excreted in urine profiles were digitized using GetData Graph Digitizer (version 2.26.0.20, S. Fedorov) [103]. Model parameter optimizations were performed using the "Parameter Identification Toolbox" in MATLAB (Natick, Massachusetts: The MathWorks Inc.) (project I) or within PKSim® (projects II-III). Sensitivity analyses were carried out within PKSim® using the implemented Sensitivity Analysis tool. PK parameters and model performance measures were calculated using MATLAB (projects I-II) and R (The R Foundation for Statistical Computing) and RStudio (RStudio, Inc., Boston, MA, USA) (project III). Graphics were generated using MATLAB (project I), R and RStudio (projects II-III). In project II, a PopPK analysis was performed using NONMEM (ICON Development Solutions, Ellicott City, MD) and for statistical analysis and graphics of the PopPK analysis SAS (SAS Institute, Cary, NC) was used. The corresponding publications for projects I-III provide more detailed information about the versions of the software and tools used for each project.

4

RESULTS

4.1 PROJECT I: PBPK MODELS FOR CYP3A4 AND P-GP DDI PREDICTION: A MODELING NETWORK OF RIFAMPICIN, ITRACONAZOLE, CLARITHROMYCIN, MIDAZOLAM, ALFENTANIL, AND DIGOXIN

4.1.1 *Reference*

Nina Hanke, Sebastian Frechen, Daniel Moj, **Hannah Britz**, Thomas Eissing, Thomas Wendl, Thorsten Lehr. PBPK Models for CYP3A4 and P-gp DDI prediction: A modeling network of rifampicin, itraconazole, clarithromycin, midazolam, alfentanil, and digoxin. CPT Pharmacometrics Syst Pharmacol. 2018;7(10): 647-659. doi: 10.1002/psp4.12343

4.1.2 *Supplementary material*

Supplementary material can be found on the accompanying storage medium. It is also available online at: supplementary material of publication I.

4.1.3 *Copyright*

4.1.4 *Author contributions*

Declaration of author contributions to the publication related to project I included in this thesis according to the CRediT [1].

Nina Hanke	Conceptualization, Data Curation, Investigation, Visualization, Writing - Original Draft, Writing - Review & Editing
Sebastian Frechen	Conceptualization, Investigation, Writing - Original Draft, Writing - Review & Editing
Daniel Moj	Investigation, Writing - Review & Editing
Hannah Britz	Investigation, Writing - Review & Editing
Thomas Eissing	Conceptualization, Writing - Original Draft, Writing - Re-

	view & Editing
Thomas Wendl	Conceptualization, Investigation, Writing - Original Draft, Writing - Review & Editing
Thorsten Lehr	Conceptualization, Investigation, Writing - Original Draft, Writing - Review & Editing

Citation: CPT Pharmacometrics Syst. Pharmacol. (2018) 7, 647–659; doi:10.1002/

ARTICLE

PBPK Models for CYP3A4 and P-gp DDI Prediction: A Modeling Network of Rifampicin, Itraconazole, Clarithromycin, Midazolam, Alfentanil, and Digoxin

Nina Hanke[1], Sebastian Frechen[2], Daniel Moj[1], Hannah Britz[1], Thomas Eissing[2], Thomas Wendl[2] and Thorsten Lehr[1,*]

According to current US Food and Drug Administration (FDA) and European Medicines Agency (EMA) guidance documents, physiologically based pharmacokinetic (PBPK) modeling is a powerful tool to explore and quantitatively predict drug-drug interactions (DDIs) and may offer an alternative to dedicated clinical trials. This study provides whole-body PBPK models of rifampicin, itraconazole, clarithromycin, midazolam, alfentanil, and digoxin within the Open Systems Pharmacology (OSP) Suite. All models were built independently, coupled using reported interaction parameters, and mutually evaluated to verify their predictive performance by simulating published clinical DDI studies. In total, 112 studies were used for model development and 57 studies for DDI prediction. 93% of the predicted area under the plasma concentration-time curve (AUC) ratios and 94% of the peak plasma concentration (C_{max}) ratios are within twofold of the observed values. This study lays a cornerstone for the qualification of the OSP platform with regard to reliable PBPK predictions of enzyme-mediated and transporter-mediated DDIs during model-informed drug development. All presented models are provided open-source and transparently documented.

CPT Pharmacometrics Syst. Pharmacol. (2018) **7**, 647–659; doi:10.1002/psp4.12343; published online on 07 September 2018.

Study Highlights

WHAT IS THE CURRENT KNOWLEDGE ON THE TOPIC?
PBPK modeling is increasingly used for DDI analysis. To investigate and predict the DDI potential of new drugs with the help of PBPK, models of index perpetrator and victim drugs are needed.

WHAT QUESTION DID THIS STUDY ADDRESS?
The aim of this study was to provide whole-body PBPK models of important CYP3A4 and P-gp perpetrator and victim drugs that are all compatible, evaluated, and fit for use in PBPK DDI modeling.

WHAT DOES THIS STUDY ADD TO OUR KNOWLEDGE?
This study adds transparently built and evaluated PBPK models of rifampicin, itraconazole, clarithromycin, midazolam, alfentanil, and digoxin, integrating the current knowledge on the relevant pharmacokinetic mechanisms of these six drugs with insights gained during model development.

HOW MIGHT THIS CHANGE DRUG DISCOVERY, DEVELOPMENT, AND/OR THERAPEUTICS?
A publicly available library, providing comprehensive PBPK models of the recommended DDI inhibitors, inducers, and substrates, evaluated and ready to use for their application in DDI modeling, has the potential to foster open collaboration and to accelerate the drug development process.

Physiologically based pharmacokinetic (PBPK) modeling is a powerful tool to explore and quantitatively predict the pharmacokinetic (PK) of drugs and the magnitude of drug-drug interactions (DDIs). It is applied at increasingly early stages during drug development and is recommended by the US Food and Drug Administration (FDA) and the European Medicines Agency (EMA) for the design of clinical DDI trials and population PK studies. Furthermore, PBPK may even offer an alternative to dedicated clinical trials, to find dosing recommendations for the co-administration of interacting substances, or the treatment of special populations.[1,2]

To investigate and predict the DDI potential of new drugs with the help of PBPK, models of index perpetrator and victim drugs are needed. A library of PBPK models of recommended DDI inhibitors, inducers, and substrates, evaluated for their application in DDI modeling, has the potential to accelerate the drug development process.

The aim of the presented work was to develop and carefully evaluate whole-body PBPK models of frequently used

[1]Clinical Pharmacy, Saarland University, Saarbrücken, Germany; [2]Clinical Pharmacometrics, Bayer AG, Leverkusen, Germany. *Correspondence: Thorsten Lehr (thorsten.lehr@mx.uni-saarland.de)
Received 05 January 2018; accepted 16 July 2018; published online on 07 September 2018. doi:10.1002/psp4.12343

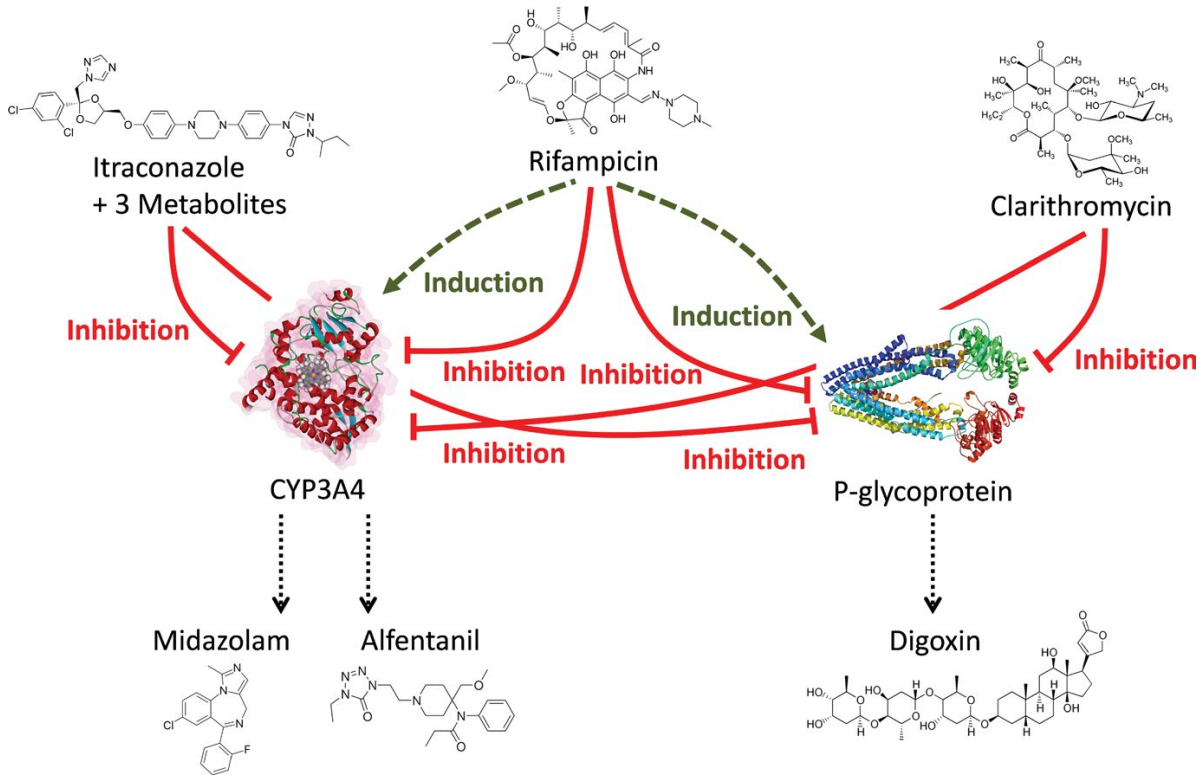

Figure 1 Physiologically based pharmacokinetic drug-drug interaction network. Schematic illustration of the modeled interaction network of cytochrome P450 (CYP)3A4 and P-glycoprotein perpetrator (upper level: itraconazole, rifampicin, and clarithromycin) and victim drugs (lower level: midazolam, alfentanil, and digoxin). Green dashed lines indicate induction; red solid lines indicate inhibition.

perpetrator and victim drugs and to provide them to the PBPK modeling community. Focusing on cytochrome P450 3A4 (CYP3A4) and P-glycoprotein (P-gp) as major interaction pathways affecting approximately half of all drugs in use,[3,4] models of rifampicin (most prominent CYP3A4 and P-gp inducer), itraconazole (competitive CYP3A4 and P-gp inhibitor), clarithromycin (mechanism-based CYP3A4 inactivator and competitive P-gp inhibitor), midazolam, alfentanil (specific CYP3A4 substrates), and digoxin (specific P-gp substrate) have been established. All selected compounds are recommended by the FDA for application in clinical DDI trials.[5]

The perpetrator and victim drug models were developed independently of each other, without the use of data from clinical DDI studies for parameter optimization. With this approach, the prediction of co-administration studies could be utilized as an additional means of model evaluation. Being recommended by the FDA for DDI potential assessment, the six selected compounds have been co-administered in different combinations in many clinical trials, providing ample data for the evaluation of DDI predictions. **Figure 1** shows the developed DDI modeling network of interacting perpetrator and victim drugs, assessing multiple combinations for mutual DDI evaluation.

Clinical DDI studies, for example, the full inhibition of an important metabolizing enzyme, provide valuable information on the fraction of victim drug that is normally eliminated via this pathway ("fraction metabolized"). Therefore, victim drug plasma concentrations during co-administration of perpetrators can serve as additional information for victim drug model evaluation. Furthermore, correct prediction of the impact of a perpetrator drug on the PK of a victim drug indicates that the model is able to describe the perpetrator concentrations at the sites of inhibition or induction. This is not trivial, as drug concentrations are generally measured in blood plasma, but the interactions take place in other compartments, such as the intracellular space of the liver or intestine. Taken together, DDI studies provide additional information on both, the perpetrator and the victim drug PKs, and their correct prediction is a challenge for both models and a valid means of model evaluation.

The aim of this study was to establish and thoroughly evaluate PBPK models of relevant DDI perpetrator and victim drugs. The presented models are whole-body PBPK models, allowing for dynamic DDI assessment in all organs expressing the affected enzyme or transporter. Evaluations indicate that the models are fit for DDI prediction. The model files have been made publicly available as supplementary material to this paper **(Data S1-S6)** and in the Open Systems Pharmacology (OSP) repository (www.open-systems-pharmacology.org), as tools for the drug development and clinical research community to assess the DDI potential of investigational drugs, to inform the design of clinical trials or to be expanded for predictions in special populations.

METHODS

Software

PBPK modeling was performed with PK-Sim and MoBi modeling software version 7.1.0 (part of the OSP Suite). The OSP Suite makes formerly commercial software tools PK-Sim and MoBi available as freeware under the GPLv2 License. The software allows the modification of system parameters and the model structure by the (qualified) user and the source code is publicly available on GitHub (accessible via www.open-systems-pharmacology.org), together with published models and tutorials. Details on how to modify a PBPK model in PK-Sim can be found, for example, in Kuepfer *et al.*,[6] the PK-Sim/MoBi user manual, and in the user forum. Parameter optimization was accomplished using the Monte Carlo algorithm of the "Parameter Identification Toolbox" in MATLAB version R2013b (The MathWorks, Natick, MA) or in PK-Sim. Sensitivity analyses were performed within PK-Sim. Plots and PK parameter analyses were compiled with MATLAB.

Model development

Models of rifampicin, itraconazole, clarithromycin, midazolam, alfentanil, and digoxin were built combining bottom-up and top-down techniques. To establish the models, an extensive literature search was conducted, collecting (i) physicochemical parameters, (ii) information on absorption, distribution, metabolism, and excretion processes, and (iii) clinical studies of intravenous and oral administration to healthy subjects in single-dosing and multiple-dosing regimens, covering the full dosing range published. All data used in this analysis has been taken from previously published human or preclinical studies.

The PBPK models were developed based on a healthy male European individual, 30 years of age, with a body weight of 73 kg, and a height of 176 cm. Physiological parameters, like organ volumes, blood flow rates, and surface permeabilities, are provided within the software.[7] Absorption, distribution, metabolism, and excretion-relevant proteins reported to govern the PK of a drug, such as metabolizing enzymes, transporters, or binding partners, were implemented into the models and tested. Whenever available and in accordance with literature protein expression, the PK-Sim expression database reverse transcription-polymerase chain reaction (RT-PCR) profiles[8] were used to define the relative tissue distribution of these proteins. For parameters that could not be informed from (*in vitro*) experimental data, parameter identification based on plasma concentration-time profiles was performed using a subset of the available clinical studies (training dataset) for optimization. The decision of which studies to include into the training dataset was based on the number of studies available and the information contained in the different studies (dosing regimen, study size, sampling times, fraction excreted measurements, etc.).

Model selection was based on the ability of the model to describe (training dataset) and predict (test dataset) plasma concentration-time profiles from all published clinical studies as well as fraction excreted unchanged to urine. Furthermore, physiological plausibility, precision and covariance of parameter estimates, and population predictions were assessed.

Model evaluation

The models were evaluated by comparison of concentration-time profiles, area under the plasma concentration-time curve (AUC), and peak plasma concentration (C_{max}) values resulting from our simulations to the values observed during clinical studies. As a quantitative measure of the descriptive and predictive performance of each model, the geometric mean fold error was calculated according to Eq. 1:

$$\mathrm{GMFE} = 10^{(\Sigma|\log_{10}(\text{pred PK parameter}/\text{obs PK parameter})|)/n}, \quad (1)$$

with GMFE = geometric mean fold error of all AUC or C_{max} predictions of the respective model, pred PK parameter = predicted AUC or C_{max}, obs PK parameter = observed AUC or C_{max}, and n = number of studies. Furthermore, models were evaluated by their ability to adequately predict the clinical data of all DDI studies available from literature. For this additional evaluation, the final perpetrator models were coupled to victim drug models using measured values (from literature) to inform the different interaction processes without further adjustment. Successful prediction of the victim drug plasma concentration-time profiles during co-administration is interpreted as indication of the correct simulation of the perpetrator drug concentration at the site where the DDI takes effect as well as of the appropriate implementation of the victim drugs' affected disposition pathways.

DDI network development

Mathematical implementation of the induction and inhibition processes in general is specified in Section 1 of **Appendix S1**. The final rifampicin model was coupled to models of midazolam, alfentanil, itraconazole, and digoxin, to assess its DDI performance with CYP3A4 and P-gp substrates. To describe the influence of rifampicin on these victim drugs, induction and simultaneous competitive inhibition of CYP3A4 and P-gp by rifampicin have been added. Furthermore, inhibition of midazolam and digoxin elimination by itraconazole and by clarithromycin were modeled and compared to observed clinical data, evaluating the performance of these two victim drug models with two different CYP3A4 and P-gp inhibitors. Inhibition of alfentanil metabolism by itraconazole or clarithromycin was not tested, as there are no clinical studies available to compare to.

All induction and inhibition processes were modeled using interaction parameter values either identified during the development of the perpetrator models if no experimental values could be found to parameterize their auto-induction or auto-inhibition (using multiple-dose perpetrator studies only, without co-administration of victim drugs), or taken from literature without further adjustment or fitting, as a means of further evaluation of the perpetrator and victim drug models.

DDI network evaluation

The DDI modeling performance was assessed by comparison of predicted vs. observed victim drug plasma concentration-time profiles during co-administration, DDI AUC ratios (Eq. 2), and DDI C_{max} ratios (Eq. 3):

$$\text{DDI AUC ratio} = \frac{\mathrm{AUC}_{\text{victim drug during co-administration}}}{\mathrm{AUC}_{\text{victim drug}}} \quad (2)$$

$$\text{DDI } C_{max} \text{ ratio} = \frac{C_{max \text{ victim drug during co-}administration}}{C_{max \text{ victim drug}}} \quad (3)$$

As a quantitative measure of the prediction accuracy of each DDI interaction, GMFEs of the predicted DDI AUC ratios and DDI C_{max} ratios were calculated according to Eq. 1.

Sensitivity analysis

Sensitivity of the final models to single parameters (local sensitivity analysis) was calculated, measured as changes of the AUC extrapolated to infinity (for single-dose administration drugs) or of the AUC of one dosing interval in steady-state conditions (for multiple-dose administration drugs) of a simulation with administration of the highest common dose. Parameters were included into the analysis if they have been optimized, if they might have a strong influence due to calculation methods used in the model (e.g., lipophilicity and fraction unbound), if they are related to optimized parameters, or if they had significant impact in other models (e.g., solubility and blood/plasma concentration ratio). Sensitivity to a parameter is calculated as the ratio of the relative change of the simulated AUC to the relative variation of the parameter around the value used in the final model (Eq. 4):

$$S = \frac{\Delta AUC}{AUC} \cdot \frac{p}{\Delta p}, \quad (4)$$

with S = sensitivity of the AUC to the examined model parameter, ΔAUC = change of the AUC, AUC = simulated AUC with the original parameter value, Δp = change of the examined model parameter value, and p = original model parameter value. A sensitivity value of +1.0 signifies that a 10% increase of the examined parameter causes a 10% increase of the simulated AUC.

Virtual population characteristics

To quantitatively predict the variability of the simulated plasma concentration-time profiles, virtual populations of 100 individuals within an age range of 20–50 years were generated. Weight, height, and many physiological parameters, such as organ volumes, blood flow rates, and gastrointestinal characteristics, were varied according to published data[7] as implemented into the software.[9] In addition to the variability in drug PK that results from these physiological differences within the virtual populations, the expression levels of the implemented drug metabolizing enzymes, transporters, and protein binding partners were varied around their reference values. If available, default population variabilities for enzyme expression in PK-Sim were used. Otherwise, log-normal distribution of the protein expression level in the population was assumed and variabilities were implemented as geometric SDs derived from literature reports. If no valid source could be found, log-normal distributions with a moderate geometric SD of 1.4 (~35% coefficient of variation) were assumed. Please refer to **Table S7** in **Appendix S1** for an overview.

Population simulations were generated and compared with observed data. Observed data were most often reported in terms of arithmetic means and SDs. To allow comparison of observed and simulated variability, simulated 68% population prediction intervals were plotted that correspond to the range span of ±1 SD around the mean assuming normal distribution.

RESULTS

Model development and evaluation

Of the total of 112 studies, in detail 16 studies of rifampicin, 27 studies of itraconazole, 17 studies of clarithromycin, 7 studies of midazolam, 7 studies of alfentanil, and 38 studies of digoxin administration, were used for model development. The respective modeling results are presented in Section 2 of **Appendix S1**. This includes tables listing the clinical studies used for model development and evaluation, with administration protocols and study population details (**Tables S1a, S2a, S3a, S4a, S5a, S6a** in **Appendix S1**), descriptions of the final models, and tables listing the respective drug-dependent parameters (**Tables S1b, S2b, S3b, S4b, S5b, S6b** in **Appendix S1**).

All models show accurate and precise descriptive and predictive performance for intravenous and oral administration. Plots of population predicted compared with observed plasma concentration-time profiles of all studies obtained from literature are shown as semilogarithmic (**Figures S1c, S2c, S3c, S4c, S5c, S6c** in **Appendix S1**) as well as linear plots (**Figures S1d, S2d, S3d, S4d, S5d, S6d** in **Appendix S1**). In addition, predicted compared to observed AUC and C_{max} values with calculated GMFEs (also listed in **Tables S1a, S2a, S3a, S4a, S5a, S6a** in **Appendix S1**) and sensitivity analysis results (**Figures S1e, S2e, S3e, S4e, S5e, S6e** in **Appendix S1**) are presented. System-dependent parameters are given in **Table S7** in **Appendix S1**.

DDI network modeling

Of the total of 57 studies, in detail 18 clinical studies of rifampicin with midazolam, 12 studies of rifampicin with alfentanil, 1 study of rifampicin with itraconazole, 10 studies of itraconazole with midazolam, 4 studies of clarithromycin with midazolam, 7 studies of rifampicin with digoxin, 1 study of itraconazole with digoxin, and 4 studies of the interaction of clarithromycin with digoxin were predicted and compared with observed data. **Table 1** lists all modeled clinical DDI studies, with administration protocols and study population details. The parameters to model the CYP3A4 and P-gp induction and inhibition processes are described in Section 3 of **Appendix S1**.

Figure 2 presents a selection of the different modeled CYP3A4 DDIs, showing population predicted compared with observed victim drug plasma concentration-time profiles of one study each of the rifampicin-midazolam, rifampicin-alfentanil, itraconazole-midazolam, and clarithromycin-midazolam DDIs, selected for their clinically relevant doses of perpetrator and victim drug. **Figure 3** presents a selection of the different modeled P-gp DDIs, showing population predicted compared with observed victim drug plasma concentration-time profiles of one study each of the rifampicin-digoxin, itraconazole-digoxin, and clarithromycin-digoxin DDIs, selected for their clinically relevant doses of perpetrator and victim drug. Please refer to

Table 1 DDI study dosing regimens, study population sizes, predicted and observed AUC ratios, and C_{max} ratios

Perpetrator (mg)	Victim (mg)	Dose gap (hours)	*n*	Males (%)	Predicted AUC_{ratio}	Observed AUC_{ratio}	Pred/Obs AUC_{ratio}	Predicted $C_{max\ ratio}$	Observed $C_{max\ ratio}$	Pred/Obs $C_{max\ ratio}$	Reference
Rifampicin	**Midazolam**										
600, q.d.	1.0, i.v. (bol)	24	9	100	0.460	0.378	1.22	–	–	–	Kharasch 1997[24]
600, q.d.	1.0, i.v. (bol)	8	10	50	0.470	0.521	0.90	–	–	–	Kharasch 2004[25]
600, q.d.	1.0, i.v. (bol)	8	6	50	0.470	0.481	0.98	–	–	–	Phimmasone 2001[26]
600, q.d.	2.0, i.v. (–)	24	8	100	0.460	0.655	0.70	–	–	–	Link 2008[27]
600, q.d.	0.05/kg, i.v. (bol)	12	3[a]	100	0.480	0.579	0.83	–	–	–	Szalat 2007[28]
600, q.d.	0.05/kg, i.v. (0.5 hours)	12	14	100	0.510	0.512	1.00	–	–	–	Gorski 2003[29]
600, q.d.	2.0, p.o. (syr)	0	11	100	0.220	0.123	1.78	0.300	0.162	1.85	Reitman 2011[12]
600, q.d.	2.0, p.o. (syr)	168	11	100	0.370	0.383	0.97	0.470	0.403	1.17	Reitman 2011[12]
600, q.d.	2.0, p.o. (syr)	336	11	100	0.910	0.815	1.12	0.940	0.731	1.29	Reitman 2011[12]
600, q.d.	3.0, p.o. (syr)	8	10	50	0.040	0.053	0.76	0.070	0.110	0.64	Kharasch 2004[25]
600, q.d.	4.0 control/6.0 DDI, p.o. (sol)	12	14	100	0.040	0.032	1.25	0.070	0.051	1.37	Gorski 2003[29]
600, q.d.	0.075/kg, p.o. (syr)	22	18	50	0.040	0.124	0.32	0.060	0.170	0.35	Chung 2006[30]
450, q.d.	7.5, p.o. (sol)	17	4	38	0.040	0.052	0.77	0.070	0.112	0.63	Eap 2004[31]
600, q.d.	7.5, p.o. (–)	24	8	100	0.040	0.016	2.57	0.060	0.035	1.72	Link 2008[27]
300, b.i.d.	8.0, p.o. (–)	2?	19	53	0.060	0.057	1.05	0.100	0.121	0.83	Gurley 2006[32]
300, b.i.d.	8.0, p.o. (–)	2	16	50	0.060	0.060	0.99	0.100	0.108	0.93	Gurley 2008a[33]
600, q.d.	15.0, p.o. (tab)	17	10	50	0.050	0.041	1.21	0.050	0.064	0.79	Backman 1996[34]
600, q.d.	15.0, p.o. (tab)	17	9	44	0.100	0.098	1.02	0.130	0.193	0.67	Backman 1998[35]
					GMFE (range)		1.30 (1.00–3.11)			1.48 (1.08–2.83)	
					Pred within twofold		16/18			11/12	
Rifampicin	**Alfentanil**										
5.0, q.d.	0.015/kg, i.v. (–)	10	12	67	0.750	0.791	0.95	–	–	–	Kharasch 2011[36]
10.0, q.d.	0.015/kg, i.v. (–)	10	12	67	0.660	0.712	0.93	–	–	–	Kharasch 2011[36]
25.0, q.d.	0.015/kg, i.v. (–)	10	12	67	0.560	0.564	0.99	–	–	–	Kharasch 2011[36]
75.0, q.d.	0.015/kg, i.v. (–)	10	12	67	0.480	0.474	1.01	–	–	–	Kharasch 2011[36]
600, q.d.	0.015/kg, i.v. (bol)	10	10	50	0.428	0.375	1.14	–	–	–	Kharasch 2004[25]
600, q.d.	0.015/kg, i.v. (bol)	12	6	50	0.426	0.433	0.98	–	–	–	Phimmasone 2001[26]
600, q.d.	0.02/kg, i.v. (bol)	24	9	100	0.425	0.362	1.17	–	–	–	Kharasch 1997[24]
600, q.d.	0.06/kg, p.o. (sol)	10	10	50	0.084	0.046	1.84	0.139	0.111	1.25	Kharasch 2004[25]
5.0, q.d.	0.075/kg, p.o. (sol)	10	12	67	0.519	0.692	0.75	0.606	0.863	0.70	Kharasch 2011[36]
10.0, q.d.	0.075/kg, p.o. (sol)	10	12	67	0.399	0.555	0.72	0.498	0.863	0.58	Kharasch 2011[36]
25.0, q.d.	0.075/kg, p.o. (sol)	10	12	67	0.270	0.295	0.92	0.365	0.490	0.75	Kharasch 2011[36]

(continues)

Table 1 (Continued)

Perpetrator (mg)	Victim (mg)	Dose gap (hours)	*n*	Males (%)	Predicted AUC_{ratio}	Observed AUC_{ratio}	Pred/Obs AUC_{ratio}	Predicted $C_{max\ ratio}$	Observed $C_{max\ ratio}$	Pred/Obs $C_{max\ ratio}$	Reference
75.0, q.d.	0.075/kg, p.o. (sol)	10	12	67	0.170	0.123	1.38	0.246	0.255	0.96	Kharasch 2011[36]
					GMFE (range)		1.19 (1.01–1.84)			1.34 (1.04–1.73)	
					Pred within twofold		12/12			5/5	
Rifampicin	**Itraconazole**										
600, q.d.	200, b.i.d. (cap), fed	12	2[b]	100	0.015	0.018	0.83	–	–	–	Tucker 1992[37]
					GMFE		1.20				
					Pred within twofold		1/1				
Itraconazole	**Midazolam**										
200, q.d. (cap), fast	0.05/kg, i.v. (bol)	2	12	58	2.360	3.220	0.73	–	–	–	Olkkola 1996[38]
50 (sol), fast	2.0, p.o. (sol)	4	6	83	2.780	2.000	1.39	–	–	–	Templeton 2010[39]
200 (sol), fast	2.0, p.o. (sol)	4	6	83	7.390	4.700	1.57	–	–	–	Templeton 2010[39]
400 (sol), fast	2.0, p.o. (sol)	4	6	83	9.700	5.400	1.80	–	–	–	Templeton 2010[39]
100, q.d. (cap), fast	7.5, p.o. (tab)	2	12	33	3.780	5.745	0.66	2.730	2.559	1.07	Ahonen 1995[40]
200 (cap), fast	7.5, p.o. (–)	2	12	58	4.680	3.423	1.37	3.080	1.750	1.76	Olkkola 1996[38]
200, q.d. (cap), fast	7.5, p.o. (tab)	1	9	22	6.220	10.77	0.58	3.480	3.409	1.02	Olkkola 1994[41]
200, q.d. (cap), fast	7.5, p.o. (–)	2	12	58	6.360	6.644	0.96	3.520	2.514	1.40	Olkkola 1996[38]
200, q.d. (cap), fast	15.0, p.o. (tab)	2	9	44	4.730	7.970	0.59	2.650	3.120	0.85	Backman 1998[35]
200, q.d. (cap), fast	15.0, p.o. (tab)	98	9	44	1.120	2.630	0.43	1.080	1.920	0.56	Backman 1998[35]
					GMFE (range)		1.55 (1.04–2.35)			1.33 (1.02–1.78)	
					Pred within twofold		9/10			6/6	
Clarithromycin	**Midazolam**										
500, b.i.d.	0.05/kg, i.v. (0.5 hours)	2	16	50	3.252	2.748	1.18	–	–	–	Gorski 1998[42]
500, b.i.d.	3.0, p.o. (sol)	0.25	11	91	5.064	5.494	0.92	–	–	–	Markert 2013[43]
500, b.i.d.	4.0, p.o. (sol)	2	16	50	8.676	7.000	1.24	3.130	2.765	1.13	Gorski 1998[42]
250, b.i.d.	15.0, p.o. (tab)	1.5	12	33	2.336	3.572	0.65	1.653	2.440	0.68	Yeates 1996[44]
					GMFE (range)		1.25 (1.08–1.53)			1.29 (1.13–1.48)	
					Pred within twofold		4/4			2/2	
Rifampicin	**Digoxin**										
600, q.d.	1.0, i.v. (0.5 hours)	8[c]	8	100	0.780	0.905	0.86	–	–	–	Greiner 1999[45]
300, b.i.d.	0.25, p.o. (–)	12	18	50	0.480	0.696	0.69	0.470	0.615	0.76	Gurley 2008b[46]
600, q.d.	0.5, p.o. (sol)	24[d]	10	50	0.510	0.817	0.62	–	–	–	Larsen 2007[47]
600, q.d.	0.5, p.o. (–)	1	11	100	0.620	1.462	0.42	0.630	1.489	0.42	Reitman 2011[12]
600, q.d.	0.5, p.o. (–)	169	11	100	0.950	0.683	1.39	0.920	0.693	1.33	Reitman 2011[12]
600, q.d.	0.5, p.o. (–)	337	11	100	1.030	0.977	1.05	1.000	0.876	1.14	Reitman 2011[12]
600, q.d.	1.0, p.o. (–)	8[c]	8	100	0.480	0.568	0.84	0.480	0.481	1.00	Greiner 1999[45]
					GMFE (range)		1.41 (1.05–2.36)			1.36 (1.00–2.36)	
					Pred within twofold		6/7			4/5	

(continues)

Table 1 (Continued)

Perpetrator (mg)	Victim (mg)	Dose gap (hours)	*n*	Males (%)	Predicted AUC_{ratio}	Observed AUC_{ratio}	Pred/Obs AUC_{ratio}	Predicted $C_{max\ ratio}$	Observed $C_{max\ ratio}$	Pred/Obs $C_{max\ ratio}$	Reference
Itraconazole	**Digoxin**										
200, q.d. (cap), fast	0.5, p.o. (tab)	1	10	10	1.399	1.610	0.87	1.465	1.340	1.09	Jalava 1997[48]
					GMFE		1.15			1.09	
					Pred within twofold		1/1			1/1	
Clarithromycin	**Digoxin**										
200, b.i.d.	0.5, i.v. (1 hours)	0	9	100	1.020	0.980	1.04	–	–	–	Tsutsumi 2002[49]
250, b.i.d.	0.01/kg, i.v. (bol)	2	3	100	1.060	1.185	0.89	–	–	–	Rengelshausen 2003[50]
500, b.i.d.	0.25, p.o. (–)	0	18	50	1.310	1.466	0.89	1.350	1.750	0.77	Gurley 2008b[46]
250, b.i.d.	0.75, p.o. (tab)	0.5	12	100	1.240	1.643	0.75	1.420	1.833	0.77	Rengelshausen 2003[50]
					GMFE (range)		1.15 (1.04–1.32)			1.29 (1.29–1.30)	
					Pred within twofold		4/4			2/2	

AUC, area under the plasma concentration-time curve; bol, bolus; cap, capsule; C_{max}, peak plasma concentration; DDI, drug-drug interaction; fast, oral administration in fasted conditions; fed, oral administration with a meal; GMFE, geometric mean fold error; obs, observed; pred, predicted; sol, solution; syr, syrup; tab, tablet.
[a]Cerebrotendinous xanthomatosis (CTX) patients,
[b]coccidioidomycosis patients,
[c]see Reitman *et al.*[12],
[d]personal communication, Rifampicin-Midazolam: 0–∞ AUC_{ratios}, Rifampicin-Alfentanil: 0–∞ AUC_{ratios}, Rifampicin-Digoxin: 3 hours AUC_{ratios}, Rifampicin-Itraconazole: 12 hours AUC_{ratio}, Itraconazole-Midazolam: 0–∞ AUC_{ratios}, Itraconazole-Digoxin: 12 hours AUC_{ratio}, Clarithromycin-Midazolam: 0–∞ or 2–4 hours AUC_{ratios}, Clarithromycin-Digoxin: 0–∞ or 24 hours AUC_{ratios}, matching reported observed values, –, not given.

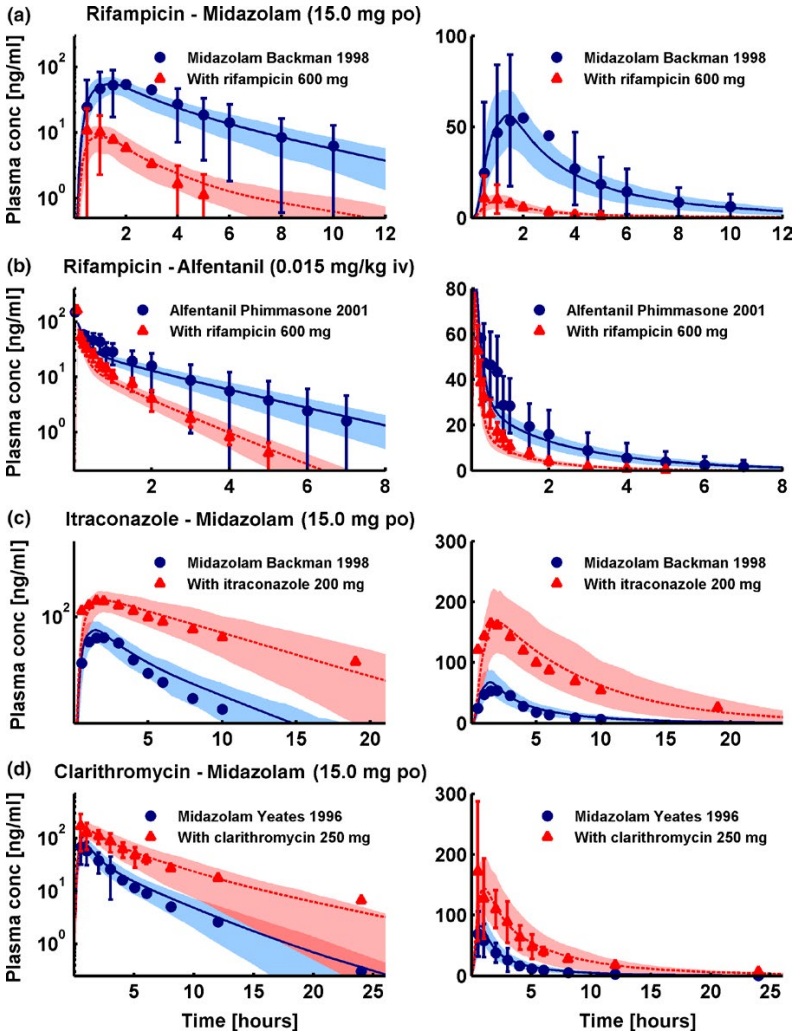

Figure 2 Cytochrome P450 3A4 drug-drug interactions (DDIs). Selection of one study each of the rifampicin-midazolam (**a**), rifampicin-alfentanil (**b**), itraconazole-midazolam (**c**), and clarithromycin-midazolam (**d**) DDIs, presented in semilogarithmic (left panel) and linear plots (right panel). Shown are population predictions compared to observed victim drug concentration-time profiles before and during perpetrator administration. Observed data are shown as blue dots (control) or red triangles (DDI) ± SD. Population simulation arithmetic means are shown as solid blue lines (control) or dashed red lines (DDI); the shaded areas illustrate the respective 68% population prediction intervals. Details on dosing regimens, study populations, predicted and observed DDI area under the plasma concentration-time curve ratios and DDI peak plasma concentration ratios are summarized in **Table 1**.

Section 3 of **Appendix S1** for the results of all 57 DDI studies, shown in **Figures S8a, S9a, S11a, S12a, S13a, S14a, S15a** in **Appendix S1** (semilogarithmic), **Figures S8b, S9b, S11b, S12b, S13b, S14b, S15b** in **Appendix S1** (linear), and **Table S10** in **Appendix S1**, demonstrating the good predictive performance for all modeled DDIs.

Modeled induction and de-induction of CYP3A4 enzyme activity in the liver and duodenum is presented in **Figure 4**. The combination of simulated intracellular rifampicin concentrations and chosen induction parameters (half-maximal effective concentration (EC_{50}) = 0.34 µmol/l, maximum effect (E_{max}) = 9) leads to CYP3A4 activity increases of 7.8-fold in the liver and of 6.7-fold in the duodenum with a 600 mg q.d. rifampicin regimen (**Figure 4a**). De-induction depends on the half-lives of the perpetrator and the induced protein; we implemented CYP3A4 with protein half-lives of 36 and 23 hours in the liver and intestine, respectively[10,11] (see **Table S7** in **Appendix S1**). De-induction kinetics were evaluated by prediction of midazolam PK when administered 1, 2, or 4 weeks after the last dose of rifampicin, as studied by Reitman *et al.*[12] The rifampicin-midazolam model successfully predicts the time course of CYP3A4 activity return to baseline after the last dose of rifampicin, shown by the correct simulation of the midazolam plasma concentration-time profiles of this study (**Figure 4b**).

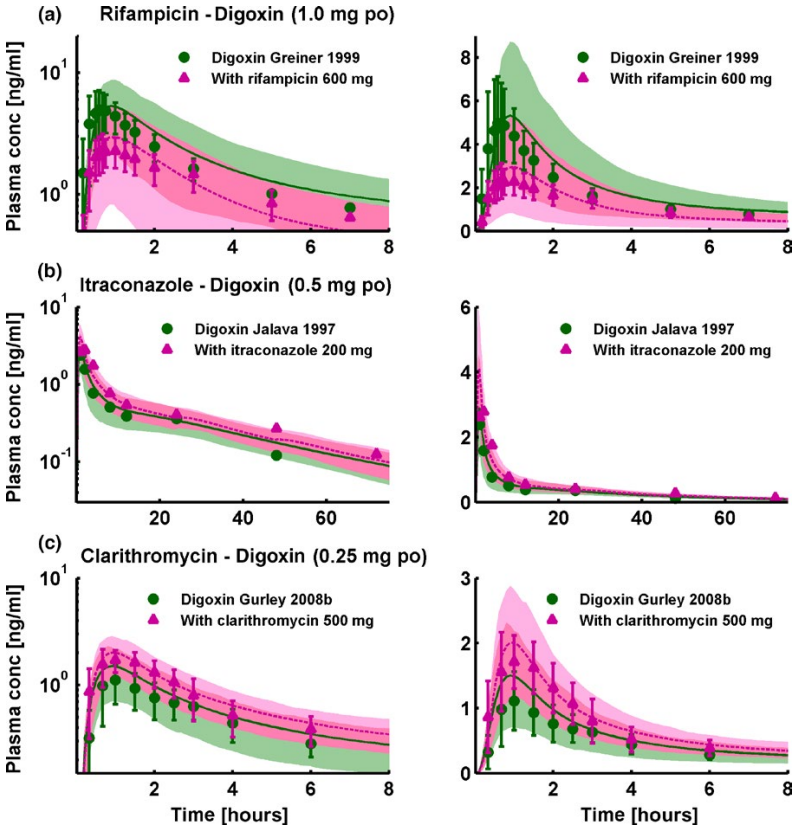

Figure 3 P-glycoprotein drug-drug interactions (DDIs). Selection of one study each of the rifampicin-digoxin (**a**), itraconazole-digoxin (**b**), and clarithromycin-digoxin (**c**) DDIs, presented in semilogarithmic (left panel) and linear plots (right panel). Shown are population predictions compared to observed victim drug concentration-time profiles before and during perpetrator administration. Observed data are shown as green dots (control) or pink triangles (DDI) ± SD. Population simulation arithmetic means are shown as solid green lines (control) or dashed pink lines (DDI); the shaded areas illustrate the respective 68% population prediction intervals. Details on dosing regimens, study populations, predicted and observed DDI area under the plasma concentration-time curve ratios and DDI peak plasma concentration ratios are summarized in **Table 1**.

All victim drug plasma concentration-time profiles before and during co-administration with the different perpetrators are well predicted over the full range of administered doses and administration protocols. Predicted compared with observed DDI AUC ratios and C_{max} ratios with calculated GMFEs for each perpetrator-victim pair are summarized in **Table 1**. Correlation of predicted to observed DDI AUC ratios and C_{max} ratios of all 57 modeled interaction studies, illustrating the performance of the entire DDI network, is presented in **Figure 5**.

DISCUSSION

Comprehensive whole-body PBPK models of rifampicin, itraconazole, clarithromycin, midazolam, alfentanil, and digoxin have been successfully developed, incorporating all current knowledge on the processes controlling the PKs of these drugs. All models were established using a large number of clinical studies and all models show a good performance over the full range of administered doses and administration protocols. Model evaluation comprised comparison of predicted with observed concentration-time profiles, AUC, and C_{max} values, calculation of GMFEs as a measure of descriptive and predictive performance, and application of the independently developed models for DDI prediction.

Sensitivity analyses demonstrate that all models are sensitive to lipophilicity, fraction unbound, and the catalytic rate constants of influential eliminating enzymes or transporters. This result is expected, as the lipophilicity values are used for calculation of membrane permeabilities and partition coefficients, fraction unbound in plasma directly controls the concentration of drug available for passive distribution, transport, and metabolization from the blood, and the catalytic rate constants of the major eliminating enzymes or transporters naturally have a large impact on the predicted clearance and AUC. Experimental values were used for parameterization wherever possible. For example, fraction unbound was fixed to reported experimental values in five of the six models. For itraconazole, the attempts to set fraction

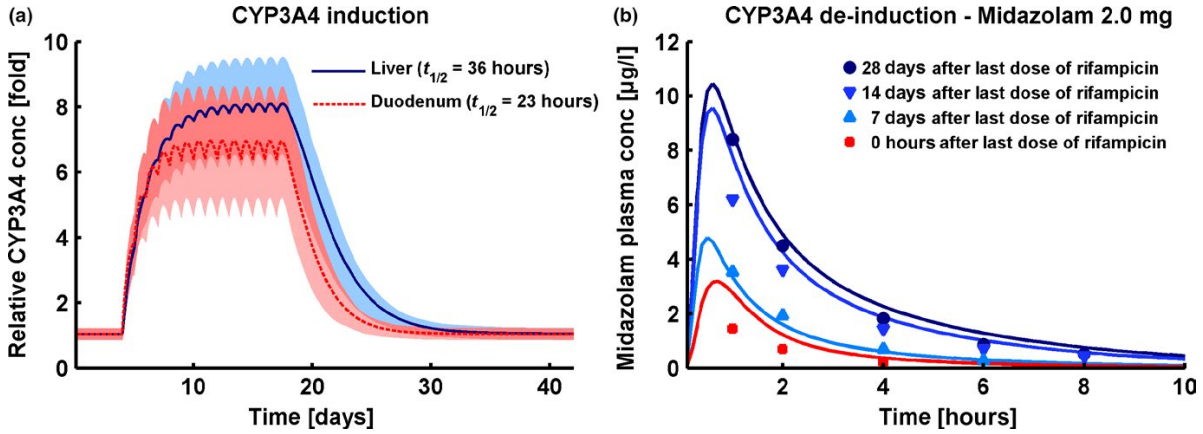

Figure 4 Cytochrome P450 (CYP)3A4 induction and de-induction. (**a**) Fold change of predicted CYP3A4 concentrations in liver (solid blue line) and duodenum (dashed red line) before, during, and after a 600 mg q.d. rifampicin regimen. Shown are population prediction arithmetic means (lines) and 68% population prediction intervals (shaded areas). (**b**) Population simulation arithmetic means (lines) and observed (squares, triangles, and dots) midazolam plasma concentration-time profiles during simultaneous administration of midazolam and rifampicin (red line and squares) or administration of midazolam 7 days (light blue line and triangles), 14 days (blue line and triangles) or 28 days (dark blue line and dots) after the last dose of a 600 mg q.d. rifampicin treatment. Observed data are from Reitman *et al.*[12] Predicted and observed DDI area under the plasma concentration-time curve ratios and DDI peak plasma concentration ratios are given in **Table 1**.

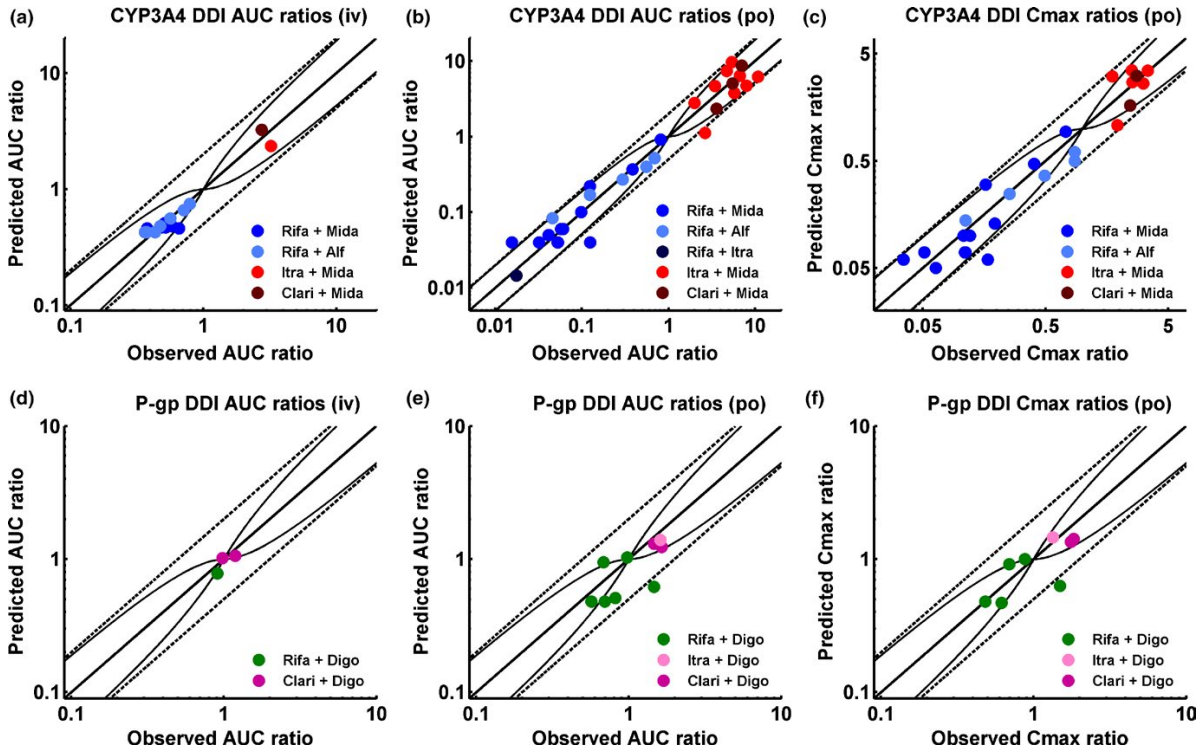

Figure 5 Correlation of predicted to observed DDI area under the plasma concentration-time curve (AUC) ratios and DDI peak plasma concentration (C_{max}) ratios. The upper panel illustrates the cytochrome P450 (CYP)3A4 DDI prediction performance, the lower panel illustrates the P-glycoprotein (P-gp) DDI prediction performance of the network. (**a**, **d**) DDI AUC ratios of intravenously administered victim drugs, (**b**, **e**) DDI AUC ratios of orally administered victim drugs, and (**c**, **f**) DDI C_{max} ratios of orally administered victim drugs. The line of identity and the prediction acceptance limits proposed by Guest *et al.*[23] are shown as solid lines. The 0.5-fold to 2.0-fold acceptance limits are shown as dashed lines. Induction of elimination pathways by rifampicin results in DDI ratios <1, inhibition of elimination pathways by itraconazole or clarithromycin results in DDI ratios >1. Study references and values of predicted and observed DDI AUC ratios and DDI C_{max} ratios are listed in **Table 1**.

unbound in plasma to one of the widely differing literature values (0.2–3.6%) did not result in a satisfactory model and, therefore, fraction unbound was optimized within the literature range (0.6%).

The presented rifampicin model accounts for metabolism by the arylacetamide deacetylase (AADAC), and transport by organic anion-transporting polypeptide (OATP)1B1 and P-gp, as described in the literature. Metabolism by CYP3A4 has not been implemented, as currently there is no conclusive evidence of rifampicin elimination via CYP3A4. Auto-induction of rifampicin clearance was implemented via induction of AADAC, OATP1B1, and P-gp expression. Furthermore, induction of CYP3A4 has been incorporated, without impact on the PK of rifampicin itself. In addition to these induction processes, the DDI application of the presented model is extended to simultaneous dynamic competitive inhibition of CYP3A4 and P-gp. Several minimal or partial PBPK models of rifampicin[13–16] and one full PBPK model[17] have been published to date, but many of them do not account for auto-induction of rifampicin or lack the induction of P-gp. Induction of further CYP isoforms and transporters by rifampicin as well as inhibition of OATP is not yet accounted for, as this requires evaluation of appropriate victim drug models and of the DDI predictions with clinical data, which is beyond the scope of this study. However, the implementation of additional interaction parameters is technically a simple and straight-forward extension of the current model.

The presented itraconazole model accounts for competitive inhibition of CYP3A4 by itraconazole itself and its three sequentially generated main metabolites. Adhering to the reported competitive mechanism of CYP3A4 inhibition by itraconazole and hydroxy-itraconazole,[18] the strong observed nonlinearity and accumulation of itraconazole could not be adequately described using the inhibitory effects of parent drug and first metabolite, only. Therefore, the second and third metabolites were included, resulting in a model that slightly overpredicts the first dose of some studies, but accurately describes the steady-state plasma concentrations of intravenous and oral multiple-dose administration. The CYP3A4 inhibition constants of itraconazole and all three metabolites were fixed to literature values.[18] Furthermore, the model correctly describes the strong food effects for both oral solution and capsule formulation, which is essential for modeling of the reported clinical studies.

The presented clarithromycin model is based on the PBPK model published by Moj *et al.*[19] with small modifications. For DDI prediction, different compounds have to be coupled in one and the same individual with a specified expression of enzymes and transporters. Therefore, the clarithromycin model was adapted to the CYP3A4 expression profile reported by Nishimura *et al.*[20] used in the other models (see **Table S7** in **Appendix S1**). Furthermore, transport by OATP1B3 was removed, according to literature,[21] and the values for pKa, lipophilicity, fraction unbound, and CYP3A4 K_M were fixed to literature values. The adapted model precisely captures the plasma concentration-time profiles of all investigated studies with very low GMFEs (1.16 for AUC values and 1.11 for C_{max} values; $n = 15$).

The presented midazolam model is a simple, very robust, and reliable model that has been successfully applied for DDI simulations with many different perpetrator models, as demonstrated in detail in Section 3 of **Appendix S1**.

The presented alfentanil model has been established as a second CYP3A4 victim drug, to further evaluate the performance of the rifampicin model. It shows an accurate and precise performance in single compound simulations as well as in DDI predictions. Due to the lack of clinical studies with other perpetrator drugs it has only been coupled to the rifampicin model so far.

For the development of the presented digoxin model, a multitude of clinical studies ($n = 38$) was available in the literature, demonstrating the high interindividual variability in the PK of digoxin. A study measuring the P-gp protein abundance in human duodenal biopsies found considerable variation of more than eightfold in a group of 25 patients.[22] Considering the large interindividual differences in the observed digoxin PK, the presented digoxin model shows a good descriptive and predictive performance. This was accomplished by incorporation of the drug target Na^+/K^+-ATPase as binding partner, and by increasing the relative P-gp expression in the intestinal mucosa, to accurately describe the plasma concentrations following intravenous as well as oral administration. This altered expression profile has been evaluated by prediction of the digoxin DDIs with rifampicin, itraconazole, and clarithromycin. Especially the prediction of the rifampicin-digoxin interaction was significantly improved applying the higher intestinal expression of P-gp.

PBPK modeling is a rapidly evolving field, including continuously improved software capabilities and steadily increasing knowledge in systems pharmacology. There are many different models for the drugs investigated in this study, built with many different software platforms, and comparing their features and performance would take a study of its own.

The presented DDI modeling network demonstrates a very good performance of the models for DDI prediction over the full range of reported DDI administration protocols. This is illustrated by concentration-time profiles, DDI AUC ratios, DDI C_{max} ratios, and corresponding GMFEs. In addition, some of the presented models have been applied for DDI prediction with currently unpublished models, which are either confidential or pending publication, also yielding good results and further increasing the confidence in their predictive capacity. Now that a core of mutually evaluated models has been established, further models can be added to this DDI network and evaluated via simulation of published clinical DDI studies utilizing the models provided in this study.

In summary, whole-body PBPK models of rifampicin, itraconazole, clarithromycin, midazolam, alfentanil, and digoxin have been thoroughly built, and tested by DDI prediction within the presented network using different kinds of perpetrator (induction, competitive inhibition, and mechanism-based inactivation) and victim drugs (CYP3A4, P-gp), demonstrating that they reliably predict the observed data of all clinical DDI studies that have been reported for combinations of these drugs. The presented models are transparently documented and provided open-source as

supplementary material to this paper **(Data S1-S6)** and in the OSP repository (www.open-systems-pharmacology.org) for the drug development community to help understand and characterize the DDI potential of investigational drugs and to inform the design of clinical trials. This study lays a cornerstone for the qualification of the OSP platform with regard to reliable PBPK predictions of enzyme-mediated and transporter-mediated DDIs during model-informed drug development.

Supporting Information

Supplementary information accompanies this paper on the *CPT: Pharmacometrics & Systems Pharmacology* website. (www.psp-journal.com)

Appendix S1. Model information and evaluation.
Data S1. Rifampicin model file.
Data S2. Itraconazole model file.
Data S3. Clarithromycin model file.
Data S4. Midazolam model file.
Data S5. Alfentanil model file.
Data S6. Digoxin model file.

Funding. This study was sponsored by Bayer AG.

Conflict of Interest. S.F., T.E., and T.W. are employees of Bayer AG. T.L. has received research funding from Bayer AG. No potential conflicts of interest were disclosed by the other authors.

Author Contributions. N.H., S.F., T.E., T.W., and T.L. wrote the manuscript. N.H., S.F., T.E., T.W., and T.L. designed the research. N.H., S.F., D.M., H.B., T.W., and T.L. performed the research.

1. U.S. Food and Drug Administration. Clinical Drug Interaction Studies – Study Design, Data Analysis, and Clinical Implications. Draft Guidance for Industry. <https://www.fda.gov/downloads/drugs/guidances/ucm292362.pdf>, (October 2017).
2. European Medicines Agency. Guideline on the Investigation of Drug Interactions. CPMP/EWP/560/95/Rev. 1 Corr. 2** <http://www.ema.europa.eu/docs/en_GB/document_library/Scientific_guideline/2012/07/WC500129606.pdf>, (21 June 2012).
3. Guengerich, F.P. Cytochrome P-450 3A4: regulation and role in drug metabolism. *Annu. Rev. Pharmacol. Toxicol.* **39**, 1–17 (1999).
4. Fenner, K.S. *et al.* Drug-drug interactions mediated through P-glycoprotein: clinical relevance and *in vitro-in vivo* correlation using digoxin as a probe drug. *Clin. Pharmacol. Ther.* **85**, 173–181 (2009).
5. U.S. Food and Drug Administration. Drug development and drug interactions: table of substrates, inhibitors and inducers. <https://www.fda.gov/Drugs/DevelopmentApprovalProcess/DevelopmentResources/DrugInteractionsLabeling/ucm093664.htm>.
6. Kuepfer, L. *et al.* Applied concepts in PBPK modeling: how to build a PBPK/PD model. *CPT Pharmacometrics Syst. Pharmacol.* **5**, 516–531 (2016).
7. Valentin, J. Basic anatomical and physiological data for use in radiological protection: reference values. A report of age- and gender-related differences in the anatomical and physiological characteristics of reference individuals. ICRP Publication 89. *Ann. ICRP* **32**, 5–265 (2002).
8. Meyer, M., Schneckener, S., Ludewig, B., Kuepfer, L. & Lippert, J. Using expression data for quantification of active processes in physiologically based pharmacokinetic modeling. *Drug Metab. Dispos.* **40**, 892–901 (2012).
9. Willmann, S. *et al.* Development of a physiology-based whole-body population model for assessing the influence of individual variability on the pharmacokinetics of drugs. *J. Pharmacokinet. Pharmacodyn.* **34**, 401–431 (2007).
10. Rowland Yeo, K., Walsky, R.L., Jamei, M., Rostami-Hodjegan, A. & Tucker, G.T. Prediction of time-dependent CYP3A4 drug-drug interactions by physiologically based pharmacokinetic modelling: impact of inactivation parameters and enzyme turnover. *Eur. J. Pharm. Sci.* **43**, 160–73 (2011).
11. Greenblatt, D.J. *et al.* Time course of recovery of cytochrome p450 3A function after single doses of grapefruit juice. *Clin. Pharmacol. Ther.* **74**, 121–129 (2003).
12. Reitman, M.L. *et al.* Rifampin's acute inhibitory and chronic inductive drug interactions: experimental and model-based approaches to drug-drug interaction trial design. *Clin. Pharmacol. Ther.* **89**, 234–242 (2011).
13. Neuhoff, S. *et al.* Application of permeability-limited physiologically-based pharmacokinetic models: part II – prediction of P-glycoprotein mediated drug-drug interactions with digoxin. *J. Pharm. Sci.* **102**, 3161–3173 (2013).
14. Almond, L.M. *et al.* Prediction of drug-drug interactions arising from CYP3A induction using a physiologically based dynamic model. *Drug Metab. Dispos.* **44**, 821–832 (2016).
15. Guo, H. *et al.* A mechanistic physiologically based pharmacokinetic-enzyme turnover model involving both intestine and liver to predict CYP3A induction-mediated drug-drug interactions. *J. Pharm. Sci.* **102**, 2819–2836 (2013).
16. Asaumi, R. *et al.* Comprehensive PBPK model of rifampicin for quantitative prediction of complex drug-drug interactions: CYP3A/2C9 induction and OATP inhibition effects. *CPT Pharmacometrics Syst. Pharmacol.* **7**, 186–196 (2018).
17. Baneyx, G., Parrott, N., Meille, C., Iliadis, A. & Lavé, T. Physiologically based pharmacokinetic modeling of CYP3A4 induction by rifampicin in human: influence of time between substrate and inducer administration. *Eur. J. Pharm. Sci.* **56**, 1–15 (2014).
18. Isoherranen, N., Kunze, K.L., Allen, K.E., Nelson, W.L. & Thummel, K.E. Role of itraconazole metabolites in CYP3A4 inhibition. *Drug Metab. Dispos.* **32**, 1121–1131 (2004).
19. Moj, D. *et al.* Clarithromycin, midazolam, and digoxin: application of PBPK modeling to gain new insights into drug-drug interactions and co-medication regimens. *AAPS J.* **19**, 298–312 (2017).
20. Nishimura, M., Yaguti, H., Yoshitsugu, H., Naito, S. & Satoh, T. Tissue distribution of mRNA expression of human cytochrome P450 isoforms assessed by high-sensitivity real-time reverse transcription PCR. *J. Pharm. Soc. Japan* **123**, 369–375 (2003).
21. Higgins, J.W., Ke, A.B. & Zamek-Gliszczynski, M.J. Clinical CYP3A inhibitor alternatives to ketoconazole, clarithromycin and itraconazole, are not transported into the liver by hepatic organic anion transporting polypeptides and organic cation transporter 1. *Drug Metab. Dispos.* **42**, 1780–1784 (2014).
22. Lown, K.S. *et al.* Role of intestinal P-glycoprotein (mdr1) in interpatient variation in the oral bioavailability of cyclosporine. *Clin. Pharmacol. Ther.* **62**, 248–260 (1997).
23. Guest, E.J., Aarons, L., Houston, J.B., Rostami-Hodjegan, A. & Galetin, A. Critique of the two-fold measure of prediction success for ratios: application for the assessment of drug-drug interactions. *Drug Metab. Dispos.* **39**, 170–173 (2011).
24. Kharasch, E.D. *et al.* The role of cytochrome P450 3A4 in alfentanil clearance. Implications for interindividual variability in disposition and perioperative drug interactions. *Anesthesiology* **87**, 36–50 (1997).
25. Kharasch, E.D., Walker, A., Hoffer, C. & Sheffels, P. Intravenous and oral alfentanil as in vivo probes for hepatic and first-pass cytochrome P450 3A activity: noninvasive assessment by use of pupillary miosis. *Clin. Pharmacol. Ther.* **76**, 452–466 (2004).
26. Phimmasone, S. & Kharasch, E.D. A pilot evaluation of alfentanil-induced miosis as a noninvasive probe for hepatic cytochrome P450 3A4 (CYP3A4) activity in humans. *Clin. Pharmacol. Ther.* **70**, 505–517 (2001).
27. Link, B. *et al.* Pharmacokinetics of intravenous and oral midazolam in plasma and saliva in humans: usefulness of saliva as matrix for CYP3A phenotyping. *Br. J. Clin. Pharmacol.* **66**, 473–484 (2008).
28. Szalat, A. *et al.* Rifampicin-induced CYP3A4 activation in CTX patients cannot replace chenodeoxycholic acid treatment. *Biochim. Biophys. Acta* **1771**, 839–844 (2007).
29. Gorski, J.C. *et al.* The effect of age, sex, and rifampin administration on intestinal and hepatic cytochrome P450 3A activity. *Clin. Pharmacol. Ther.* **74**, 275–287 (2003).
30. Chung, E., Nafziger, A.N., Kazierad, D.J. & Bertino, J.S. Comparison of midazolam and simvastatin as cytochrome P450 3A probes. *Clin. Pharmacol. Ther.* **79**, 350–361 (2006).
31. Eap, C.B. *et al.* Oral administration of a low dose of midazolam (75 microg) as an in vivo probe for CYP3A activity. *Eur. J. Clin. Pharmacol.* **60**, 237–246 (2004).
32. Gurley, B. *et al.* Assessing the clinical significance of botanical supplementation on human cytochrome P450 3A activity: comparison of a milk thistle and black cohosh product to rifampin and clarithromycin. *J. Clin. Pharmacol.* **46**, 201–213 (2006).
33. Gurley, B.J. *et al.* Supplementation with goldenseal (Hydrastis canadensis), but not kava kava (Piper methysticum), inhibits human CYP3A activity in vivo. *Clin. Pharmacol. Ther.* **83**, 61–69 (2008).
34. Backman, J.T., Olkkola, K.T. & Neuvonen, P.J. Rifampin drastically reduces plasma concentrations and effects of oral midazolam. *Clin. Pharmacol. Ther.* **59**, 7–13 (1996).
35. Backman, J.T., Kivistö, K.T., Olkkola, K.T. & Neuvonen, P.J. The area under the plasma concentration-time curve for oral midazolam is 400-fold larger during

treatment with itraconazole than with rifampicin. *Eur. J. Clin. Pharmacol.* **54**, 53–58 (1998).
36. Kharasch, E.D. *et al.* Sensitivity of intravenous and oral alfentanil and pupillary miosis as minimal and noninvasive probes for hepatic and first-pass CYP3A induction. *Clin. Pharmacol. Ther.* **90**, 100–108 (2011).
37. Tucker, R.M. *et al.* Interaction of azoles with rifampin, phenytoin, and carbamazepine: *in vitro* and clinical observations. *Clin. Infect. Dis.* **14**, 165–174 (1992).
38. Olkkola, K.T., Ahonen, J. & Neuvonen, P.J. The effects of the systemic antimycotics, itraconazole and fluconazole, on the pharmacokinetics and pharmacodynamics of intravenous and oral midazolam. *Anesth. Analg.* **82**, 511–516 (1996).
39. Templeton, I. *et al.* Accurate prediction of dose-dependent CYP3A4 inhibition by itraconazole and its metabolites from in vitro inhibition data. *Clin. Pharmacol. Ther.* **88**, 499–505 (2010).
40. Ahonen, J., Olkkola, K.T. & Neuvonen, P.J. Effect of itraconazole and terbinafine on the pharmacokinetics and pharmacodynamics of midazolam in healthy volunteers. *Br. J. Clin. Pharmacol.* **40**, 270–272 (1995).
41. Olkkola, K.T., Backman, J.T. & Neuvonen, P.J. Midazolam should be avoided in patients receiving the systemic antimycotics ketoconazole or itraconazole. *Clin. Pharmacol. Ther.* **55**, 481–485 (1994).
42. Gorski, J.C. *et al.* The contribution of intestinal and hepatic CYP3A to the interaction between midazolam and clarithromycin. *Clin. Pharmacol. Ther.* **64**, 133–143 (1998).
43. Markert, C. *et al.* Interaction of ambrisentan with clarithromycin and its modulation by polymorphic SLCO1B1. *Eur. J. Clin. Pharmacol.* **69**, 1785–1793 (2013).
44. Yeates, R.A., Laufen, H. & Zimmermann, T. Interaction between midazolam and clarithromycin: comparison with azithromycin. *Int. J. Clin. Pharmacol. Ther.* **34**, 400–405 (1996).
45. Greiner, B. *et al.* The role of intestinal P-glycoprotein in the interaction of digoxin and rifampin. *J. Clin. Invest.* **104**, 147–153 (1999).
46. Gurley, B.J., Swain, A., Williams, D.K., Barone, G. & Battu, S.K. Gauging the clinical significance of P-glycoprotein-mediated herb-drug interactions: comparative effects of St. John's wort, Echinacea, clarithromycin, and rifampin on digoxin pharmacokinetics. *Mol. Nutr. Food Res.* **52**, 772–779 (2008).
47. Larsen, U.L. *et al.* Human intestinal P-glycoprotein activity estimated by the model substrate digoxin. *Scand. J. Clin. Lab. Invest.* **67**, 123–134 (2007).
48. Jalava, K.M., Partanen, J. & Neuvonen, P.J. Itraconazole decreases renal clearance of digoxin. *Ther. Drug Monit.* **19**, 609–613 (1997).
49. Tsutsumi, K. *et al.* The effect of erythromycin and clarithromycin on the pharmacokinetics of intravenous digoxin in healthy volunteers. *J. Clin. Pharmacol.* **42**, 1159–1164 (2002).
50. Rengelshausen, J. *et al.* Contribution of increased oral bioavailability and reduced nonglomerular renal clearance of digoxin to the digoxin-clarithromycin interaction. *Br. J. Clin. Pharmacol.* **56**, 32–38 (2003).

4.2 PROJECT II: PHYSIOLOGICALLY-BASED PHARMACOKINETIC MODELS FOR CYP1A2 DRUG-DRUG INTERACTION PREDICTION: A MODELING NETWORK OF FLUVOXAMINE, THEOPHYLLINE, CAFFEINE, RIFAMPICIN, AND MIDAZOLAM

4.2.1 *Reference*

Hannah Britz, Nina Hanke, Anke-Katrin Volz, Olav Spigset, Matthias Schwab, Thomas Eissing, Thomas Wendl, Sebastian Frechen, Thorsten Lehr. Physiologically-based pharmacokinetic models for CYP1A2 drug-drug interaction prediction: A modeling network of fluvoxamine, theophylline, caffeine, rifampicin, and midazolam. CPT Pharmacometrics Syst Pharmacol. 2019;8(5):296-307. doi: 10.1002/-psp4.12397

4.2.2 *Supplementary material*

Supplementary material can be found on the accompanying storage medium. It is also available online at: supplementary material of publication II.

4.2.3 *Copyright*

4.2.4 *Author contributions*

Declaration of author contributions to the publication related to project II included in this thesis according to the CRediT [1].

Hannah Britz	Conceptualization, Data Curation, Investigation, Visualization, Writing - Original Draft, Writing - Review & Editing
Nina Hanke	Conceptualization, Investigation, Writing - Original Draft, Writing - Review & Editing
Anke-Katrin Volz	Investigation, Visualization, Writing - Original Draft, Writing - Review & Editing
Olav Spigset	Resources, Investigation, Writing - Review & Editing
Matthias Schwab	Conceptualization, Writing - Review & Editing
Thomas Eissing	Conceptualization, Writing - Review & Editing
Thomas Wendl	Conceptualization, Writing - Review & Editing

Sebastian Frechen	Conceptualization, Investigation, Writing - Review & Editing
Thorsten Lehr	Conceptualization, Investigation, Visualization, Writing - Original Draft, Writing - Review & Editing

Citation: CPT Pharmacometrics Syst. Pharmacol. (2019) 8, 296–307; doi:10.1002/psp4.

ARTICLE

Physiologically-Based Pharmacokinetic Models for CYP1A2 Drug–Drug Interaction Prediction: A Modeling Network of Fluvoxamine, Theophylline, Caffeine, Rifampicin, and Midazolam

Hannah Britz[1], Nina Hanke[1], Anke-Katrin Volz[1], Olav Spigset[2,3], Matthias Schwab[4,5,6], Thomas Eissing[7], Thomas Wendl[7], Sebastian Frechen[7] and Thorsten Lehr[1,*]

This study provides whole-body physiologically-based pharmacokinetic models of the strong index cytochrome P450 (CYP)1A2 inhibitor and moderate CYP3A4 inhibitor fluvoxamine and of the sensitive CYP1A2 substrate theophylline. Both models were built and thoroughly evaluated for their application in drug–drug interaction (DDI) prediction in a network of perpetrator and victim drugs, combining them with previously developed models of caffeine (sensitive index CYP1A2 substrate), rifampicin (moderate CYP1A2 inducer), and midazolam (sensitive index CYP3A4 substrate). Simulation of all reported clinical DDI studies for combinations of these five drugs shows that the presented models reliably predict the observed drug concentrations, resulting in seven of eight of the predicted DDI area under the plasma curve (AUC) ratios (AUC during DDI/AUC control) and seven of seven of the predicted DDI peak plasma concentration (C_{max}) ratios (C_{max} during DDI/C_{max} control) within twofold of the observed values. Therefore, the models are considered qualified for DDI prediction. All models are comprehensively documented and publicly available, as tools to support the drug development and clinical research community.

Study Highlights

WHAT IS THE CURRENT KNOWLEDGE ON THE TOPIC?
☑ Physiologically-based pharmacokinetic (PBPK) models are a valuable tool to investigate and predict the drug–drug interaction (DDI) potential of investigational drugs. A publicly available library of thoroughly and transparently evaluated models of relevant perpetrator and victim drugs used in clinical studies is needed to accelerate the drug development process.

WHAT QUESTION DID THIS STUDY ADDRESS?
☑ The aim of this study was to provide whole-body PBPK models of the most important cytochrome (CYP)1A2 perpetrator and victim drugs and to evaluate them for their application in PBPK DDI modeling.

WHAT DOES THIS STUDY ADD TO OUR KNOWLEDGE?
☑ This study provides publicly available and transparently built and evaluated PBPK models of fluvoxamine and theophylline. Both models integrate the current knowledge on relevant pharmacokinetic (PK) mechanisms, including the impact of different genotypes and smoking on the PK of fluvoxamine.

HOW MIGHT THIS CHANGE DRUG DISCOVERY, DEVELOPMENT, AND/OR THERAPEUTICS?
☑ The developed PBPK models are ready to use for their application in DDI modeling and might help to support the drug development process.

Cytochrome P450 (CYP)1A2 is an important enzyme for the metabolism of several endogenous substances (e.g., melatonin), and it is involved in the elimination of 15% of all therapeutic drugs.[1] CYP1A2 is exclusively expressed in the liver, where it accounts for about 13% of total CYP content in liver microsomes.[2] The expression of CYP1A2 can be markedly induced by smoking, whereas rifampicin, a strong CYP3A4 inducer, shows only a moderate potential to induce CYP1A2.[1,3] Well-known substrates of CYP1A2 include caffeine and theophylline, which are mainly metabolized via CYP1A2 (fractions metabolized of 0.95[4] and 0.7,[5,6] respectively) and can, therefore, be used as sensitive CYP1A2 substrates to evaluate the activity of CYP1A2 *in vivo*.[7] The most important inhibitor of CYP1A2 is fluvoxamine.

[1]Clinical Pharmacy, Saarland University, Saarbrücken, Germany; [2]Department of Clinical and Molecular Medicine, Norwegian University of Science and Technology, Trondheim, Norway; [3]Department of Clinical Pharmacology, St. Olav University Hospital, Trondheim, Norway; [4]Dr. Margarete Fischer-Bosch-Institute of Clinical Pharmacology, Stuttgart, Germany; [5]Department of Clinical Pharmacology, University Hospital Tübingen, Tübingen, Germany; [6]Department of Pharmacy and Biochemistry, University Tübingen, Tübingen, Germany; [7]Clinical Pharmacometrics, Bayer AG, Leverkusen, Germany. *Correspondence: Thorsten Lehr (thorsten.lehr@mx.uni-saarland.de)
Received: November 8, 2018; accepted: January 30, 2019. doi:10.1002/psp4.12397

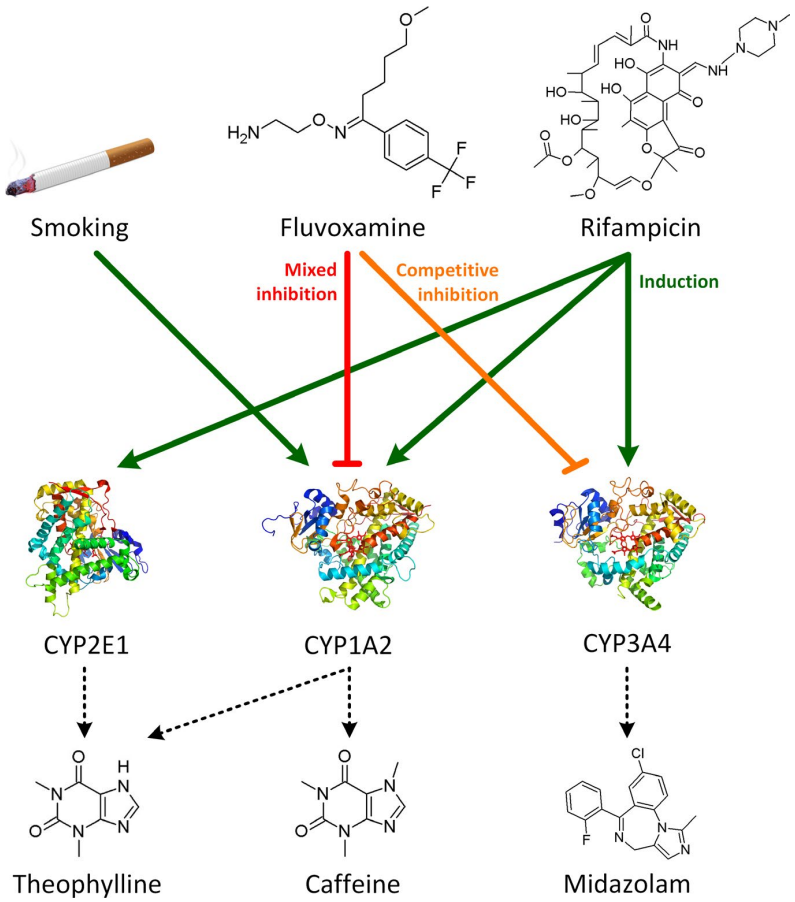

Figure 1 Cytochrome P450 (CYP) 1A2 drug–drug interaction (DDI) network. Schematic illustration of the developed CYP1A2 DDI network with fluvoxamine and rifampicin as CYP1A2 perpetrator drugs and theophylline and caffeine as CYP1A2 victim drugs. Midazolam was used as CYP3A4 victim drug for fluvoxamine. Dark green lines indicate induction by rifampicin or smoking, and the red and orange lines indicate inhibition by fluvoxamine.

The US Food and Drug Administration (FDA) specifies caffeine as a sensitive clinical index substrate and fluvoxamine as a strong clinical index inhibitor for CYP1A2. Furthermore, they recommend considering a clinical study in smokers for investigational drugs that are CYP1A2 substrates.[8] Theophylline is classified as a sensitive clinical substrate and rifampicin as moderate clinical inducer of CYP1A2.[9]

Physiologically-based pharmacokinetic (PBPK) modeling is a valuable method, recognized by the FDA and the European Medicines Agency, to explore and quantitatively predict the pharmacokinetics (PK) of drugs, to evaluate drug–drug interactions (DDIs), and to support clinical study design, dose selection, and labeling.[8,10–12] The FDA furthermore supports the prediction of DDI studies with weak and moderate index inhibitors and inducers as an alternative to prospective clinical studies, if the sponsors can demonstrate adequate model performance using clinical data from DDI studies with strong index perpetrators.[8]

The aim of this study was to develop a PBPK DDI network for CYP1A2 and thereby to extend the library of publicly available PBPK models for DDI prediction.[13,14] For this purpose, whole-body PBPK models of fluvoxamine and theophylline have been developed and existing models of

Figure 2 Fluvoxamine plasma concentrations. (**a**) Population predictions of selected fluvoxamine plasma concentration-time profiles compared with observed data in linear (left panel) and semilogarithmic plots (right panel). The upper panel shows i.v. application, the lower panel p.o. administration of fluvoxamine. Observed data are shown as dots ± SD.[34,35] Population simulation arithmetic means are shown as lines; the shaded areas illustrate the 68% population prediction intervals. (**b**) Predicted compared with observed fluvoxamine plasma concentration values of all clinical studies. Line of identity and 0.5-fold to 2.0-fold acceptance limits are shown as black lines. The 0.8-fold to 1.25-fold limits are shown as grey lines. Details on dosing regimens and study populations are listed in **Table S1a of Supplement S1**. Predicted and observed pharmacokinetic parameters are summarized in **Table S1d of Supplement S1**.

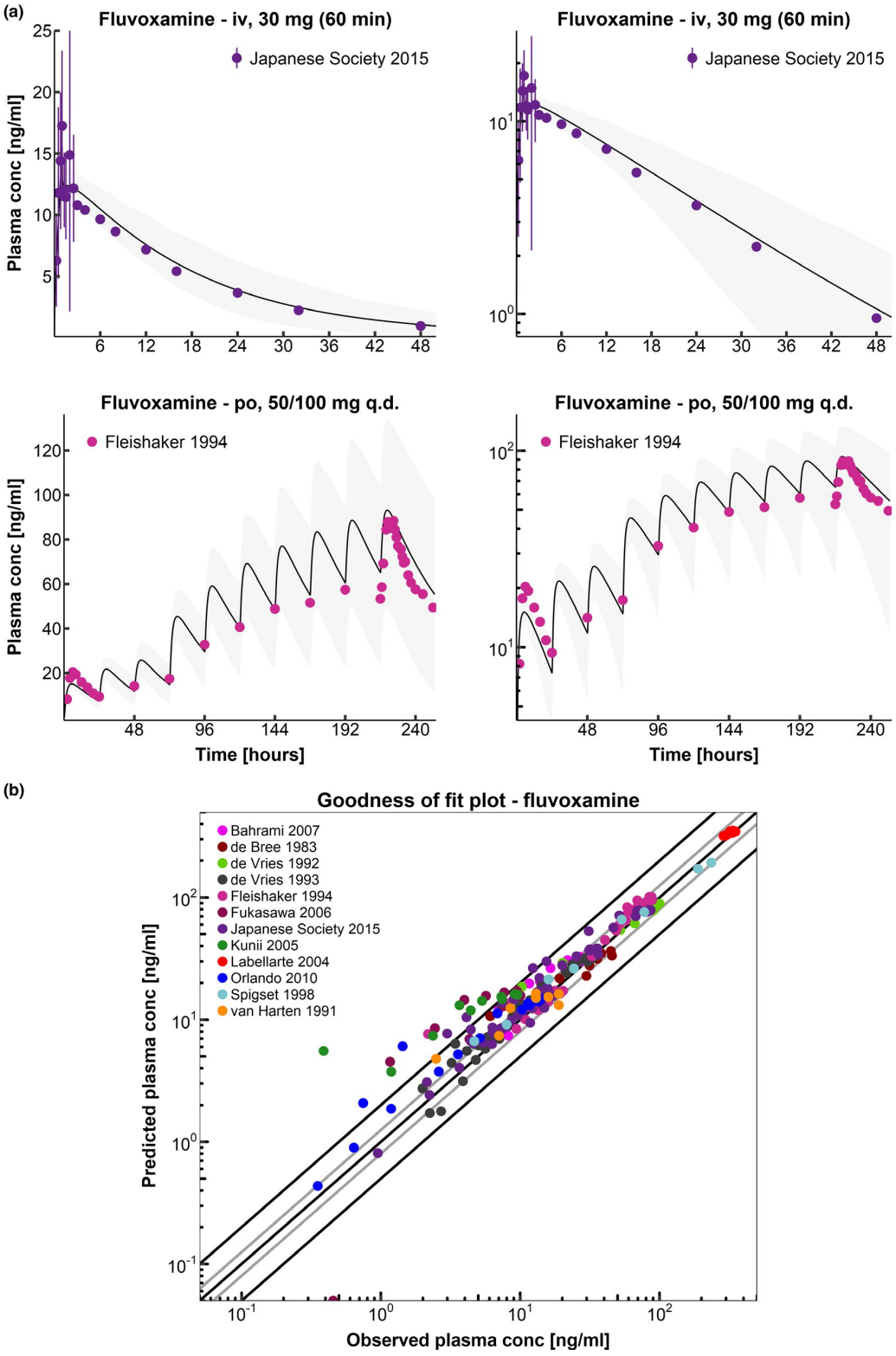
(a)
Fluvoxamine - iv, 30 mg (60 min)
Japanese Society 2015
Plasma conc [ng/ml]
Fluvoxamine - po, 50/100 mg q.d.
Fleishaker 1994
Time [hours]
(b)
Goodness of fit plot - fluvoxamine
Bahrami 2007
de Bree 1983
de Vries 1992
de Vries 1993
Fleishaker 1994
Fukasawa 2006
Japanese Society 2015
Kunii 2005
Labellarte 2004
Orlando 2010
Spigset 1998
van Harten 1991
Predicted plasma conc [ng/ml]
Observed plasma conc [ng/ml]

caffeine,[15] rifampicin,[13] and midazolam[13] have been expanded and coupled for mutual validation of the DDI performance of these five models. The evaluation of the single models and of the network was accomplished by prediction of multiple clinical DDI studies, demonstrating their performance with different victim or perpetrator drugs. **Figure 1** shows the successfully developed CYP1A2 PBPK DDI network, with caffeine and theophylline as sensitive substrates, fluvoxamine as a strong inhibitor, and rifampicin and smoking as moderate inducers (owing to the lack of strong CYP1A2 inducers). The evaluation of the final fluvoxamine PBPK model, including the fluvoxamine fraction metabolized via CYP2D6, was supported by a *post hoc* population pharmacokinetic (PopPK) analysis to confirm the PBPK results concerning the impact of CYP2D6 poor metabolism and smoking on the metabolism of fluvoxamine. The supplementary document (**Supplement S1**) to this paper was devised as comprehensive documentation and reference guide and provides detailed information on the single models and modeled DDI studies, including all model parameters, plots, and quantitative assessments of model performance.

METHODS

Software

PBPK modeling was performed with PK-Sim and MoBi modeling software version 7.3.0 (part of the Open Systems Pharmacology Suite,[16] www.open-systems-pharmacology.org). Parameter optimization was accomplished using the Monte Carlo algorithm implemented in PK-Sim. Sensitivity analysis was performed within PK-Sim. PopPK analysis was performed with NONMEM version 7.3 (ICON Development Solutions, Ellicott City, MD). Digitization of published plasma concentration-time profiles was accomplished using GetData Graph Digitizer version 2.26.0.20 (S. Fedorov). PK parameter analysis was performed with MATLAB version R2013b (The MathWorks, Natick, MA). Graphics were compiled with R version 3.5.1 (The R Foundation for Statistical Computing, Vienna, Austria) and RStudio version 1.1.453 (RStudio, Boston, MA). SAS version 9.4 (SAS Institute, Cary, NC) was used for statistical analysis and graphics of the PopPK analysis.

PBPK model building

Fluvoxamine and theophylline PBPK model building was started with an extensive literature search to collect physicochemical parameters, information on absorption, distribution, metabolism, and excretion processes and clinical studies of i.v. and p.o. administration of fluvoxamine and theophylline in single-dose and multiple-dose regimens.

The PBPK models were built based on healthy individuals, using the reported mean values for age, weight, height, and genetic background for each study protocol. If no information on these parameters could be found, a healthy male European individual, 30 years of age, with a body weight of 73 kg and a height of 176 cm was used.

To model the specific metabolic clearance, relevant CYP enzymes were implemented in accordance with literature, using the PK-Sim expression database reverse transcription-polymerase chain reaction profiles[17] to define their relative expression in the different organs of the body. For more details see **Table S6 in Supplement S1**. Glomerular filtration and enterohepatic cycling were enabled, as they are active under physiological conditions.

To build the data sets for PBPK modeling, the reported observed plasma concentration-time profiles were digitized and divided into "training data set" and "test data set." Model parameters that could not be informed from experimental reports were optimized by simultaneously fitting the model to all measured plasma concentration-time profiles assigned to the training data set. To limit the parameters to be optimized during model building, the minimal number of processes necessary was implemented into the model. Model evaluation was carried out based on the clinical data of the test data set. Descriptive (training data set) and predictive (test data set) performance of the model for all published clinical studies is transparently presented in **Supplement S1**.

PBPK model evaluation

Model performance was evaluated with different methods. The predicted population plasma concentration-time profiles were compared with the plasma concentration-time profiles observed in the clinical studies. Furthermore, predicted plasma concentration values of all studies were compared with the observed plasma concentrations in goodness-of-fit plots. In addition, the performance was evaluated by comparison of predicted to observed area under the plasma curve (AUC) and peak plasma concentration (C_{max}) values. As quantitative measures of the descriptive and predictive performance of the models, the mean relative deviation (MRD) according to Edginton *et al.*[18] and the geometric mean fold error (GMFE) were calculated. MRD was calculated for all observed plasma concentrations according to Eq. 1.

$$\mathrm{MRD} = 10^{x}; x = \sqrt{\frac{\sum_{i=1}^{N} (\log_{10} c_{\mathrm{obs}} - \log_{10} c_{\mathrm{pred}})^2}{N}} \qquad (1)$$

with $\log_{10} c_{obs}$ = logarithm of the observed plasma concentration, $\log_{10} c_{pred}$ = logarithm of the predicted plasma concentration, and N = number of observed values. An MRD value ≤ 2 characterizes an adequate prediction.

Figure 3 Theophylline plasma concentrations. (**a**) Population predictions of selected theophylline plasma concentration-time profiles compared with observed data in linear (left panel) and semilogarithmic plots (right panel). The upper panel shows i.v. application, the lower panel p.o. administration of theophylline. Observed data are shown as dots ± SD.[36,37] Population simulation arithmetic means are shown as lines, and the shaded areas illustrate the 68% population prediction intervals. (**b**) Predicted compared with observed theophylline plasma concentration values of all clinical studies. Line of identity and 0.5-fold to 2.0-fold acceptance limits are shown as black lines. The 0.8-fold to 1.25-fold limits are shown as grey lines. Details on dosing regimens and study populations are listed in **Table S2a of Supplement S1**. Predicted and observed pharmacokinetic parameters are summarized in **Table S2d of Supplement S1**.

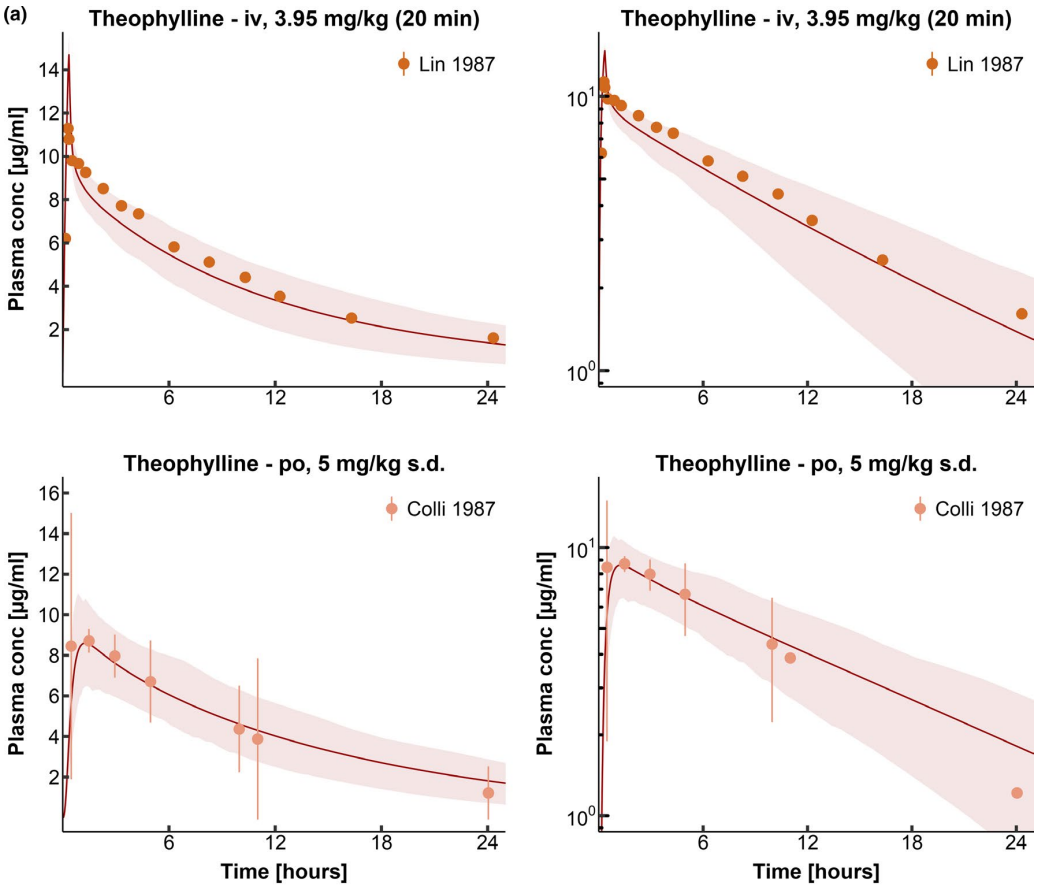
(a)
Theophylline - iv, 3.95 mg/kg (20 min)
Lin 1987
Plasma conc [µg/ml]
Theophylline - po, 5 mg/kg s.d.
Colli 1987
Time [hours]

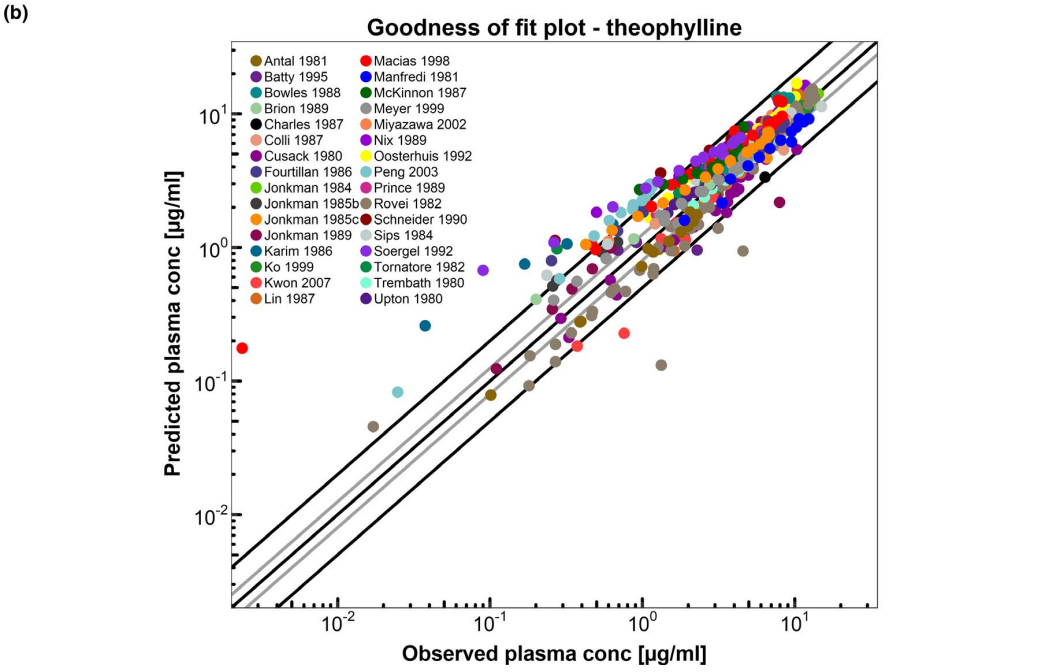
(b)
Goodness of fit plot - theophylline
Antal 1981
Batty 1995
Bowles 1988
Brion 1989
Charles 1987
Colli 1987
Cusack 1980
Fourtillan 1986
Jonkman 1984
Jonkman 1985b
Jonkman 1985c
Jonkman 1989
Karim 1986
Ko 1999
Kwon 2007
Lin 1987
Macias 1998
Manfredi 1981
McKinnon 1987
Meyer 1999
Miyazawa 2002
Nix 1989
Oosterhuis 1992
Peng 2003
Prince 1989
Rovei 1982
Schneider 1990
Sips 1984
Soergel 1992
Tornatore 1982
Trembath 1980
Upton 1980
Predicted plasma conc [µg/ml]
Observed plasma conc [µg/ml]

The GMFE was calculated for all observed AUC and C_{max} values according to Eq. 2.

$$GMFE = 10^{\left(\Sigma\left|\log_{10}\left(\frac{\text{pred PK parameter}}{\text{obs PK parameter}}\right)\right|\right)/n} \quad (2)$$

with pred PK parameter = predicted AUC or C_{max} value, obs PK parameter = observed AUC or C_{max} value, and n = number of studies. A GMFE value below two characterizes an adequate prediction.

PopPK model building and evaluation

Fluvoxamine PBPK model evaluation was supported by a *post hoc* PopPK analysis to quantify the effect of CYP2D6 poor metabolism and the impact of smoking on fluvoxamine clearance and to compare the results to the effect sizes predicted by the PBPK model.

PopPK analysis, model evaluation, and simulation were performed using nonlinear mixed-effects modeling techniques implemented in NONMEM. A full description of the PopPK methodology is available in **Supplement S1**.

DDI network building

In addition to the evaluation methods described above, a CYP1A2 DDI network was built to evaluate the DDI performance of the developed models (**Figure 1**). Fluvoxamine was used as a CYP1A2 and CYP3A4 inhibitor theophylline and caffeine as CYP1A2 victim drugs, rifampicin as CYP1A2 and CYP2E1 inducer, and midazolam as a CYP3A4 victim drug. Mathematical implementation of the drug interaction processes in general is specified in **Supplement S1**. All induction and inhibition processes were modeled using interaction parameter values from *in vitro* experimental reports without further adjustment or fitting.

DDI network evaluation

All predicted DDI simulations were evaluated by comparison of predicted vs. observed victim drug plasma concentration-time profiles alone and during coadministration, DDI AUC ratios (Eq. 3), and DDI C_{max} ratios (Eq. 4).

$$\text{DDI AUC ratio} = \frac{AUC_{\text{victim drug during coadministration}}}{AUC_{\text{victim drug alone}}} \quad (3)$$

$$\text{DDI } C_{max}\text{ratio} = \frac{C_{max_{\text{victim drug during coadministration}}}}{C_{max_{\text{victim drug alone}}}} \quad (4)$$

As a quantitative measure of the prediction accuracy for each DDI interaction, GMFEs of the predicted DDI AUC ratios and DDI C_{max} ratios were calculated according to Eq. 2.

Sensitivity analysis

Sensitivity of the final PBPK models to single parameters (local sensitivity analysis) was calculated, measured as relative changes of the AUC of one dosing interval in steady-state conditions for simulations of the highest recommended doses for fluvoxamine (300 mg once daily) and theophylline (500 mg once daily), respectively.

Parameters were included into the analysis if they have been optimized (**Table S1b or S2b in Supplement S1**), if they might have a strong influence due to calculation methods used in the model (fraction unbound) or if they had significant impact in former models (solubility, blood/plasma ratio, and glomerular filtration rate fraction).

Sensitivity to a parameter is calculated as the ratio of the relative change of the simulated AUC to the relative variation of the parameter around the value used in the final model according to Eq. 5.

$$S = \frac{\Delta AUC}{AUC} * \frac{p}{\Delta p} \quad (5)$$

with S = sensitivity of the AUC to the examined model parameter, ΔAUC = change of the AUC, AUC = simulated AUC with the original parameter value, Δp = change of the examined model parameter value, and p = original model parameter value. A sensitivity value of + 1.0 signifies that a 10% increase of the examined parameter causes a 10% increase of the simulated AUC.

Virtual population characteristics

To predict the variability of the simulated plasma concentration-time profiles, virtual populations of 100 individuals were generated, containing European, Asian, or Japanese individuals. The percentage of male and female individuals and the age and weight ranges were set corresponding with the reported demographics. If not specified, virtual populations containing 50 male and 50 female individuals 20–50 years of age were used, without specific body weight or height restriction as implemented in the software. For details on study populations see **Tables S1a, S2a, S7a, S8a, S9a, and S10a in Supplement S1**. In the generated virtual populations, corresponding organ volumes, tissue compositions, blood flow rates, etc. were varied by an implemented algorithm within the limits of the International Commission on Radiological Protection,[19,20] Tanaka and Kawamura,[21] or Japanese[22] databases. In addition, the reference concentrations of the implemented CYP enzymes were set to be distributed with the default variabilities for their expression available in PK-Sim. **Table S6 in Supplement S1** summarized the implemented enzymes with their reference concentrations and variabilities.

With these populations, simulations were generated and compared with observed data. As the observed data were

Figure 4 Plasma concentration-time profiles of the drug–drug interaction (DDI) network. Population predictions of selected plasma concentration-time profiles compared with observed data for the fluvoxamine-theophylline, rifampicin-theophylline, fluvoxamine-caffeine, and fluvoxamine-midazolam DDIs in linear (left panel) and semilogarithmic plots (right panel). Observed data are shown as dots ± SD.[38-41] Population simulation arithmetic means are shown as lines, and the shaded areas illustrate the 68% population prediction intervals. Details on dosing regimens and study populations are listed in **Tables S7a, S8a, S9a, and S10a of Supplement S1**. Predicted and observed pharmacokinetic parameters are summarized in **Tables S7b, S8b, S9b, and S10b of Supplement S1**.

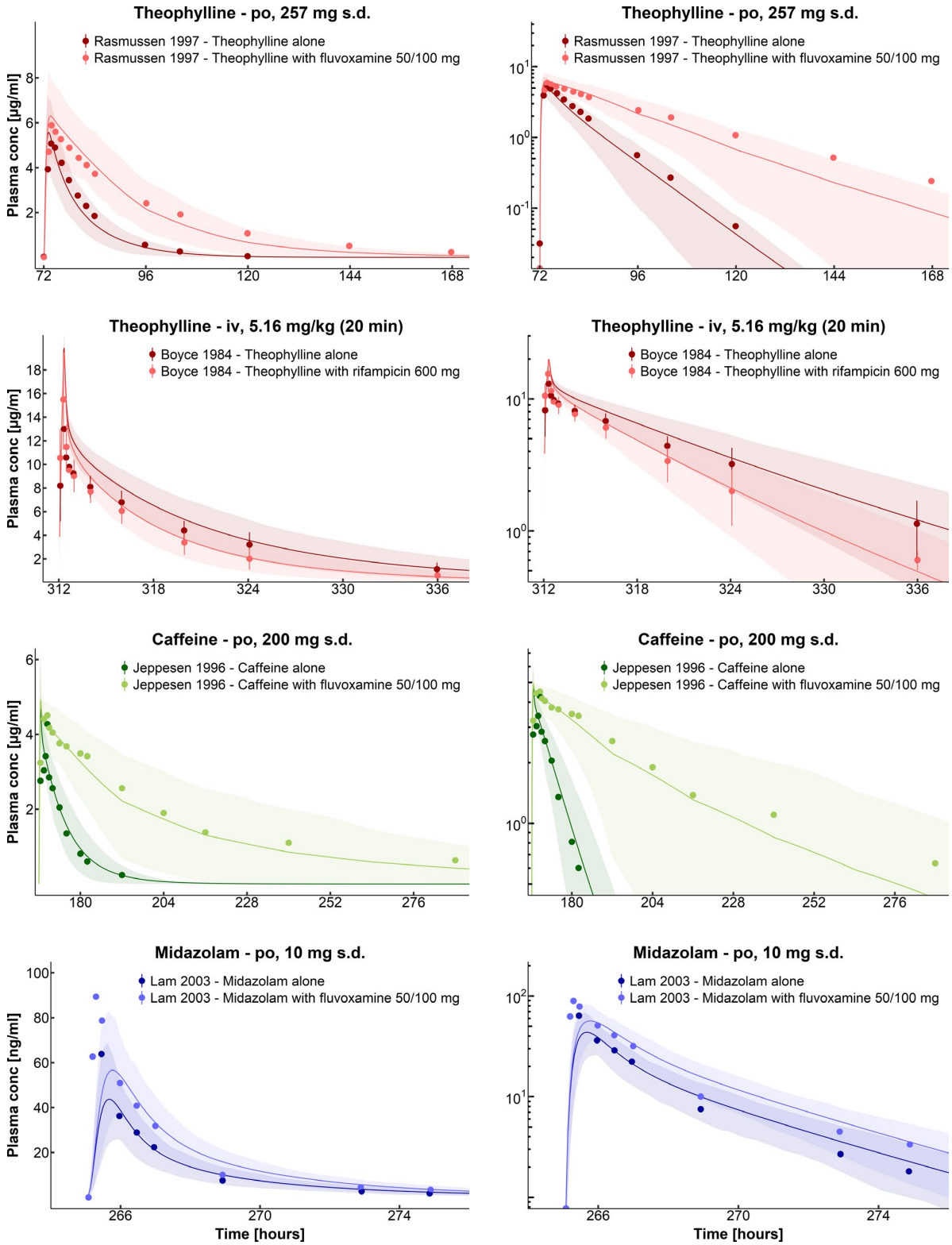
Theophylline - po, 257 mg s.d.
Rasmussen 1997 - Theophylline alone
Rasmussen 1997 - Theophylline with fluvoxamine 50/100 mg
Plasma conc [µg/ml]
Theophylline - iv, 5.16 mg/kg (20 min)
Boyce 1984 - Theophylline alone
Boyce 1984 - Theophylline with rifampicin 600 mg
Caffeine - po, 200 mg s.d.
Jeppesen 1996 - Caffeine alone
Jeppesen 1996 - Caffeine with fluvoxamine 50/100 mg
Midazolam - po, 10 mg s.d.
Lam 2003 - Midazolam alone
Lam 2003 - Midazolam with fluvoxamine 50/100 mg
Plasma conc [ng/ml]
Time [hours]

reported in terms of arithmetic means and SDs, simulated 68% population prediction intervals were plotted that correspond to the range span of ± 1 SD around the mean assuming normal distribution.

RESULTS

PBPK model building and evaluation

The final PBPK models of fluvoxamine and theophylline precisely describe and predict the plasma concentration-time profiles following i.v. and p.o. administration for a large range of administered doses.

Plots of population predicted compared with observed plasma concentration-time profiles of all studies obtained from literature are shown in linear as well as in semilogarithmic plots in **Figure 2a** (selected fluvoxamine studies), **Figure 3a** (selected theophylline studies), and **Figures S1a, S1b, S2a, and S2b of Supplement S1** (all studies). Goodness-of-fit plots are presented in **Figure 2b** (fluvoxamine), **Figure 3b** (theophylline), and **Figures S1c and S2c of Supplement S1**. MRD values of all studies are listed in **Tables S1c and S2c of Supplement S1**.

Predicted compared with observed AUC and C_{max} values of all studies with calculated GMFEs are listed in **Tables S1d and S2d of Supplement S1**. Plots showing the correlation of predicted to observed AUC and C_{max} values of all studies are presented in **Figures S1f and S2d of Supplement S1**.

For fluvoxamine PBPK model development, 26 different clinical studies with PK blood sampling were used, with 9 studies assigned to the training data set (**Table S1a in Supplement S1**). The fluvoxamine PBPK model applies metabolism by CYP1A2, CYP2D6, and glomerular filtration.

To distinguish between fluvoxamine metabolism in CYP2D6 extensive metabolizers (EMs) and poor metabolizers (PMs), the CYP2D6 catalytic rate constant (k_{cat}) of PMs was set to zero. This assumption was made because CYP2D6 PMs were characterized by absent CYP2D6 enzymatic activity,[23] which results in a predicted 1.5-fold increase of the fluvoxamine AUC in CYP2D6 PMs compared with CYP2D6 EMs (observed: 1.3-fold increase[24]). Population predictions of fluvoxamine plasma concentration-time profiles compared with observed data for CYP2D6 EMs and PMs are shown in **Figure S1d of Supplement S1**.

Furthermore, the final model is able to describe the influence of smoking on the PK of fluvoxamine. Smoking is the strongest known inducer of CYP1A2 and results in higher metabolism of CYP1A2 substrates.[1] As no detailed information on the frequency, duration, and amount of smoking was available from literature, the induction of CYP1A2 was implemented as a static 1.38-fold increase in enzyme activity. This factor was optimized based on the study of Spigset *et al.*,[25] resulting in a 39% reduction of the fluvoxamine AUC in smokers (observed: 31% reduction). Population predictions of fluvoxamine plasma concentration-time profiles compared with observed data for nonsmokers and smokers are shown in **Figure S1e of Supplement S1**. Drug-dependent parameters of the final fluvoxamine model are listed in **Table S1b of Supplement S1**. System-dependent parameters are given in **Table S6 of Supplement S1**.

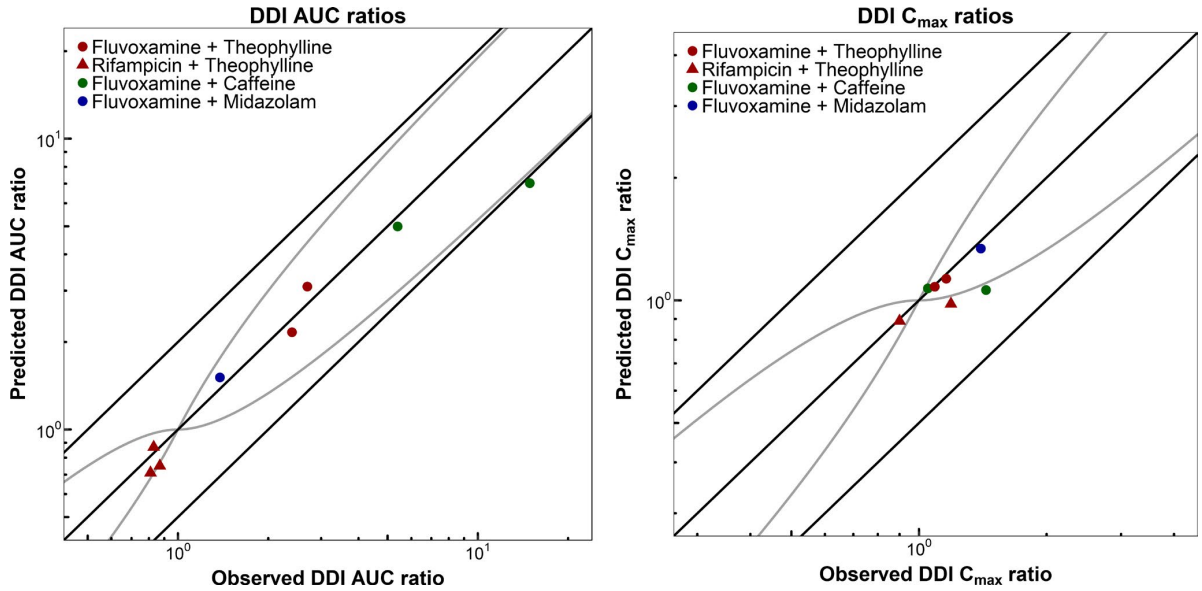

Figure 5 Correlation of predicted to observed drug–drug interaction (DDI) area under the curve (AUC) ratios, and DDI peak plasma concentration (C_{max}) ratios. The left panel illustrates the predicted compared with observed DDI AUC ratios, the right panel illustrates the predicted compared with observed DDI C_{max} ratios of the fluvoxamine-theophylline, rifampicin-theophylline, fluvoxamine-caffeine, and fluvoxamine-midazolam DDIs. Fluvoxamine interaction studies are shown as dots and rifampicin interaction studies are shown as triangles. The colors represent the different victim drugs. The line of identity and the 0.5-fold to 2.0-fold acceptance limits are shown as straight black lines. The curved grey lines are the prediction acceptance limits proposed by Guest *et al.*[42] Study references, dosing regimens, and values of predicted and observed DDI AUC ratios and DDI C_{max} ratios are listed in **Table 1**.

Sensitivity analysis of a simulation of 300 mg fluvoxamine p.o. once daily with a sensitivity threshold of 0.5 reveals that the fluvoxamine model is sensitive to the values of lipophilicity (optimized), CYP2D6 catalytic rate constant (optimized), CYP2D6 Michaelis-Menten constant (literature value), and fraction unbound (literature value; see **Figure S1g of Supplement S1**).

For theophylline PBPK model development, 40 different clinical studies with PK blood sampling and additional fraction excreted unchanged to urine measurements and CYP1A2 fraction metabolized information were used, with 13 clinical studies assigned to the training data set (**Table S2a in Supplement S1**). The theophylline PBPK model applies metabolism by CYP1A2, CYP2E1, and glomerular filtration with reabsorption in the renal tubulus.

In the model, CYP1A2 metabolizes theophylline with high affinity but low capacity, whereas CYP2E1 metabolizes theophylline with low affinity and high capacity, as described in the literature,[26] resulting in a good prediction of the observed concentration dependency of theophylline metabolism. About 95% of an administered theophylline dose are excreted with the urine but only 14–17% as unchanged drug.[27,28] Due to the lack of valid *in vitro* data on renal tubular reabsorption transporters for theophylline, the glomerular filtration rate fraction was optimized to a value of 0.22 to describe the fraction of theophylline excreted unchanged to urine. Drug-dependent parameters of the final theophylline model are listed in **Table S2b of Supplement S1**. System-dependent parameters are given in **Table S6 of Supplement S1**.

Sensitivity analysis of a simulation of 500 mg theophylline p.o. once daily with a sensitivity threshold of 0.5 reveals that the theophylline model is sensitive to the values of fraction unbound (literature value), CYP1A2 catalytic rate constant (optimized), and CYP1A2 Michaelis-Menten constant (literature value; see **Figure S2e of Supplement S1**).

DDI network modeling

For the CYP1A2 DDI network modeling, eight different clinical DDI studies were available, consisting of two studies of fluvoxamine with theophylline, three studies

Table 1 DDI AUC ratios, DDI C_{max} ratios, and GMFE values of DDI studies

Perpetrator drug	Victim drug	Observed DDI AUC ratio	Predicted DDI AUC ratio	Pred/Obs DDI AUC ratio	Observed DDI C_{max} ratio	Predicted DDI C_{max} ratio	Pred/Obs DD C_{max} ratio	Reference
Fluvoxamine	*Theophylline*							
50 mg p.o., q.d./b.i.d.	3.21 mg/kg p.o., s.d.	2.40	2.16	0.90	1.09	1.08	0.99	Orlando 2006[43]
50/100 mg p.o., q.d.	257 mg p.o., s.d.	2.70	3.10	1.15	1.16	1.13	0.97	Rasmussen 1997[38]
			GMFE (range)	1.13 (1.11–1.15)			1.02 (1.01–1.03)	
			Pred/Obs within twofold	2/2			2/2	
Rifampicin	*Theophylline*							
600 mg p.o., q.d.	3.95 mg/kg i.v. (30 minutes)	0.83	0.87	1.05		0.98		Powell-Jackson 1985[44]
600 mg p.o., q.d.	5.19 mg/kg i.v. (20 minutes)	0.81	0.71	0.89	1.19	0.98	0.82	Boyce 1984[39]
600 mg p.o., q.d.	355.5 mg p.o., s.d.	0.87	0.75	0.87	0.90	0.89	0.99	Powell-Jackson 1985[44]
			GMFE (range)	1.12 (1.05–1.16)			1.11 (1.01–1.21)	
			Pred/Obs within twofold	3/3			2/2	
Fluvoxamine	*Caffeine*							
50/100 mg p.o., q.d.	200 mg p.o., s.d.	5.40	4.99	0.92	1.06	1.07	1.01	Jeppesen 1996[40]
100 mg p.o., b.i.d	250 mg p.o., s.d.	14.90	7.03	0.47	1.44	1.06	0.74	Culm-Merdek 2005[45]
			GMFE (range)	1.51 (1.08–2.12)			1.17 (1.01–1.36)	
			Pred/Obs within twofold	1/2			2/2	
Fluvoxamine	*Midazolam*							
50 mg p.o., b.i.d.	10 mg p.o., s.d.	1.38	1.51	1.09	1.40	1.34	0.95	Lam 2003[41]
			GMFE	1.09			1.04	
			Pred/Obs within twofold	1/1			1/1	

AUC, area under the plasma concentration-time curve; C_{max}, peak plasma concentration; DDI, drug-drug interaction; GMFE, geometric mean fold error; Pred/Obs, predicted/observed; -, no data available.

of rifampicin with theophylline, two studies of fluvoxamine with caffeine, and one study of fluvoxamine with midazolam. The victim drug plasma concentration-time profiles of these studies, before and during perpetrator treatment, were predicted and compared with observed data. **Tables S7a, S8a, S9a, and S10a of Supplement S1** list the administration protocols and study population details of the clinical DDI studies. The parameters to model the CYP1A2, CYP2E1, and CYP3A4 induction and inhibition processes are described in **Supplement S1**. Population predictions of plasma concentration-time profiles of the different victim drugs before and during coadministration are presented in linear as well as semi-logarithmic plots in **Figure 4** (selected studies) and **Figures S7a, S8a, S9a, and S10a of Supplement S1** (all studies). All victim drug plasma concentration-time profiles before and during coadministration with fluvoxamine or rifampicin are well-predicted over the full range of reported administration protocols.

Figure 5 shows the correlation of predicted to observed DDI AUC ratios and DDI C_{max} ratios of the modeled DDI studies as a visualization of the performance of the entire network. **Table 1** lists the corresponding DDI AUC ratio and DDI C_{max} ratio values shown in **Figure 5**, with calculated GMFE values for each perpetrator–victim drug combination, demonstrating the good performance of the developed models when applied for DDI prediction.

PopPK modeling of fluvoxamine

The PK of fluvoxamine were best described by a one-compartment model with zero-order absorption with a lag time and linear elimination from the central compartment. As shown in **Table S11 of Supplement S1**, parameter estimates were precise. Goodness-of-fit plots (**Figure S11a in Supplement S1**) and visual predictive checks (**Figure S11b in Supplement S1**) demonstrate the good descriptive performance of the model.

The impact of CYP2D6 phenotype on total clearance of fluvoxamine was best described as a categorical covariate. Volunteers who are CYP2D6 PMs show a 22% lower total clearance of fluvoxamine compared with EMs. Furthermore, fluvoxamine clearance was found to be 28% higher in smokers compared with nonsmokers.

DISCUSSION

The developed PBPK models of fluvoxamine and theophylline reliably describe and predict plasma concentration-time profiles over the full range of published doses and administration protocols. Their good descriptive and predictive performance has been demonstrated by comparison of predicted to observed plasma concentration-time profiles, AUC and C_{max} values, calculation of MRDs and GMFEs, as well as with the prediction of different DDIs. Although the populations used for model predictions were carefully generated according to the reported study demographics, CYP1A2 and CYP2D6 show high interindividual variability, and information on smoking status and CYP2D6 phenotype were lacking in most of the study reports. This could explain why a small percentage of the fluvoxamine and theophylline studies cannot be accurately predicted using the same k_{cat} values for all studies.

There are two previously published PBPK models of fluvoxamine: a minimal PBPK model (three compartments)[29] and a model built on the basis of few clinical studies (four studies).[30] For theophylline, one PBPK model has been previously reported, developed to predict the disposition of theophylline during pregnancy.[31] All three models have not been challenged by prediction of DDIs. The whole-body PBPK models presented in this study have been built using a multitude of clinical studies, are transparently documented, and they have been evaluated in a DDI network.

To describe the metabolism of fluvoxamine, CYP1A2 and CYP2D6 were implemented into the PBPK model. Model building was started with the working hypothesis that CYP2D6 accounts for up to 60% of fluvoxamine metabolism.[32] However, our PBPK analysis suggested a higher fraction of fluvoxamine metabolized by CYP1A2 than by CYP2D6. This result was supported by the finding that fluvoxamine total apparent clearance (CL/F) in CYP2D6 PMs (no CYP2D6 activity) was only 25% lower than in CYP2D6 EMs.[32] (Taking into account that CYP2D6 is also expressed in the intestine, CYP2D6 PMs might show a higher bioavailability of fluvoxamine, reducing CL/F, and thereby further reducing the impact of CYP2D6 poor metabolism on fluvoxamine clearance.)

To confirm this relatively small impact of CYP2D6 poor metabolism on fluvoxamine PK, a PopPK analysis of fluvoxamine was conducted. The reduction of fluvoxamine CL/F in CYP2D6 PMs compared with EMs was quantified at 22%. This is the first reported compartmental analysis of fluvoxamine, which is in very good agreement with the noncompartmental result for reduction of CL/F in CYP2D6 PMs of 25%.[32]

Simulation of fluvoxamine fraction metabolized using the final PBPK model and a single dose of 50 mg predicts fractions metabolized of 20% by CYP2D6 and of 71% by CYP1A2, which is very close to the PopPK analysis result. Neither fraction metabolized information nor the CYP2D6 PM fluvoxamine plasma profiles were used during the final PBPK model parameter optimization. Fitting the catalytic rate constants of CYP2D6 and CYP1A2 and, therefore, the contribution of both enzymes to fluvoxamine metabolism to get a good description of the nonlinear PK of fluvoxamine for the different doses administered already resulted in a model that accurately describes the fractions metabolized.

The inducing effect of smoking on the metabolism of fluvoxamine is also well-described by the PBPK model, with AUC ratios smoking/nonsmoking of 0.61 predicted and 0.69 observed. The fluvoxamine PopPK analysis gives a 28% higher CL/F of fluvoxamine in smokers compared with nonsmokers. The small overprediction of the fluvoxamine C_{max} in smokers could be attributed to gastrointestinal effects of smoking that reduce the absorption of fluvoxamine but were not accounted for in the model. However, due to a lack of more detailed information on the frequency, duration, and amount of smoking, the induction of CYP1A2 could only be implemented as a static increase of the enzyme activity. To model this CYP induction in a mechanistic and dynamic

way, for example, to predict the return of CYP1A2 activity to baseline when smoking is stopped before a surgical intervention, as well as to validate the estimated factor on CYP1A2 enzyme activity for the smoking population, more data are needed.

The developed theophylline model can be used for prediction of plasma concentration-time profiles following i.v. administration or p.o. administration of syrup, solution, or immediate-release formulations. As the reported plasma concentration profiles of the different sustained release dosage forms strongly vary with the mechanism used for prolongation of drug release, sustained release or enteric coated theophylline formulations were not considered in the current investigation. If needed, the model can be easily extended by implementation of sustained release drug dissolution profiles.[33]

The DDIs presented in this study have been modeled using reported experimental values to inform all necessary interaction parameters. This approach is followed as an additional means of model evaluation, predicting all available reported clinical DDI studies, and comparing the observed data to model predictions. The caffeine,[15] rifampicin,[13] and midazolam[13] PBPK models applied have been evaluated and described elsewhere. The existing rifampicin model has been extended to predict the induction of CYP1A2 and CYP2E1 by rifampicin. The DDI performance of the enhanced rifampicin model has been successfully evaluated with the data of three different clinical rifampicin-theophylline DDI studies.

The presented CYP1A2 DDI network demonstrates the good performance of all models for DDI prediction over the full range of reported DDI study protocols. This has been shown by victim drug concentration-time profiles, DDI AUC ratios, DDI C_{max} ratios, and corresponding GMFE values. All DDIs of fluvoxamine with the sensitive CYP1A2 victim drugs theophylline and caffeine are well predicted. The moderate inhibition of CYP3A4 by fluvoxamine was successfully implemented and evaluated by prediction of the fluvoxamine-midazolam DDI. Due to the present lack of models for CYP2C19 victim drugs, the strong inhibition of CYP2C19 by fluvoxamine could not be tested. However, fluvoxamine CYP2C19 interaction parameters are reported and can be easily implemented into the presented fluvoxamine PBPK model.

In summary, a PBPK CYP1A2 DDI network has been successfully developed. Whole-body PBPK models of fluvoxamine and theophylline have been carefully built and evaluated by DDI prediction using different kinds of perpetrator (induction, competitive inhibition, and mixed inhibition) and victim drugs (CYP1A2 and CYP3A4). Furthermore, a previously developed model of rifampicin has been expanded with parameters for CYP1A2 and CYP2E1 interaction and tested. The resulting PBPK network of fluvoxamine, theophylline, caffeine, rifampicin, and midazolam adequately predicts the observed data of all clinical DDI studies reported for combinations of these drugs and, therefore, all models are considered ready to use for DDI prediction. The newly developed models of fluvoxamine and theophylline are transparently documented and the model files, also including DDI model files, are provided as **Supplementary Material** to this paper (**Data S1-S6**) as well as in the Open Systems Pharmacology repository (www.open-systems-pharmacology.org), to extend the library of publicly available PBPK models for DDI prediction. They can be applied to help understand and characterize the DDI potential of investigational drugs, to inform the design of clinical trials, or to generate dose recommendations for comedication.

Supporting Information. Supplementary information accompanies this paper on the *CPT: Pharmacometrics & Systems Pharmacology* website (www.psp-journal.com).

Supplement S1. Model information and evaluation.
Data S1. Fluvoxamine model file.
Data S2. Theophylline model file.
Data S3. Fluvoxamine-theophylline DDI model file.
Data S4. Rifampicin-theophylline DDI model file.
Data S5. Fluvoxamine-caffeine DDI model file.
Data S6. Fluvoxamine-midazolam DDI model file.

Funding. This project has received funding from the European Union's Horizon 2020 Research and Innovation Programme under grant agreement No. 668353. M.S. was supported by the Robert Bosch Stiftung, Stuttgart, Germany.

Conflict of Interest. T.E., T.W., and S.F. are employees of Bayer AG. A.K.V. performed this work at the Saarland University. Since January 2018, she is an employee of the Federal Institute for Drugs and Medical Devices (BfArM) and declares no potential conflicts of interest with respect to the research, authorship, and/or publication of this article. No potential conflicts of interest were disclosed by the other authors.

Author Contributions. H.B., N.H., A.K.V., and T.L. wrote the manuscript. N.H., O.S., M.S., T.E., T.W., S.F., and T.L. designed the research. H.B., N.H., A.K.V., S.F., and T.L. performed the research.

Disclaimer. The views expressed in this article are the views of A.K.V. and do not necessarily reflect the views and opinions of the BfArM.

1. Zhou, S.F., Yang, L.P., Zhou, Z.W., Liu, Y.H. & Chan, E. Insights into the substrate specificity, inhibitors, regulation, and polymorphisms and the clinical impact of human cytochrome P450 1A2. *AAPS J.* **11**, 481–494 (2009).
2. Shimada, T., Yamazaki, H., Mimura, M., Inui, Y. & Guengerich, F.P. Interindividual variations in human liver cytochrome P-450 enzymes involved in the oxidation of drugs, carcinogens and toxic chemicals: studies with liver microsomes of 30 Japanese and 30 caucasians. *J. Pharmacol. Exp. Ther.* **270**, 414–423 (1994).
3. Chen, Y., Liu, L., Laille, E., Kumar, G. & Surapaneni, S. In vitro assessment of cytochrome P450 inhibition and induction potential of azacitidine. *Cancer Chemother. Pharmacol.* **65**, 995–1000 (2010).
4. Kalow, W. & Tang, B. The use of caffeine for enzyme assays: a critical appraisal. *Clin. Pharmacol. Ther.* **53**, 503–514 (1993).
5. Karjalainen, M.J., Neuvonen, P.J. & Backman, J.T. Rofecoxib is a potent, metabolism-dependent inhibitor of CYP1A2: implications for in vitro prediction of drug interactions. *Drug Metab. Dispos.* **34**, 2091–2096 (2006).
6. Lu, P. *et al.* Mechanism-based inhibition of human liver microsomal cytochrome P450 1A2 by zileuton, a 5-lipoxygenase inhibitor. *Drug Metab. Dispos.* **31**, 1352–1360 (2003).
7. Faber, M.S., Jetter, A. & Fuhr, U. Assessment of CYP1A2 activity in clinical practice: why, how, and when? *Basic Clin. Pharmacol. Toxicol.* **97**, 125–134 (2005).
8. US Food and Drug Administration. Clinical drug interaction studies - study design, data analysis, implications for dosing, and labeling recommendations. Draft Guidance for Industry <https://www.fda.gov/downloads/drugs/guidancecomplianceregulatoryinformation/guidances/ucm292362.pdf> (2017).
9. US Food and Drug Administration. Drug development and drug interactions: table of substrates, inhibitors and inducers. <https://www.fda.gov/Drugs/DevelopmentApprovalProcess/DevelopmentResources/DrugInteractionsLabeling/ucm093664.htm> (2017). Accessed October 2, 2018.

10. European Medicines Agency. Guideline on the investigation of drug interactions. <https://www.ema.europa.eu/documents/scientific-guideline/guideline-investigation-drug-interactions_en.pdf> (2015).
11. European Medicines Agency. Draft guideline on the qualification and reporting of physiologically based pharmacokinetic (PBPK) modelling and simulation. <https://www.ema.europa.eu/documents/scientific-guideline/draft-guideline-qualification-reporting-physiologically-based-pharmacokinetic-pbpk-modelling_en.pdf> (2016).
12. US Food and Drug Administration. Physiologically based pharmacokinetic analyses - format and content. Guidance for Industry. <https://www.fda.gov/downloads/Drugs/GuidanceComplianceRegulatoryInformation/Guidances/UCM531207.pdf> (2018).
13. Hanke, N. *et al.* PBPK models for CYP3A4 and P-gp DDI prediction: a modeling network of rifampicin, itraconazole, clarithromycin, midazolam, alfentanil, and digoxin. *CPT Pharmacometrics Syst. Pharmacol.* **7**, 647–659 (2018).
14. Open Systems Pharmacology (OSP). OSP repository. <https://github.com/Open-Systems-Pharmacology> (2018). Accessed October 2, 2018.
15. Open Systems Pharmacology (OSP). OSP repository: caffeine template model. <https://github.com/Open-Systems-Pharmacology/Example_Caffeine/blob/master/Caffeine.pksim5> (2018). Accessed October 2, 2018.
16. Eissing, T. *et al.* A computational systems biology software platform for multiscale modeling and simulation: integrating whole-body physiology, disease biology, and molecular reaction networks. *Front. Physiol.* **2**, 1–10 (2011).
17. Meyer, M., Schneckener, S., Ludewig, B., Kuepfer, L. & Lippert, J. Using expression data for quantification of active processes in physiologically-based pharmacokinetic modeling. *Drug Metab. Dispos.* **40**, 892–901 (2012).
18. Edginton, A.N., Schmitt, W. & Willmann, S. Development and evaluation of a generic physiologically based pharmacokinetic model for children. *Clin. Pharmacokinet.* **45**, 1013–1034 (2006).
19. Valentin, J. Basic anatomical and physiological data for use in radiological protection: reference values. A report of age- and gender-related differences in the anatomical and physiological characteristics of reference individuals. ICRP Publication 89. *Ann. ICRP* **32**, 5–265 (2002).
20. Willmann, S. *et al.* Development of a physiology-based whole-body population model for assessing the influence of individual variability on the pharmacokinetics of drugs. *J. Pharmacokinet. Pharmacodyn.* **34**, 401–431 (2007).
21. Tanaka, G. & Kawamura, H. Anatomical and physiological characteristics for Asian reference man: male and female of different ages: Tanaka model. Division of Radioecology, National Institute of Radiological Sciences. Hitachinaka 311-12 Japan. NIRS-M-115 (1996).
22. Open Systems Pharmacology Suite. Open Systems Pharmacology Suite Manual, Version 7.0.0. (2017).
23. Crews, K.R. *et al.* Clinical Pharmacogenetics Implementation Consortium guidelines for cytochrome P450 2D6 genotype and codeine therapy: 2014 update. *Clin. Pharmacol. Ther.* **95**, 376–382 (2014).
24. Spigset, O., Granberg, K., Hägg, S., Norström, A. & Dahlqvist, R. Relationship between fluvoxamine pharmacokinetics and CYP2D6/CYP2C19 phenotype polymorphisms. *Eur. J. Clin. Pharmacol.* **52**, 129–133 (1997).
25. Spigset, O., Carleborg, L., Hedenmalm, K. & Dahlqvist, R. Effect of cigarette smoking on fluvoxamine pharmacokinetics in humans. *Clin. Pharmacol. Ther.* **58**, 399–403 (1995).
26. Zhang, Z. & Kaminsky, L.S. Characterization of human cytochromes P450 involved in theophylline 8-hydroxylation. *Biochem. Pharmacol.* **50**, 205–211 (1995).
27. Macias, W.L. *et al.* Lack of effect of olanzapine on the pharmacokinetics of a single aminophylline dose in healthy men. *Pharmacotherapy* **18**, 1237–1248 (1998).
28. Rovei, V., Chanoine, F. & Strolin Benedetti, M. Pharmacokinetics of theophylline: a dose-range study. *Br. J. Clin. Pharmacol.* **14**, 769–778 (1982).
29. Iga, K. Use of three-compartment physiologically based pharmacokinetic modeling to predict hepatic blood levels of fluvoxamine relevant for drug-drug interactions. *J. Pharm. Sci.* **104**, 1478–1491 (2015).
30. Alqahtani, S. & Kaddoumi, A. Development of a physiologically based pharmacokinetic/pharmacodynamic model to predict the impact of genetic polymorphisms on the pharmacokinetics and pharmacodynamics represented by receptor/transporter occupancy of central nervous system drugs. *Clin. Pharmacokinet.* **55**, 957–969 (2016).
31. Ke, A.B. *et al.* A physiologically based pharmacokinetic model to predict disposition of CYP2D6 and CYP1A2 metabolized drugs in pregnant women. *Drug Metab. Dispos.* **41**, 801–813 (2013).
32. Spigset, O., Axelsson, S., Norström, A., Hägg, S. & Dahlqvist, R. The major fluvoxamine metabolite in urine is formed by CYP2D6. *Eur. J. Clin. Pharmacol.* **57**, 653–658 (2001).
33. Thelen, K., Coboeken, K., Willmann, S., Dressman, J.B. & Lippert, J. Evolution of a detailed physiological model to simulate the gastrointestinal transit and absorption process in humans, part II: extension to describe performance of solid dosage forms. *J. Pharm. Sci.* **101**, 1267–1280 (2012).
34. Japanese Society of Hospital Pharmacists. Pharmaceutical interview form (Article in Japanese). <https://www.abbvie.co.jp/content/dam/abbviecorp/japan/docs/if_luvox_201412.pdf> (2015). Accessed October 2, 2018.
35. Fleishaker, J. & Hulst, L. A pharmacokinetic and pharmacodynamic evaluation of the combined administration of alprazolam and fluvoxamine. *Eur. J. Clin. Pharmacol.* **46**, 35–39 (1994).
36. Lin, J.H., Chremos, A.N., Chiou, R., Yeh, K.C. & Williams, R. Comparative effect of famotidine and cimetidine on the pharmacokinetics of theophylline in normal volunteers. *Br. J. Clin. Pharmacol.* **24**, 669–672 (1987).
37. Colli, A. *et al.* Ticlopidine-theophylline interaction. *Clin. Pharmacol. Ther.* **41**, 358–362 (1987).
38. Rasmussen, B.B., Jeppesen, U., Gaist, D. & Brøsen, K. Griseofulvin and fluvoxamine interactions with the metabolism of theophylline. Ther. Drug Monit. **19**, 56–62 (1997).
39. Boyce, E.G. The effect of rifampin on theophylline pharmacokinetic parameters (following intravenous aminophylline) in normal volunteers. (1984).
40. Jeppesen, U., Loft, S., Poulsen, H.E. & Brøsen, K. A fluvoxamine-caffeine interaction study. Pharmacogenetics **6**, 213–222 (1996).
41. Lam, Y.W.F., Alfaro, C.L., Ereshefsky, L. & Miller, M. Pharmacokinetic and pharmacodynamic interactions of oral midazolam with ketoconazole, fluoxetine, fluvoxamine, and nefazodone. J. Clin. Pharmacol. **43**, 1274–1282 (2003).
42. Guest, E.J., Aarons, L., Houston, J.B., Rostami-Hodjegan, A. & Galetin, A. Critique of the two-fold measure of prediction success for ratios: application for the assessment of drug-drug interactions. Drug Metab. Dispos. **39**, 170–173 (2011).
43. Orlando, R., *et al.* Liver dysfunction markedly decreases the inhibition of cytochrome P450 1A2-mediated theophylline metabolism by fluvoxamine. Clin. Pharmacol. Ther. **79**, 489–499 (2006).
44. Powell-Jackson, P.R., Jamieson, A.P., Gray, B.J., Moxham, J. & Williams, R. Effect of rifampicin administration on theophylline pharmacokinetics in humans. Am. Rev. Respir. Dis. **131**, 939–940 (1985).
45. Culm-Merdek, K.E., von Moltke, L.L., Harmatz, J.S. & Greenblatt, D.J. Fluvoxamine impairs single-dose caffeine clearance without altering caffeine pharmacodynamics. Br. J. Clin. Pharmacol. **60**, 486–493 (2005).

4.3 PROJECT III: PHYSIOLOGICALLY BASED PHARMACOKINETIC MODELS OF PROBENECID AND FUROSEMIDE TO PREDICT TRANSPORTER MEDIATED DRUG-DRUG INTERACTIONS

4.3.1 *Reference*

Hannah Britz, Nina Hanke, Mitchell E Taub, Ting Wang, Bhagwat Prasad, Éric Fernandez, Peter Stopfer, Valerie Nock, Thorsten Lehr. Physiologically based pharmacokinetic models of probenecid and furosemide to predict transporter mediated drug-drug interactions. Pharm Res. 2020;37(12):250. The final publication is available at Springer via doi: 10.1007/s11095-020-02964-z

4.3.2 *Supplementary material*

Supplementary material can be found on the accompanying storage medium. It is also available online at: supplementary material of publication III.

4.3.3 *Copyright*

4.3.4 *Author contributions*

Declaration of author contributions to the publication related to project III included in this thesis according to the CRediT [1].

Hannah Britz	Conceptualization, Data Curation, Investigation, Visualization, Writing - Original Draft, Writing - Review & Editing
Nina Hanke	Conceptualization, Investigation, Writing - Original Draft, Writing - Review & Editing
Mitchell E Taub	Resources, Investigation, Writing - Review & Editing
Ting Wang	Resources, Investigation, Writing - Review & Editing
Bhagwat Prasad	Resources, Investigation, Writing - Review & Editing
Éric Fernandez	Conceptualization, Writing - Review & Editing
Peter Stopfer	Conceptualization, Resources, Writing - Review & Editing
Valerie Nock	Conceptualization, Writing - Review & Editing
Thorsten Lehr	Conceptualization, Investigation, Writing - Original Draft, Writing - Review & Editing

Pharm Res (2020) 37:250
https://doi.org/10.1007/s11095-020-02964-z

RESEARCH PAPER

Physiologically Based Pharmacokinetic Models of Probenecid and Furosemide to Predict Transporter Mediated Drug-Drug Interactions

Hannah Britz[1] • Nina Hanke[1] • Mitchell E. Taub[2] • Ting Wang[2] • Bhagwat Prasad[3] • Éric Fernandez[4] • Peter Stopfer[4] • Valerie Nock[4] • Thorsten Lehr[1]

Received: 24 August 2020 / Accepted: 26 October 2020

ABSTRACT

Purpose To provide whole-body physiologically based pharmacokinetic (PBPK) models of the potent clinical organic anion transporter (OAT) inhibitor probenecid and the clinical OAT victim drug furosemide for their application in transporter-based drug-drug interaction (DDI) modeling.

Methods PBPK models of probenecid and furosemide were developed in PK-Sim®. Drug-dependent parameters and plasma concentration-time profiles following intravenous and oral probenecid and furosemide administration were gathered from literature and used for model development. For model evaluation, plasma concentration-time profiles, areas under the plasma concentration–time curve (AUC) and peak plasma concentrations (C_{max}) were predicted and compared to observed data. In addition, the models were applied to predict the outcome of clinical DDI studies.

Results The developed models accurately describe the reported plasma concentrations of 27 clinical probenecid studies and of 42 studies using furosemide. Furthermore, application of these models to predict the probenecid-furosemide and probenecid-rifampicin DDIs demonstrates their good performance, with 6/7 of the predicted DDI AUC ratios and 4/5 of the predicted DDI C_{max} ratios within 1.25-fold of the observed values, and all predicted DDI AUC and C_{max} ratios within 2.0-fold.

Conclusions Whole-body PBPK models of probenecid and furosemide were built and evaluated, providing useful tools to support the investigation of transporter mediated DDIs.

KEY WORDS drug-drug interaction (DDI) · furosemide · organic anion transporter (OAT) · physiologically based pharmacokinetic modeling (PBPK) · probenecid

ABBREVIATIONS

AADAC	Arylacetamide deacetylase
ADME	Absorption, distribution, metabolism and excretion
AUC_{last}	Area under the plasma concentration-time curve (AUC) from the time of drug administration to the time of the last concentration measurement
C_{max}	Peak plasma concentration
DDI	Drug-drug interaction
EMA	European Medicines Agency
FDA	U.S. Food and Drug Administration
GFR	Glomerular filtration rate
GMFE	Geometric mean fold error
MRD	Mean relative deviation
MRP	Multidrug resistance-associated protein
OAT	Organic anion transporter
OATP	Organic anion transporting polypeptide
PBPK	Physiologically based pharmacokinetics
Pgp	P-glycoprotein
SLC	Solute carrier
T_{max}	Time to peak plasma concentration
UGT	Uridine 5′-diphospho-glucuronosyltransferase

✉ Thorsten Lehr
thorsten.lehr@mx.uni-saarland.de

[1] Clinical Pharmacy, Saarland University, Campus C2 2, 66123 Saarbrücken, Germany

[2] Drug Metabolism and Pharmacokinetics, Boehringer Ingelheim Pharmaceuticals Inc., Ridgefield, Connecticut, USA

[3] Department of Pharmaceutical Sciences, Washington State University, Spokane, Washington, USA

[4] Translational Medicine and Clinical Pharmacology, Boehringer Ingelheim Pharma GmbH & Co. KG, Biberach, Germany

INTRODUCTION

Many important drug transporters are members of the solute carrier (SLC) family, which is widely expressed throughout the human body and mediates influx or efflux of endogenous and exogenous substrates (1). For the approval of new drugs, the U.S. Food and Drug Administration (FDA) and the European Medicines Agency (EMA) require various *in vitro*, and in many cases, clinical studies to characterize the transporter mediated drug-drug interaction (DDI) potential of investigational drugs. Based on the outcome of these investigations, recommendations for dose adjustments are given in the accompanying label of a new drug (2,3).

Organic anion transporter (OAT) 1 and OAT3 are members of the SLC transporter family (*SLC22A6*, *SLC22A8*) and recognized as important drug transporters from the perspective of their potential to be involved in clinically relevant DDIs. OAT1 and OAT3 are predominantly expressed in the kidney at the basolateral membrane of proximal tubule cells (4), where they facilitate the uptake of endogenous (e.g. p-aminohippurate, estrone sulfate) and exogenous (e.g. diuretic drugs) organic anions from the blood into the proximal tubule cells (5), from where they can be secreted into the nephron lumen for excretion with the urine. Several polymorphisms have been identified and investigated; however, variants of OAT1 or OAT3 have not been shown to significantly impact the renal clearance of OAT substrates in clinical studies (6,7). To characterize the OAT mediated DDI potential, the FDA recommends furosemide as clinical OAT1/OAT3 substrate and probenecid as clinical OAT1/OAT3 inhibitor (8). In addition, probenecid can also be used to investigate organic anion transporting polypeptide (OATP) 1B1 mediated DDIs (9).

OATP1B1, another clinically relevant member of the SLC transporter family (*SLCO1B1*), is exclusively expressed at the sinusoidal membrane of hepatocytes, where it is responsible for the uptake of endogenous (e.g. bile acids) and exogenous (e.g. statins, rifampicin) organic anions from the blood into the hepatocytes (10,11). As probenecid also inhibits OATP1B1, the prediction of the probenecid-rifampicin DDI was included into the presented study, to further evaluate the performance of the probenecid model as a DDI perpetrator.

Physiologically based pharmacokinetic (PBPK) modeling is encouraged and supported by the FDA and EMA as a valuable tool to quantitatively describe and predict the pharmacokinetics of drugs, to evaluate DDI potential and to support clinical study design, dose selection and labeling during drug development (2,3,12–14). The objectives of this study were to provide whole-body PBPK models of probenecid and furosemide, incorporating the transporters and enzymes involved in the pharmacokinetics of these drugs. *In vitro* measurements were used to parametrize the respective incorporated processes. The models were built and evaluated to adequately predict the plasma concentration-time profiles and the fractions excreted unchanged in urine. Furthermore, the models were used to predict probenecid DDIs, with probenecid as potent clinical OAT1/OAT3 inhibitor (8,15), moderate OATP1B1 inhibitor (9), weak inhibitor of multidrug resistance-associated protein (MRP) 4 (16) and weak inhibitor of uridine 5′-diphospho-glucuronosyltransferase (UGT) 1A9 (in-house measurement), furosemide as clinical OAT1/OAT3 substrate and rifampicin as OATP1B1 substrate. The comprehensive Electronic Supplementary Material (ESM) to this manuscript provides detailed information on the developed PBPK models, including all model parameters and a complete documentation of the extensive model evaluation. The model files will be shared in the Open Systems Pharmacology PBPK model library (www.open-systems-pharmacology.org).

METHODS

Software

PBPK modeling was performed with the open source PK-Sim® and MoBi® modeling software (version 8.0, part of the Open Systems Pharmacology Suite (17,18), www.open-systems-pharmacology.org). Published plasma concentration-time profiles were digitized using GetData Graph Digitizer (version 2.26.0.20, S. Fedorov) (19). Parameter optimizations were accomplished with the Monte Carlo algorithm as well as the Levenberg-Marquardt algorithm using the "multiple random starting values" function implemented in PK-Sim®. The final optimizations were run using the Levenberg-Marquardt algorithm. PK parameter analysis and calculation of model performance measures was performed with R (version 3.6.2, The R Foundation for Statistical Computing) and graphics were compiled with R and RStudio (version 1.2.5033, RStudio, Inc., Boston, MA, USA). Sensitivity analysis was performed using the implemented Sensitivity Analysis tool in PK-Sim® (20).

PBPK Model Building

PBPK model building was started with an extensive literature search to collect physicochemical parameters, information on absorption, distribution, metabolism and excretion (ADME) processes and clinical studies of intravenous and oral administration of probenecid and furosemide in single- and multiple dose regimens.

To build the datasets for PBPK model development, the reported observed plasma concentration-time profiles were digitized and divided into a training dataset for model building and a test dataset for model evaluation. Model input parameters that could not be informed from experimental reports were optimized by fitting the model simultaneously

to the observed data of all studies assigned to the training dataset. To limit the parameters to be optimized during model building, the minimal number of processes necessary to mechanistically describe the pharmacokinetics and DDIs of the modeled drugs were implemented into the models. If two transporters show very similar expression patterns and affinity for the same compound, optimizing the transport rate constants of both transporters would lead to identifiability issues. Therefore, only the transporter with the higher affinity for the respective substrate was implemented, to describe a transport that probably is accomplished by both transporters *in vivo*.

Model evaluation was carried out based on the clinical data of the test dataset. Descriptive (training dataset) and predictive (test dataset) performance of the model for all analyzed clinical studies is transparently documented in the ESM.

Virtual Individuals

The PBPK models were built based on data from healthy individuals, using the reported sex, ethnicity and mean values for age, weight and height from each study protocol. If no demographic information was provided, the following default values were substituted: male, European, 30 years of age, 73 kg body weight and 176 cm body height (characteristics from the PK-Sim® population database (21,22)). ADME transporters and enzymes were implemented in accordance with literature, using the PK-Sim® expression database to define their relative expression in the different organs of the body (23). Table S7.0.1 summarizes all system-dependent parameters on the implemented transporters and enzymes.

Virtual Population Characteristics

To predict the variability of the simulated plasma concentration-time profiles, virtual populations of 100 individuals were generated, consisting of either European or Asian individuals. The percentage of female individuals and the ranges of age, weight and height were set according to the reported demographics. If not specified, virtual populations containing 100 male subjects 20–50 years of age were used, with body weight and height restrictions from the PK-Sim® population database (22). For details on the study populations see Tables S2.2.1, S3.2.1, S5.2.1 and S6.2.1.

In the generated virtual populations, organ volumes, tissue compositions, blood flow rates, etc. were varied by an implemented algorithm within the limits of the International Commission on Radiological Protection (ICRP) (21,22) or Tanaka (24) databases. In addition, the reference concentrations of the implemented transporters and enzymes were log-normally distributed around their mean values, using reported variabilities for their expression from the PK-Sim® database (25) or from literature. Table S7.0.1 summarizes the modeled transporters and enzymes with their reference concentrations and variabilities.

As the clinical plasma concentration data from literature is mostly reported as arithmetic means ± standard deviation, population prediction arithmetic means and 68% prediction intervals were plotted, that correspond to a range of ±1 standard deviation around the mean assuming normal distribution.

PBPK Model Evaluation

Model performance was evaluated using various methods. The population predicted plasma concentration-time profiles were compared to the data observed in the clinical studies. Furthermore, predicted plasma concentrations of all studies were compared to the observed plasma concentrations in goodness-of-fit plots. In addition, the model performance was evaluated by comparison of predicted to observed areas under the plasma concentration-time curve (AUC) from the time of drug administration to the time of the last concentration measurement (AUC_{last}) and peak plasma concentration (C_{max}) values. As quantitative measures of the model performance, the mean relative deviation (MRD) of all predicted plasma concentrations (Eq. 1) and the geometric mean fold error (GMFE) of all predicted AUC_{last} and C_{max} values (Eq. 2) were calculated. MRD and GMFE values ≤2 characterize an adequate model performance.

$$\mathrm{MRD} = 10^{x};\quad x = \sqrt{\frac{1}{k}\sum_{i=1}^{k}\left(\log_{10}c_{\mathrm{predicted,i}} - \log_{10}c_{\mathrm{observed,i}}\right)^{2}} \tag{1}$$

where $c_{predicted,\ i}$ = predicted plasma concentration, $c_{observed,\ i}$ = corresponding observed plasma concentration and k = number of observed values.

$$\mathrm{GMFE} = 10^{x};\quad x = \frac{1}{m}\sum_{i=1}^{m}\left|\log_{10}\left(\frac{\text{predicted PK parameter}_i}{\text{observed PK parameter}_i}\right)\right| \tag{2}$$

where predicted PK parmeter$_i$ = predicted AUC_{last} or C_{max}, observed PK parameter$_i$ = corresponding observed AUC_{last} or C_{max} and m = number of studies.

Furthermore, sensitivity analysis results were assessed. A detailed description of the sensitivity calculation is provided in the ESM.

PBPK DDI Modeling

As an additional means of model evaluation, the DDI performance of the developed models was assessed. To model the probenecid-furosemide DDI, inhibition of OAT3, UGT1A9

and MRP4 by probenecid was implemented. To predict the probenecid-rifampicin DDI, inhibition of OATP1B1 by probenecid was incorporated (Fig. 1). The rifampicin model applied was developed by Hanke *et al.* (26) and is freely available in the Open Systems Pharmacology repository on GitHub (27). The model includes rifampicin transport via OATP1B1 and P-glycoprotein (Pgp), metabolism via the arylacetamide deacetylase (AADAC), as well as auto-induction of OATP1B1, Pgp and AADAC (26). The good DDI performance of the model was demonstrated in many different applications (26,28–31). Mathematical implementation of the DDI processes is specified in Section 1 of the ESM.

Inhibition constants characterizing the inhibition of OAT3, UGT1A9 (in-house measurement) and OATP1B1 by probenecid were taken from *in vitro* experimental reports (9,15). Short descriptions of the respective *in vitro* assay conditions are provided in Sections 5.1 and 6.1 of the ESM. To describe the competitive inhibition of MRP4 by probenecid, the corresponding inhibition constant was optimized during the furosemide PBPK model parameter identification, using the clinical data of one of the probenecid-furosemide interaction studies (32) (see Table S5.2.1). The DDI parameter values are listed in the probenecid drug-dependent parameter table (Table S2.3.1).

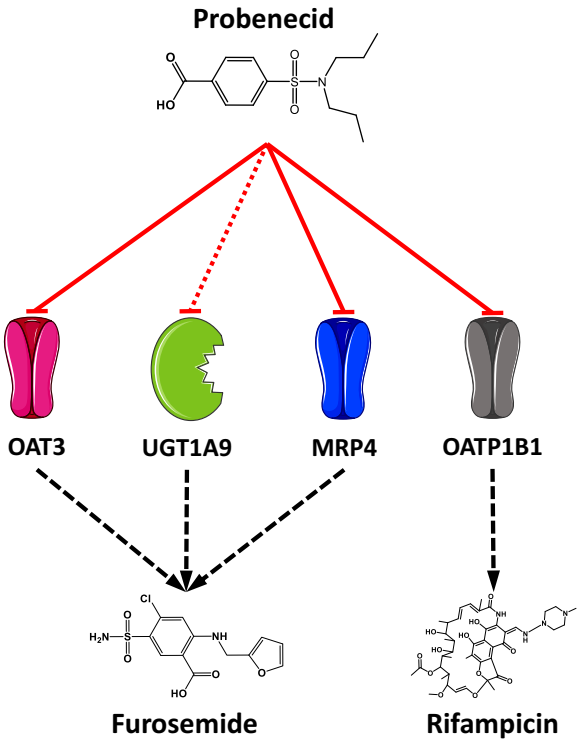

Fig. 1 Probenecid DDIs. Schematic illustration of the modeled DDIs with probenecid as OAT3, UGT1A9, MRP4 and OATP1B1 perpetrator drug, furosemide as OAT3, UGT1A9 and MRP4 victim drug and rifampicin as OATP1B1 victim drug. The red solid lines indicate competitive inhibition, the red dotted line indicates non-competitive inhibition by probenecid. The black dashed lines indicate transport or metabolism. Drawings by Servier Medical Art, licensed under CC BY 3.0. **MRP4:** multidrug resistance-associated protein 4, **OAT3:** organic anion transporter 3, **OATP1B1:** organic anion transporting polypeptide 1B1, **UGT1A9:** uridine 5′-diphosphoglucuronosyltransferase 1A9.

Fig. 2 Probenecid plasma concentrations. (**a**) Selected population predictions of probenecid plasma concentration-time profiles compared to observed data in semilogarithmic (upper panel) and linear plots (lower panel). Observed data are shown as dots ± standard deviation (42,54,55). Population simulation arithmetic means are shown as lines; the shaded areas illustrate the predicted population variation ($Q_{16} - Q_{84}$). (**b**) Predicted compared to observed probenecid plasma concentration values of all analyzed clinical studies. The solid line marks the line of identity. The dotted lines indicate 1.25-fold, the dashed lines indicate 2-fold deviation. Details on dosing regimens, study populations and literature references are summarized in Table S2.2.1. **iv:** intravenous, **po:** oral, **sd:** single dose, **tab:** tablet.

PBPK DDI Performance Evaluation

All DDI predictions were evaluated by comparison of predicted *versus* observed victim drug plasma concentration-time profiles alone and during co-administration, DDI AUC_{last} ratios and DDI C_{max} ratios (Eq. 3).

$$\text{DDI PK parameter ratio} = \frac{\text{PK parameter}_{\text{victim drug during co-administration}}}{\text{PK parameter}_{\text{victim drug alone}}} \quad (3)$$

where PK parameter = AUC_{last} or C_{max}.

As quantitative measure of the DDI prediction accuracy, GMFEs of the predicted DDI AUC_{last} ratios and DDI C_{max} ratios were calculated according to Eq. 2.

RESULTS

PBPK Model Building and Evaluation

The probenecid PBPK model was developed using 27 different clinical studies, including intravenous (single dose) and oral (single- and multiple dose) administration. A complete list of the clinical studies used in the presented analysis is provided in Table S2.2.1. In addition, five studies reported fraction excreted unchanged in urine profiles following oral administration. In the intravenous studies, probenecid was administered in doses of 464–1860 mg. In the oral studies, probenecid was administered in doses of 250–2000 mg. The training dataset included 11 probenecid plasma concentration-time profiles and one fraction excreted unchanged in urine profile. The final probenecid model applies uptake into kidney cells via OAT3, glucuronidation mainly in the renal cells by UGT1A9, glomerular filtration and tubular reabsorption,

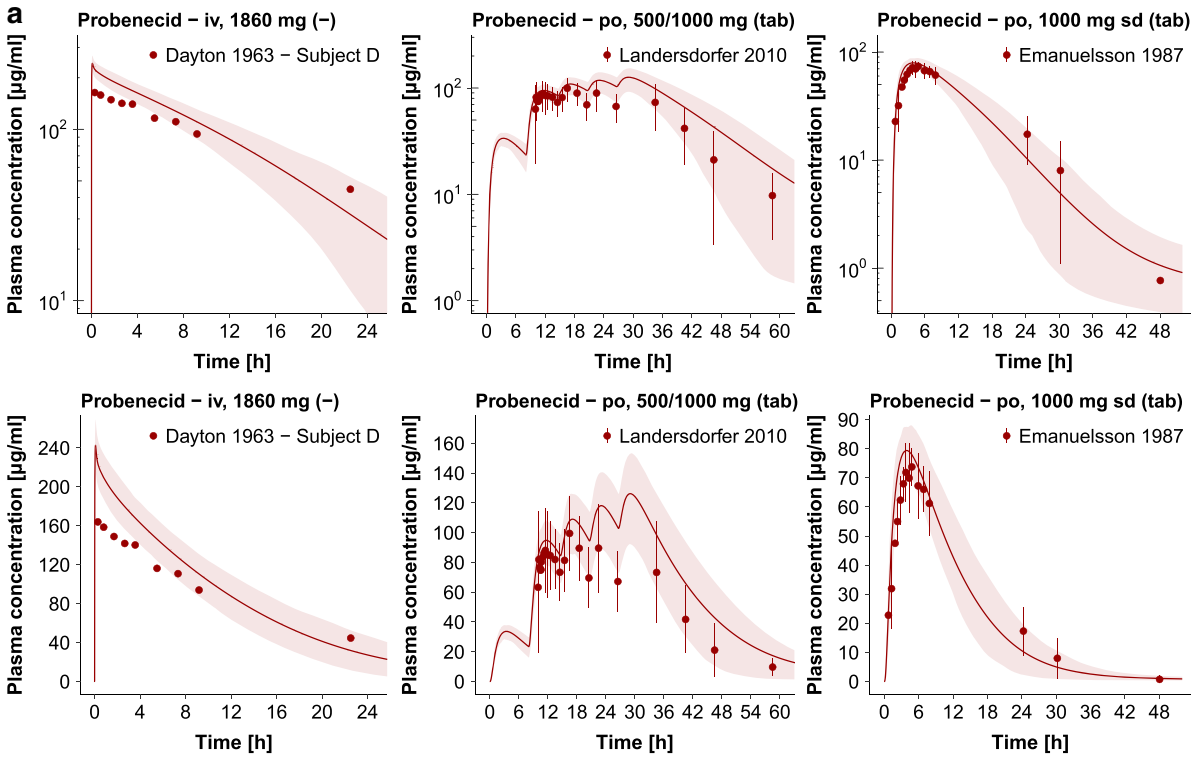
a
Probenecid – iv, 1860 mg (–)
Dayton 1963 – Subject D
Probenecid – po, 500/1000 mg (tab)
Landersdorfer 2010
Probenecid – po, 1000 mg sd (tab)
Emanuelsson 1987
Plasma concentration [µg/ml]
Time [h]

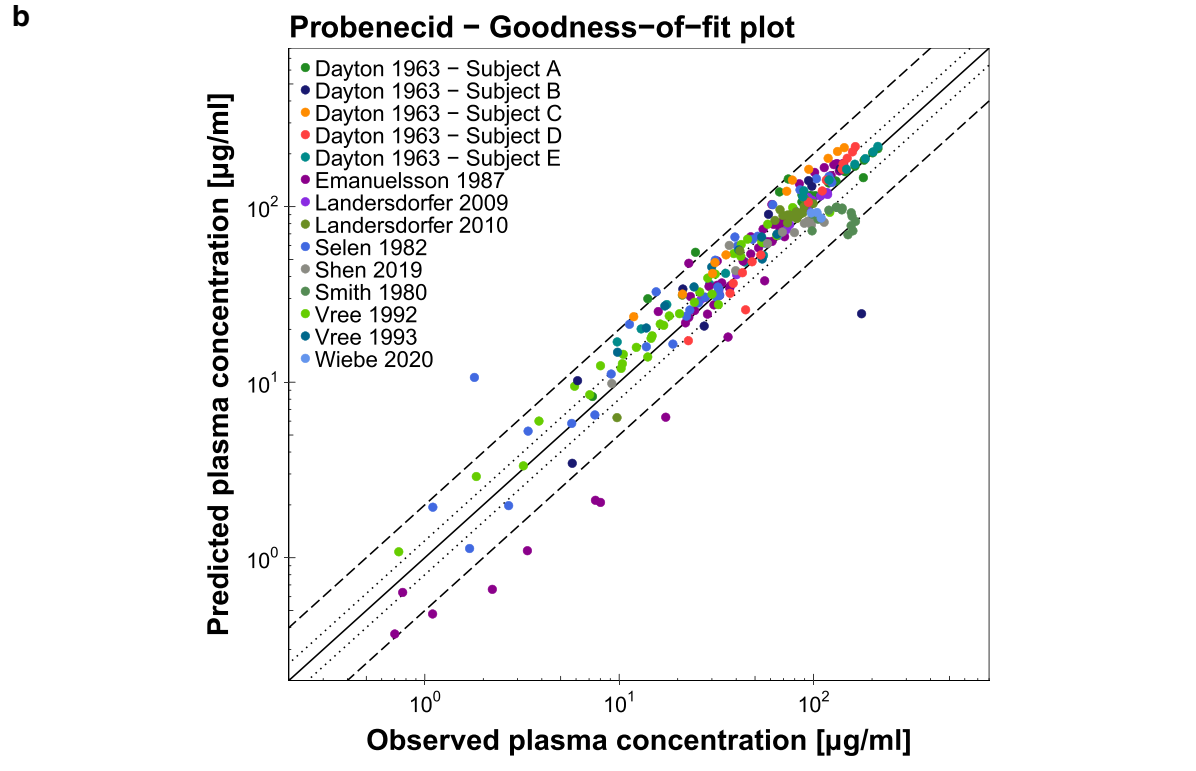
b
Probenecid – Goodness–of–fit plot
Dayton 1963 – Subject A
Dayton 1963 – Subject B
Dayton 1963 – Subject C
Dayton 1963 – Subject D
Dayton 1963 – Subject E
Emanuelsson 1987
Landersdorfer 2009
Landersdorfer 2010
Selen 1982
Shen 2019
Smith 1980
Vree 1992
Vree 1993
Wiebe 2020
Predicted plasma concentration [µg/ml]
Observed plasma concentration [µg/ml]

which was modeled as a reduction of the glomerular filtration rate (GFR fraction <1). The drug-dependent parameters are summarized in Table S2.3.1.

Population predicted compared to observed plasma concentration-time profiles of selected studies as well as the probenecid goodness-of-fit plot with the predicted plasma concentrations of all studies are presented in Fig. 2. Semilogarithmic and linear plots of the plasma profiles of all 27 clinical studies included in the analysis are shown in the ESM. Population predicted compared to observed fraction excreted unchanged in urine profiles are also presented in the ESM. Table S2.5.1 lists the MRD values of all 27 studies.

The correlation of predicted and observed probenecid AUC_{last} and C_{max} values is presented in Fig. 3, further demonstrating the good model performance with 27/27 predicted AUC_{last} and 18/18 predicted C_{max} values within 2-fold of the observed data. The individual values, mean GMFE values and ranges are listed in Table S2.5.2.

The sensitivity analysis results of a simulation of 500 mg probenecid twice daily as a tablet are illustrated in Fig. S2.5.3. Applying a threshold of 0.5, the probenecid model is sensitive to the values of the UGT1A9 catalytic rate constant (optimized) and Michaelis-Menten constant (literature value), the probenecid fraction unbound in plasma (literature value), the OAT3 catalytic rate constant (optimized) and the probenecid lipophilicity (optimized).

The furosemide PBPK model was developed using 42 different clinical studies, including intravenous (single dose) and oral (single- and multiple dose) administration. A complete list of the clinical studies used in the presented analysis is provided in Table S3.2.1. In addition, 27 studies reported fraction excreted unchanged in urine profiles following intravenous and oral administration. In the intravenous studies, furosemide was administered in doses of 20–80 mg. In the oral studies, furosemide was administered in doses of 1–80 mg. The training dataset included 14 furosemide plasma concentration-time profiles, 11 fraction excreted unchanged in urine profiles and one plasma concentration-time profile with corresponding fraction excreted unchanged in urine data of furosemide during co-administration of probenecid (32). The final furosemide model applies uptake into kidney cells via OAT3, glucuronidation by UGT1A9, secretion into urine via MRP4 and glomerular filtration. The drug-dependent parameters are summarized in Table S3.3.1.

Population predicted compared to observed plasma concentration-time profiles of selected studies as well as the furosemide goodness-of-fit plot with the predicted plasma concentrations of all studies are presented in Fig. 4. Semilogarithmic and linear plots of the plasma profiles of all

Fig. 4 Furosemide plasma concentrations. (**a**) Selected population predictions of furosemide plasma concentration-time profiles compared to observed data in semilogarithmic (upper panel) and linear plots (lower panel). Observed data are shown as dots ± standard deviation (56–58). Population simulation arithmetic means are shown as lines; the shaded areas illustrate the predicted population variation (Q_{16} – Q_{84}). (**b**) Predicted compared to observed furosemide plasma concentration values of all analyzed clinical studies. The solid line marks the line of identity. The dotted lines indicate 1.25-fold, the dashed lines indicate 2-fold deviation. Details on dosing regimens, study populations and literature references are summarized in Table S3.2.1. **iv:** intravenous, **po:** oral, **qd:** once daily, **sd:** single dose, **sol:** solution, **tab:** tablet.

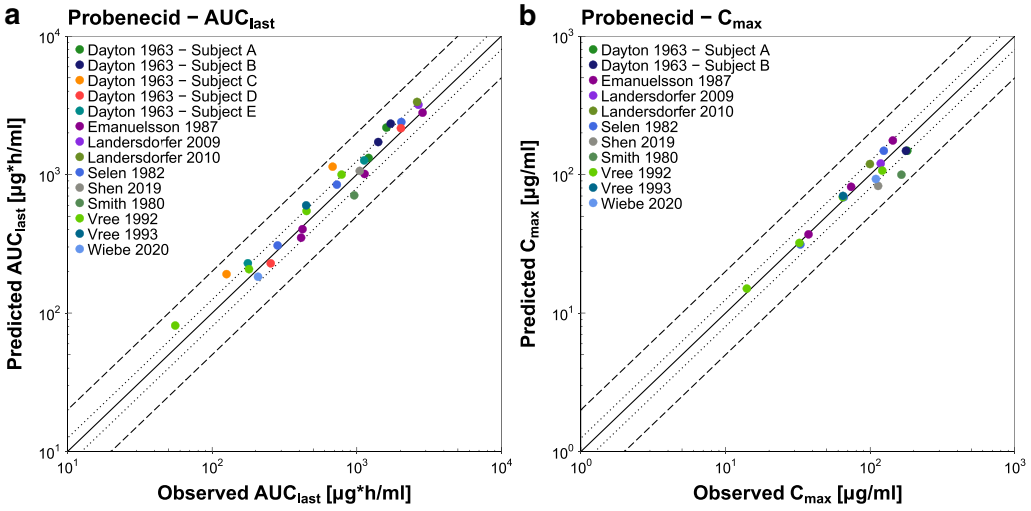

Fig. 3 Probenecid AUC_{last} and C_{max} values. Predicted compared to observed probenecid (**a**) AUC_{last} and (**b**) C_{max} values of all analyzed clinical studies. The solid line marks the line of identity. The dotted lines indicate 1.25-fold, the dashed lines indicate 2-fold deviation. Details on dosing regimens, study populations and literature references are summarized in Table S2.2.1. The individual AUC_{last} and C_{max} values, mean GMFE values and ranges are listed in Table S2.5.2. **AUC_{last}:** area under the plasma concentration-time curve from the time of drug administration to the time of the last concentration measurement, **C_{max}:** peak plasma concentration.

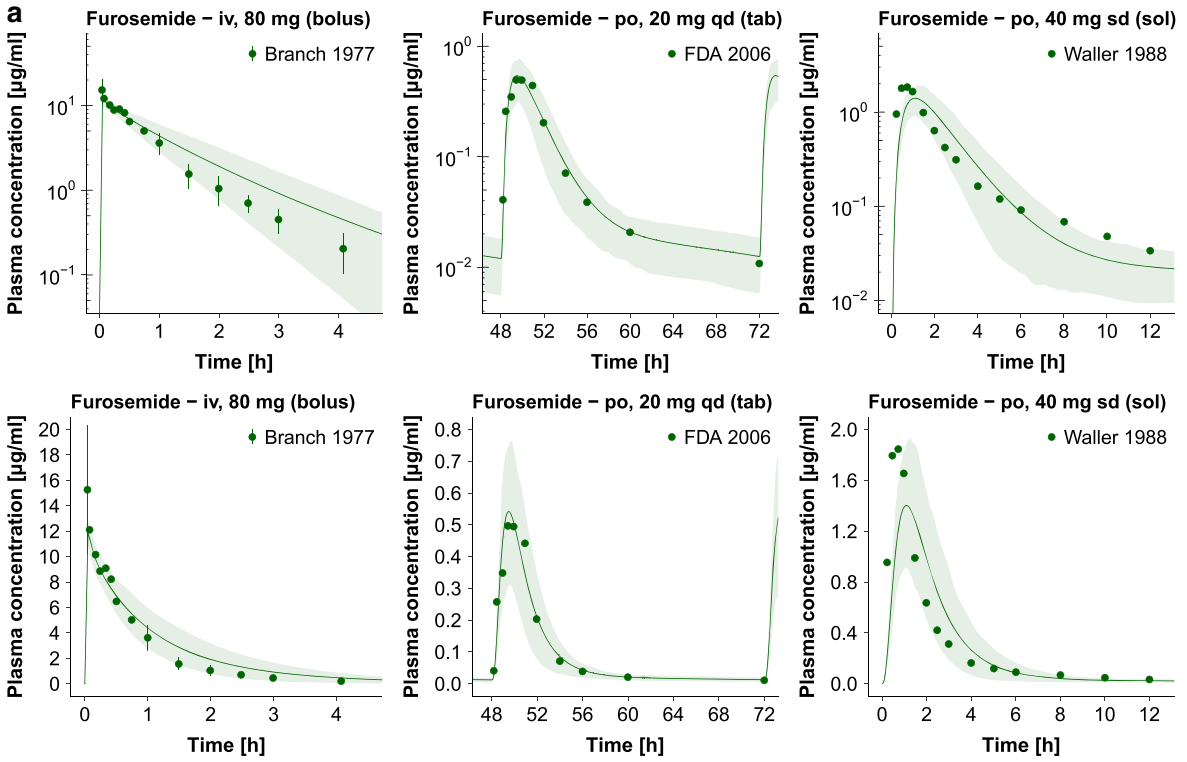
a
Furosemide − iv, 80 mg (bolus)
Branch 1977
Furosemide − po, 20 mg qd (tab)
FDA 2006
Furosemide − po, 40 mg sd (sol)
Waller 1988
Plasma concentration [µg/ml]
Time [h]

Furosemide − iv, 80 mg (bolus)
Branch 1977
Furosemide − po, 20 mg qd (tab)
FDA 2006
Furosemide − po, 40 mg sd (sol)
Waller 1988
Plasma concentration [µg/ml]
Time [h]

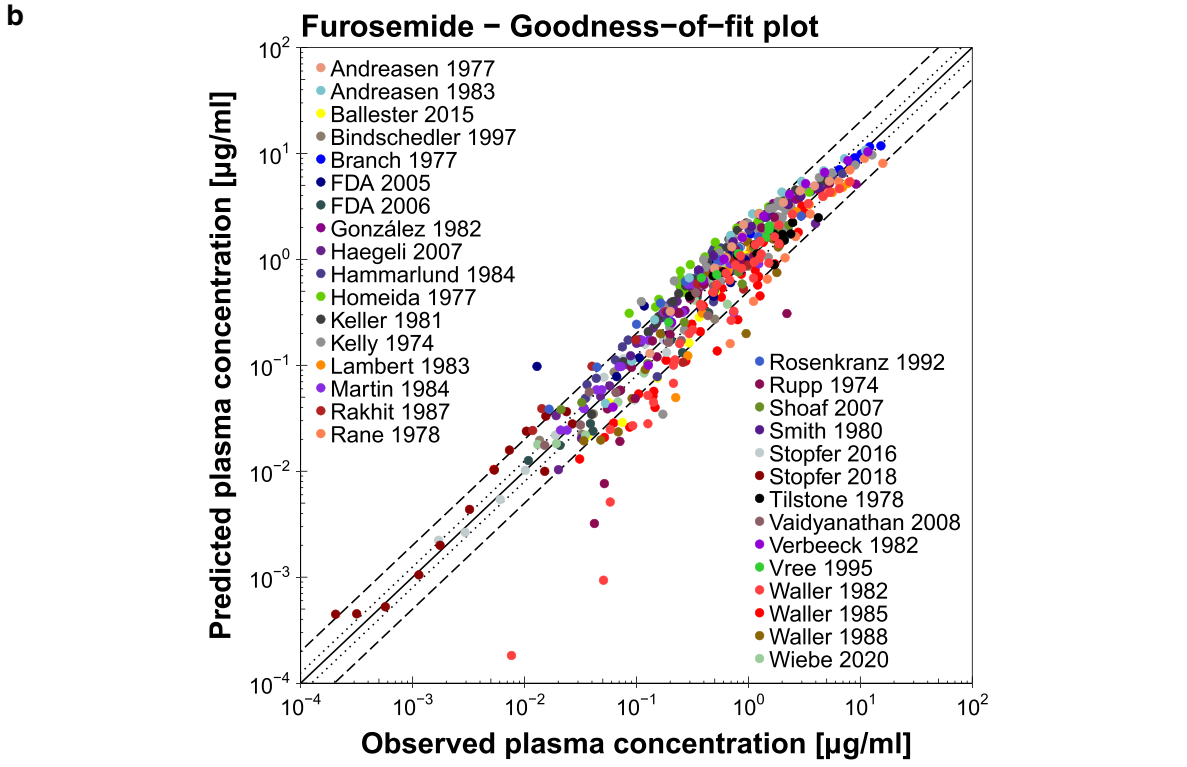
b
Furosemide − Goodness−of−fit plot
Predicted plasma concentration [µg/ml]
Observed plasma concentration [µg/ml]
Andreasen 1977
Andreasen 1983
Ballester 2015
Bindschedler 1997
Branch 1977
FDA 2005
FDA 2006
González 1982
Haegeli 2007
Hammarlund 1984
Homeida 1977
Keller 1981
Kelly 1974
Lambert 1983
Martin 1984
Rakhit 1987
Rane 1978
Rosenkranz 1992
Rupp 1974
Shoaf 2007
Smith 1980
Stopfer 2016
Stopfer 2018
Tilstone 1978
Vaidyanathan 2008
Verbeeck 1982
Vree 1995
Waller 1982
Waller 1985
Waller 1988
Wiebe 2020

42 clinical studies included in the analysis are shown in the ESM. Population predicted compared to observed fraction excreted unchanged in urine profiles are also presented in the ESM. Table S3.5.1 lists the MRD values of all 42 studies.

The correlation of predicted and observed furosemide AUC_{last} and C_{max} values is presented in Fig. 5, further demonstrating the good model performance with 41/42 predicted AUC_{last} and 24/25 predicted C_{max} values within 2-fold of the observed data. The individual values, mean GMFE values and ranges are listed in Table S3.5.2.

The sensitivity analysis results of a simulation of 80 mg furosemide once daily as a tablet are illustrated in Fig. S3.5.3. Applying a threshold of 0.5, the furosemide model is sensitive to the values of furosemide fraction unbound in plasma (literature value) and the OAT3 catalytic rate constant (optimized).

PBPK DDI Modeling and Evaluation

The developed PBPK models were applied to model the probenecid-furosemide and probenecid-rifampicin DDIs and the DDI performance was evaluated using the clinical data of six studies investigating the probenecid-furosemide DDI and one study of the probenecid-rifampicin DDI. For all studies, plasma concentration-time profiles of the victim drugs, administered alone and during probenecid co-administration, were predicted and compared to observed data. In addition, four studies of the probenecid-furosemide DDI reported fraction excreted unchanged in urine profiles, allowing the comparison of predicted and observed urinary excretion under control and DDI conditions. Administration protocols, study population details and references of the clinical DDI studies are listed in Tables S5.2.1 and S6.2.1.

To predict the probenecid-furosemide DDI, competitive inhibition of OAT3 (K_i = 5.41 µmol/l) (15) and non-competitive inhibition of UGT1A9 (K_i = 242.0 µmol/l) (in-house measurement) by probenecid were implemented using interaction parameter values measured *in vitro*. As no information regarding the inhibition of MRP4 could be obtained, the K_i to describe the competitive inhibition of MRP4 (K_i = 87.4 µmol/l) by probenecid was optimized during the parameter identification of the furosemide model. To predict the probenecid-rifampicin DDI, competitive inhibition of OATP1B1 (K_i = 39.8 µmol/l) (9) was implemented using an interaction parameter value measured *in vitro*.

The coupled models adequately describe and predict all furosemide and rifampicin plasma concentration-time profiles, as well as fraction excreted unchanged in urine profiles of furosemide, under control conditions and during probenecid co-administration, over the full range of reported DDI administration protocols. Population predicted compared to observed plasma profiles of furosemide and rifampicin, administered alone and during the DDIs, are presented in Fig. 6 (selected DDI studies). Semilogarithmic and linear plots of all 7 clinical DDI studies included in the analysis are shown in Sections 5.3 and 6.3 of the ESM. Predicted compared to observed furosemide fraction excreted unchanged in urine profiles, administered alone and during probenecid co-administration, are presented in the ESM.

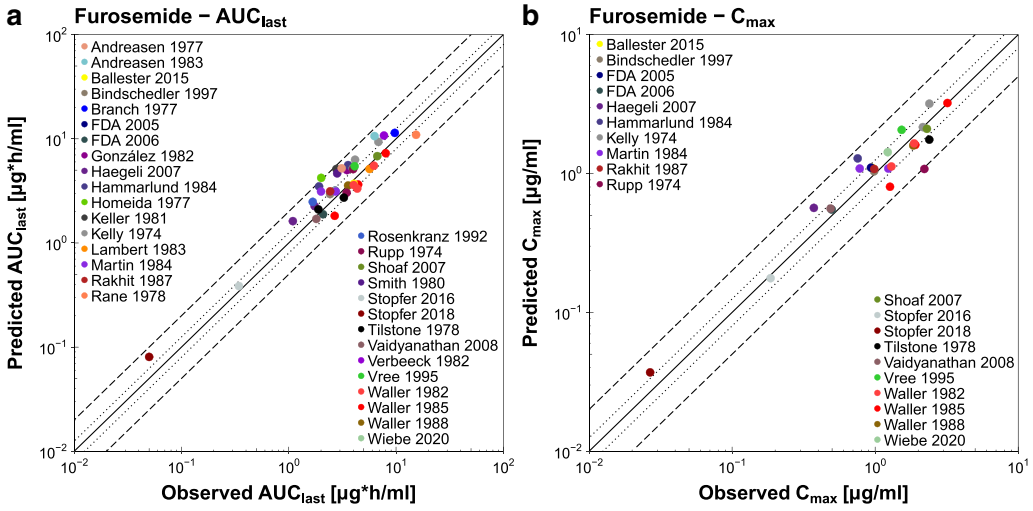

Fig. 5 Furosemide AUC_{last} and C_{max} values. Predicted compared to observed furosemide (**a**) AUC_{last} and (**b**) C_{max} values of all analyzed clinical studies. The solid line marks the line of identity. The dotted lines indicate 1.25-fold, the dashed lines indicate 2-fold deviation. Details on dosing regimens, study populations and literature references are summarized in Table S3.2.1. The individual AUC_{last} and C_{max} values, mean GMFE values and ranges are listed in Table S3.5.2. **AUC_{last}:** area under the plasma concentration-time curve from the time of drug administration to the time of the last concentration measurement, **C_{max}:** peak plasma concentration.

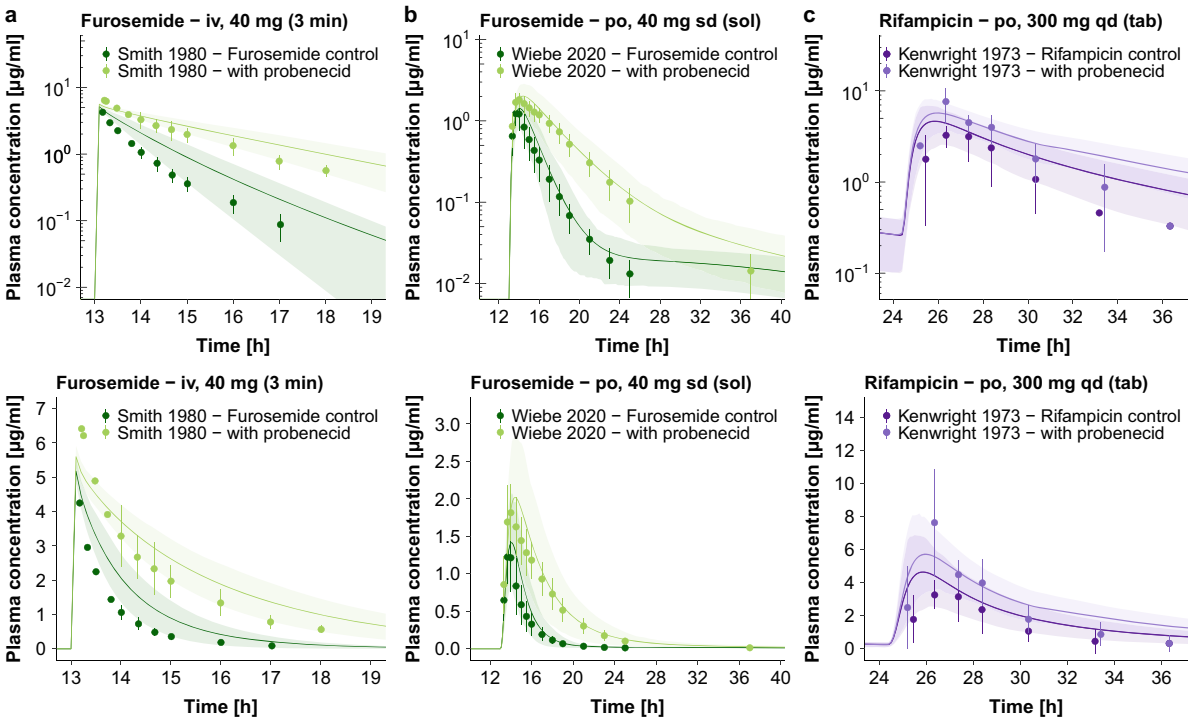

Fig. 6 DDI plasma concentration-time profiles. Selected population predictions of the victim drug plasma concentration-time profiles compared to observed data for the (**a, b**) probenecid-furosemide and **(c)** probenecid-rifampicin DDIs in semilogarithmic (upper panel) and linear plots (lower panel). Observed data are shown as dots ± standard deviation (32,59,60). Population simulation arithmetic means are shown as lines; the shaded areas illustrate the corresponding predicted population variation (Q_{16} – Q_{84}). Details on dosing regimens, study populations and literature references are summarized in Tables S5.2.1 and S6.2.1. **iv:** intravenous, **po:** oral, **qd:** once daily, **sd:** single dose, **tab:** tablet.

The correlation of predicted and observed DDI AUC_{last} ratios and DDI C_{max} ratios of all analyzed clinical DDI studies is shown in Fig. 7, further demonstrating the good DDI performance with all predicted DDI ratios within 2-fold of the observed data. The individual ratios, mean GMFE values and ranges for both DDI combinations are listed in Table I.

DISCUSSION

The newly developed whole-body PBPK models for probenecid and furosemide accurately describe the observed plasma concentration-time profiles and fraction excreted unchanged in urine data over the full range of reported doses and administration protocols. Furthermore, these models adequately describe the available clinical data from probenecid-furosemide and probenecid-rifampicin clinical DDI studies.

Various other PBPK models of probenecid and furosemide with different applications have been published previously (33–38). For probenecid, three PBPK models are available describing DDIs with drugs that are OAT substrates. However, none of these analyses considered the probenecid-furosemide DDI or extended the model to include UGT1A9, MRP4 or OATP1B1 inhibition (33–35). The previously developed furosemide PBPK models were not built or evaluated for use in DDI prediction (36–38).

Development of the probenecid model was particularly challenging. The number of published clinical studies is low and the quality of the available data varies considerably, as probenecid was approved in the late 1940s. Hence, careful consideration of the study protocols and the presented data was required, and studies in patients or elderly volunteers, studies with co-medication and studies using others than the marketed formulation were excluded for probenecid model development. In addition, information on the ADME processes that govern the pharmacokinetics of probenecid is very limited.

Probenecid shows a low solubility and permeability, indicating an important role of transporters in its absorption and distribution. However, neither *in vitro* nor *in vivo* studies describing transporters involved in probenecid absorption, organ uptake, secretion or reabsorption are available in literature. Therefore, probenecid absorption was described by optimization of the passive transcellular intestinal permeability (optimized value: $3.97 \cdot 10^{-4}$ cm/min, lipophilicity based calculated value: $3.12 \cdot 10^{-6}$ cm/min). The uptake of probenecid into the kidney, which is its site of action and metabolism (39–41), was assumed

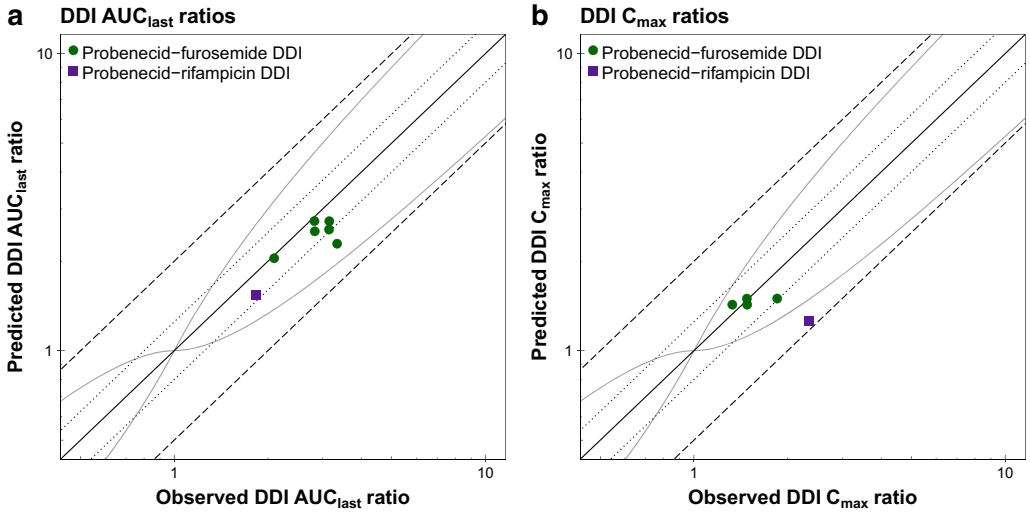

Fig. 7 DDI AUC_{last} and C_{max} ratios. Predicted compared to observed (**a**) DDI AUC_{last} ratios and (**b**) DDI C_{max} ratios of the probenecid-furosemide and probenecid-rifampicin DDIs. The solid line marks the line of identity. The dotted lines indicate 1.25-fold, the dashed lines indicate 2-fold deviation. The curved grey lines show the prediction acceptance limits proposed by Guest *et al.* (61). Details on dosing regimens, the individual DDI AUC_{last} and DDI C_{max} ratios, mean GMFE values and ranges are listed in Table I. **AUC_{last}:** area under the plasma concentration-time curve from the time of drug administration to the time of the last concentration measurement, **C_{max}:** peak plasma concentration, **DDI:** drug-drug interaction.

to be mediated by OAT3. The parameters (K_M, k_{cat}) to describe this transport were optimized during parameter identification (see Table S2.3.1). Furthermore, a low renal clearance (42) and fraction excreted unchanged in urine of only 0.3% to 5% (43,44) are reported, indicating tubular reabsorption. Due to our current lack of knowledge regarding transporters that may contribute to probenecid reabsorption, the GFR fraction was optimized to 0.03. This reduced GFR fraction substitutes for the implementation of active reabsorption processes of probenecid (20) and correctly captures the low probenecid fraction excreted unchanged in urine.

In the clinical studies conducted by Vree *et al.* (43,44), probenecid tablets were broken in half prior to oral administration. The corresponding plasma concentration-time profiles display an earlier time to peak plasma concentration (T_{max}) of 1.6 h compared to the other clinical studies with a T_{max} of 3.3 h. Given the low solubility of probenecid it is possible that the broken tablets show a different dissolution behavior, resulting in faster release and absorption. Therefore, a different dissolution profile was used to describe the studies by Vree *et al.* (43,44). The parameters to model the two different dissolution profiles are listed in Table S2.3.1.

Similar to probenecid, furosemide also demonstrates low solubility and permeability and is classified as a BCS class IV drug (45). Therefore, transporters play an essential role in furosemide absorption, distribution and elimination. Furosemide bioavailability is highly variable (37%–83%) (46), and influenced by dosage form and fasted/fed state of the patient (46). For the absorption of furosemide, Flanagan *et al.* postulate a saturable active transport process and passive diffusion with paracellular contribution in Caco-2 cells (47). As no further information on transporters that may contribute to the absorption of furosemide is available, absorption was modeled as passive transcellular ($5.06 \cdot 10^{-7}$ cm/min) and paracellular ($2.32 \cdot 10^{-6}$ cm/min) intestinal permeability. These processes together allow a rapid absorption in the small intestine to describe the early furosemide T_{max} of 1.0–1.5 h (46), while limiting the furosemide absorption in the large intestine. Other crucial transport processes take place in the kidney, which is the main organ for furosemide metabolism and excretion (fraction excreted unchanged in urine: 20%–80% (46)).

Uptake of furosemide into renal cells *in vivo* is probably facilitated via OAT1 and OAT3. Both transporters are predominantly expressed in the kidney (48) and show a similar affinity to furosemide (OAT1 furosemide K_M = 38.9 µmol/l, OAT3 furosemide K_M = 21.5 µmol/l (49)). Without additional information to distinguish the furosemide transport via these two transporters, the furosemide OAT1 and OAT3 transport rate constants would be highly correlated in a model parameter optimization. To avoid indentifiability issues, renal uptake of furosemide was incorporated via OAT3 only, as a substitute for transport by both, OAT1 and OAT3. The probenecid inhibition potency towards these transporters is also similar (probenecid OAT1 K_i = 11.4 µmol/l, probenecid OAT3 K_i = 5.41 µmol/l (15) and the DDI was predicted via inhibition of OAT3. Furosemide metabolism was modeled using UGT1A9 (50). The pronounced urinary excretion is accomplished by glomerular filtration and active tubular

Table I Predicted and Observed DDI AUC_{last} Ratios and DDI C_{max} Ratios with Mean GMFE Values and Ranges

Probenecid administration		Victim drug administration			DDI AUC_{last} ratio			DDI C_{max} ratio				Reference
Dose [mg]	Route	Dose [mg]	Route	Dose gap [h]	Pred	Obs	Pred/obs	Pred	Obs	Pred/obs	T_{last} [h]	
Intravenous furosemide												
500	po (−), qid (D1-D3)	40	iv (bolus), sd (D4)	2	2.52	2.83	0.89	–	–	–	3.0	Homeida 1977 (62)
1000	po (−), sd (D4)											
1000	po (tab), bid (D1)	40	iv (3 min), sd (D1)	1	2.29	3.34	0.69	–	–	–	4.0	Smith 1980 (59)
GMFE					**1.29 (1.12–1.45)**					–		
					2/2 with GMFE ≤ 2					–		
Oral furosemide												
1000	po (tab), bid (D1)	1	po (sol), sd (D1)	1	2.73	2.82	0.97	1.43	1.33	1.08	12.0	Wiebe 2020 (32)
1000	po (tab), bid (D1)	40	po (sol), sd (D1)	1	2.73	3.15	0.87	1.43	1.48	0.97	12.0	Wiebe 2020 (32)
1000	po (tab), sd (D1)	40	po (tab), sd (D1)	1	2.56	3.14	0.82	1.50	1.85	0.81	12.0	Shen 2019 (63)
1000	po (tab), sd (D1)	80	po (tab), sd (D1)	1	2.05	2.10	0.98	1.50	1.48	1.01	5.0	Vree 1995 (64)
GMFE					**1.11 (1.02–1.22)**			**1.09 (1.01–1.23)**				
					4/4 with GMFE ≤ 2			**4/4 with GMFE ≤ 2**				
Overall GMFE of the probenecid-furosemide DDI					**1.17 (1.02–1.45)**			**1.09 (1.01–1.23)**				
					6/6 with GMFE ≤ 2			**4/4 with GMFE ≤ 2**				
DDI ratios within in the prediction success limits of Guest *et al*. (61)					**6/6 DDI AUC_{last} ratios**			**4/4 DDI C_{max} ratios**				
Oral rifampicin												
2000	po (−), sd (D2)	300	po (tab), qd (D1-D2)	0.33	1.54	1.83	0.84	1.26	2.34	0.54	11.0	Kenwright 1973 (60)
1500	po (−), sd (D2)[a]											
Overall GMFE of the probenecid-rifampicin DDI					**1.19**			**1.85**				
					1/1 with GMFE ≤ 2			**1/1 with GMFE ≤ 2**				
DDI ratios within in the prediction success limits of Guest *et al*. (61)					**1/1 DDI AUC_{last} ratio**			**0/1 DDI C_{max} ratio**				

[a] 2000 mg probenecid 0.33 h before and 1500 mg 6 h after rifampicin administration, **AUC_{last}:** area under the plasma concentration-time curve from the time of drug administration to the time of the last concentration measurement, **bid:** twice daily, **C_{max}:** peak plasma concentration, **D:** day of administration, **DDI:** drug-drug interaction, **GMFE:** geometric mean fold error, **iv:** intravenous, **obs:** observed, **po:** oral, **pred:** predicted, **qid:** four times daily, **qd:** once daily, **route:** route of administration, **sd:** single dose, **sol:** solution, **tab:** tablet, **T_{last}:** time of the last concentration measurement. GMFE values are means and ranges

Bold text marks the main results

secretion. Renal secretion was incorporated via MRP4 (51,52), based on *in vitro* furosemide transport measurements.

In the goodness-of-fit plot, there seems to be an underprediction of the lower furosemide plasma concentrations for two of the intravenous studies (Rupp 1974 and Waller 1982). These are the only two studies that published furosemide plasma concentrations later than 6 h after intravenous dosing, and they did not report their lower limits of quantification. The model is therefore not qualified for the prediction of plasma concentrations later than 6 h after intravenous administration of furosemide. However, this does not affect the prediction of higher plasma concentrations and AUC_{last} values, and the developed model shows a good performance, with 41/42 predicted AUC_{last} and 24/25 predicted C_{max} values within 2-fold of the observed data.

To model the probenecid-furosemide DDI, inhibition of OAT3 alone, using published *in vitro* inhibition parameters, was not sufficient to describe the clinically observed data. Therefore, inhibition of UGT1A9 and MRP4 were added to adequately capture the impact of probenecid on the furosemide pharmacokinetics. Inhibition parameter values for OAT3 (15) and UGT1A9 (in-house measurement) were available from *in vitro* studies. Van Aubel *et al.* reported MRP4 inhibition by probenecid (16), but so far, no inhibition parameter values have been published. Therefore, competitive MRP4 inhibition was assumed and the K_i value was optimized during parameter identification of the furosemide model. Applying the inhibition of OAT3, UGT1A9 and MRP4, all reported plasma concentration time-profiles and fraction excreted unchanged in urine profiles of furosemide during

probenecid co-administration are well described by the presented models.

The probenecid-rifampicin DDI was predicted using a probenecid OATP1B1 inhibition value measured with 2′,7′-dichlorofluorescein as the substrate (9). For OATP1B1, it has been demonstrated that its inhibition can strongly depend on the employed substrate (53). However, since there are no *in vitro* reports of probenecid OATP1B1 inhibition using rifampicin, the DDI was predicted applying the probenecid OATP1B1 K_i = 39.8 µmol/l measured with 2′,7′-dichlorofluorescein (9). Rifampicin is typically not used as OATP1B1 victim drug, but rather as OATP1B1/OATP1B3 inhibitor. However, as the clinical data of this probenecid-rifampicin trial were published, we wanted to utilize them to test our probenecid model. In addition to OATP1B1/OATP1B3 inhibition, rifampicin is also inhibiting and inducing further enzymes and transporters (13). Therefore, an impact of rifampicin on the perpetrator drug probenecid may have influenced the results of this particular DDI administration protocol. Taking into account that the only available clinical study has been published in 1973 and that the reported rifampicin plasma concentrations show considerable standard deviations, this DDI is also well described (see Fig. 6 and Table I).

CONCLUSIONS

The presented whole-body PBPK models of probenecid and furosemide have been carefully built and evaluated for their ability to predict the pharmacokinetics of these drugs, using a multitude of clinical studies. In addition, the models adequately describe the available clinical data of the probenecid-furosemide and probenecid-rifampicin DDIs and will be shared in the Open Systems Pharmacology PBPK model library (www.open-systems-pharmacology.org) as tools to support the investigation of the DDI potential of new compounds during drug development. The ESM to this paper has been compiled to serve as transparent and comprehensive documentation of the probenecid and furosemide model development and evaluation.

SUPPLEMENTARY INFORMATION

The online version contains supplementary material available at https://doi.org/10.1007/s11095-020-02964-z.

ACKNOWLEDGMENTS AND DISCLOSURES

We would like to thank Solvo Biotechnology (Budapest, Hungary) for providing MRP4 vesicles used in the transporter studies. *In vitro* work on MRP4 mediated furosemide transport kinetics was conducted by Revathi Chapa and Bhagwat Prasad at the Department of Pharmaceutics, University of Washington, Seattle, WA, USA. Mitchell E. Taub, Ting Wang, Éric Fernandez, Peter Stopfer and Valerie Nock are employees of Boehringer Ingelheim. Thorsten Lehr has received research grants from Boehringer Ingelheim Pharma GmbH & Co. KG. Hannah Britz, Nina Hanke and Bhagwat Prasad declare that they have no conflict of interest.

FUNDING

Open Access funding enabled and organized by Projekt DEAL. This project has received funding from Boehringer Ingelheim Pharma GmbH & Co. KG.

REFERENCES

1. Liang Y, Li S, Chen L. The physiological role of drug transporters. Protein Cell. 2015;6(5):334–50.
2. U.S. Food and Drug Administration. *In Vitro* Drug Interaction Studies - Cytochrome P450 Enzyme- and Transporter-Mediated Drug Interactions. Guidance for Industry. 2020.
3. European Medicines Agency. Guideline on the investigation of drug interactions. 2015.
4. Motohashi H, Sakurai Y, Saito H, Masuda S, Urakami Y, Goto M, *et al.* Gene expression levels and immunolocalization of organic ion transporters in the human kidney. J Am Soc Nephrol. 2002;13(4):866–74.
5. Mathialagan S, Piotrowski MA, Tess DA, Feng B, Litchfield J, Varma MV. Quantitative prediction of human renal clearance and drug-drug interactions of organic anion transporter substrates using *in vitro* transport data: a relative activity factor approach. Drug Metab Dispos. 2017;45(4):409–17.
6. Vormfelde S, Schirmer M, Hagos Y, Toliat M, Engelhardt S, Meineke I, *et al.* Torsemide renal clearance and genetic variation in luminal and basolateral organic anion transporters. Br J Clin Pharmacol. 2006;62(3):323–35.
7. Nishizato Y, Ieiri I, Suzuki H, Kimura M, Kawabata K, Hirota T, *et al.* Polymorphisms of OATP-C (SLC21A6) and OAT3 (SLC22A8) genes: consequences for pravastatin pharmacokinetics. Clin Pharmacol Ther. 2003;73(6):554–65.

8. U.S. Food and Drug Administration. Drug development and drug interactions: table of substrates, inhibitors and inducers. 2017 [cited 2020 May 19]. Available from: https://www.fda.gov/Drugs/DevelopmentApprovalProcess/DevelopmentResources/DrugInteractionsLabeling/ucm093664.htm
9. Izumi S, Nozaki Y, Komori T, Takenaka O, Maeda K, Kusuhara H, *et al.* Investigation of fluorescein derivatives as substrates of organic anion transporting polypeptide (OATP) 1B1 to develop sensitive fluorescence-based OATP1B1 inhibition assays. Mol Pharm. 2016;13(2):438–48.
10. Kitamura S, Maeda K, Wang Y, Sugiyama Y. Involvement of multiple transporters in the Hepatobiliary transport of Rosuvastatin. Drug Metab Dispos. 2008;36(10):2014–23.
11. Tirona R, Leake B, Wolkoff A, Kim R. Human organic anion transporting polypeptide-C (SLC21A6) is a major determinant of rifampin-mediated pregnane X receptor activation. J Pharmacol Exp Ther. 2003;304(1):223–8.
12. European Medicines Agency. Guideline on the reporting of physiologically based pharmacokinetic (PBPK) modelling and simulation. 2018.
13. U.S. Food and Drug Administration. Clinical Drug Interaction Studies - Study Design, Data Analysis, Implications for Dosing, and Labeling Recommendations. Draft Guidance for Industry. 2017.
14. U.S. Food and Drug Administration. Physiologically Based Pharmacokinetic Analyses - Format and Content. Guidance for Industry. 2018.
15. Tsuruya Y, Kato K, Sano Y, Imamura Y, Maeda K, Kumagai Y, *et al.* Investigation of endogenous compounds applicable to drug-drug interaction studies involving the renal organic anion transporters, OAT1 and OAT3, in humans. Drug Metab Dispos. 2016;44(12):1825–933.
16. Van Aubel RAMH, Smeets PHE, Peters JGP, Bindels RJM, Russel FGM. The MRP4/ABCC4 gene encodes a novel apical organic anion transporter in human kidney proximal tubules: putative efflux pump for urinary cAMP and cGMP. J Am Soc Nephrol. 2002;13(3):595–603.
17. Eissing T, Kuepfer L, Becker C, Block M, Coboeken K, Gaub T, *et al.* A computational systems biology software platform for multiscale modeling and simulation: integrating whole-body physiology, disease biology, and molecular reaction networks. Front Physiol. 2011;2(February):1–10.
18. Lippert J, Burghaus R, Edginton A, Frechen S, Karlsson M, Kovar A, *et al.* Open systems pharmacology community - an open access, open source, open science approach to modeling and simulation in pharmaceutical sciences. CPT Pharmacometrics Syst Pharmacol. 2019;8(12):878–82.
19. Wojtyniak J, Britz H, Selzer D, Schwab M, Lehr T. Data digitizing: accurate and precise data extraction for quantitative systems pharmacology and physiologically-based pharmacokinetic modeling. CPT Pharmacometrics Syst Pharmacol. 2020;9(6):322–31.
20. Open Systems Pharmacology Suite Community. Open Systems Pharmacology Suite Manual. 2018 [cited 2020 May 19]. Available from: https://docs.open-systems-pharmacology.org/
21. Valentin J. Basic anatomical and physiological data for use in radiological protection: reference values. A report of age- and gender-related differences in the anatomical and physiological characteristics of reference individuals. ICRP publication 89. Ann ICRP. 2002;32(3–4):5–265.
22. Willmann S, Höhn K, Edginton A, Sevestre M, Solodenko J, Weiss W, *et al.* Development of a physiology-based whole-body population model for assessing the influence of individual variability on the pharmacokinetics of drugs. J Pharmacokinet Pharmacodyn. 2007;34(3):401–31.
23. Meyer M, Schneckener S, Ludewig B, Kuepfer L, Lippert J. Using expression data for quantification of active processes in physiologically based pharmacokinetic modeling. Drug Metab Dispos. 2012;40(5):892–901.
24. Tanaka G, Kawamura H. Anatomical and physiological characteristics for asian reference man: male and female of different ages: Tanaka model. Division of Radioecology National Institute of Radiological Sciences Hitachinaka 311–12 Japan. 1996;NIRS-M-115.
25. Open Systems Pharmacology Suite Community. PK-Sim® Ontogeny Database Documentation, Version 7.3. 2018 [cited 2020 May 19]. Available from: https://github.com/Open-Systems-Pharmacology/OSPSuite.Documentation/blob/master/PK-Sim Ontogeny Database Version 7.3.pdf.
26. Hanke N, Frechen S, Moj D, Britz H, Eissing T, Wendl T, *et al.* PBPK models for CYP3A4 and P-gp DDI prediction: a modeling network of rifampicin, itraconazole, clarithromycin, midazolam, alfentanil, and digoxin. CPT Pharmacometrics Syst Pharmacol. 2018;7(10):647–59.
27. Open Systems Pharmacology. OSP repository. 2020 [cited 2020 May 19]. Available from: https://github.com/Open-Systems-Pharmacology
28. Türk D, Hanke N, Wolf S, Frechen S, Eissing T, Wendl T, *et al.* Physiologically based pharmacokinetic models for prediction of complex CYP2C8 and OATP1B1 (SLCO1B1) drug–drug–gene interactions: a modeling network of gemfibrozil, repaglinide, pioglitazone, rifampicin, clarithromycin and itraconazole. Clin Pharmacokinet. 2019;58(12):1595–607.
29. Britz H, Hanke N, Volz A, Spigset O, Schwab M, Eissing T, *et al.* Physiologically-based pharmacokinetic models for CYP1A2 drug-drug interaction prediction: a modeling network of fluvoxamine, theophylline, caffeine, rifampicin, and midazolam. CPT Pharmacometrics Syst Pharmacol. 2019;8(5):296–307.
30. Hanke N, Türk D, Selzer D, Wiebe S, Fernandez É, Stopfer P, *et al.* A mechanistic, Enantioselective, physiologically based pharmacokinetic model of verapamil and Norverapamil, built and evaluated for drug–drug interaction studies. Pharmaceutics. 2020;12(6):556.
31. Kovar L, Schräpel C, Selzer D, Kohl Y, Bals R, Schwab M, *et al.* Physiologically-based pharmacokinetic (PBPK) modeling of buprenorphine in adults. Children and Preterm Neonates Pharmaceutics. 2020;12(6):578.
32. Wiebe S, Giessmann T, Hohl K, Schmidt-Gerets S, Hauel E, Jambrecina A, *et al.* Validation of a drug transporter probe cocktail using the prototypical inhibitors rifampin, probenecid, verapamil, and cimetidine. Clin Pharmacokinet. 2020.
33. Ball K, Jamier T, Parmentier Y, Denizot C, Mallier A, Chenel M. Prediction of renal transporter-mediated drug-drug interactions for a drug which is an OAT substrate and inhibitor using PBPK modelling. Eur J Pharm Sci. 2017;106:122–32.
34. Hsu V, de L. T. Vieira M, Zhao P, Zhang L, Zheng J, Nordmark A, *et al.* Towards quantitation of the effects of renal impairment and probenecid inhibition on kidney uptake and efflux transporters, using physiologically based pharmacokinetic modelling and simulations. Clin Pharmacokinet 2014;53(3):283–293.
35. Posada M, Cannady E, Payne C, Zhang X, Bacon J, Pak Y, *et al.* Prediction of transporter-mediated drug-drug interactions for baricitinib. Clin Transl Sci. 2017;10(6):509–19.
36. Hansmann S, Darwich A, Margolskee A, Aarons L, Dressman J. Forecasting oral absorption across biopharmaceutics classification system classes with physiologically based pharmacokinetic models. J Pharm Pharmacol. 2016;68(12):1501–15.
37. Otsuka K, Wagner C, Selen A, Dressman J. Prediction of in-vivo pharmacokinetic profile for immediate and modified release oral dosage forms of furosemide using an in-vitro-in-silico-in-vivo approach. J Pharm Pharmacol. 2015;67(5):651–65.
38. Schlender J, Meyer M, Thelen K, Krauss M, Willmann S, Eissing T, *et al.* Development of a whole-body physiologically based

pharmacokinetic approach to assess the pharmacokinetics of drugs in elderly individuals. Clin Pharmacokinet. 2016;55(12):1573–89.
39. Ito Y, Fukami T, Yokoi T, Nakajima M. An orphan esterase ABHD10 modulates probenecid acyl glucuronidation in human liver. Drug Metab Dispos. 2014;42(12):2109–16.
40. Margaillan G, Rouleau M, Fallon JK, Caron P, Villeneuve L, Turcotte V, *et al.* Quantitative profiling of human renal UDP-glucuronosyltransferases and glucuronidation activity: a comparison of normal and tumoral kidney tissues. Drug Metab Dispos. 2015;43(4):611–9.
41. Enomoto A, Kimura H, Chairoungdua A, Shigeta Y, Jutabha P, Cha SH, *et al.* Molecular identification of a renal urate-anion exchanger that regulates blood urate levels. Nature. 2002;417(6887):447–52.
42. Dayton P, Yu T, Chen W, Berger L, West L, Gutman A. The physiological disposition of probenecid, including renal clearance, in man, studied by an improved method for its estimation in biological material. J Pharmacol Exp Ther. 1963;140:278–86.
43. Vree T, Van Ewijk-Beneken KE, Wuis E, Hekster Y. Capacity-limited renal glucuronidation of probenecid by humans. A pilot Vmax-finding study. Pharm Weekbl Sci. 1992;14(5):325–31.
44. Vree T, Van Ewijk-Beneken KE, Wuis E, Hekster Y, Broekman M. Interindividual variation in the capacity-limited renal glucuronidation of probenecid by humans. Pharm World Sci. 1993;15(5):197–202.
45. Granero G, Longhi M, Mora M, Junginger H, Midha K, Shah V, *et al.* Biowaiver monographs for immediate release solid oral dosage forms: furosemide. J Pharm Sci. 2010;99(6):2544–56.
46. Ponto L, Schoenwald R. Furosemide (frusemide). A pharmacokinetic/pharmacodynamic review (part I). Clin Pharmacokinet. 1990;18(5):381–408.
47. Flanagan S, Takahashi L, Liu X, Benet L. Contributions of saturable active secretion, passive transcellular, and paracellular diffusion to the overall transport of furosemide across adenocarcinoma (Caco-2) cells. J Pharm Sci. 2002;91(4):1169–77.
48. Sun W, Wu R, Van Poelje P, Erion M. Isolation of a family of organic anion transporters from human liver and kidney. Biochem Biophys Res Commun. 2001;283(2):417–22.
49. Ebner T, Ishiguro N, Taub M. The use of transporter probe drug cocktails for the assessment of transporter-based drug–drug interactions in a clinical setting - proposal of a four component transporter cocktail. J Pharm Sci. 2015;104(9):3220–8.
50. Kerdpin O, Knights KM, Elliot DJ, Miners JO. *In vitro* characterisation of human renal and hepatic frusemide glucuronidation and identification of the UDP-glucuronosyltransferase enzymes involved in this pathway. Biochem Pharmacol. 2008;76(2):249–57.
51. Hasegawa M, Kusuhara H, Adachi M, Schuetz J, Takeuchi K, Sugiyama Y. Multidrug resistance-associated protein 4 is involved in the urinary excretion of hydrochlorothiazide and furosemide. J Am Soc Nephrol. 2007;18(1):37–45.
52. Flanagan S, Cummins C, Susanto M, Liu X, Takahashi L, Benet L. Comparison of furosemide and vinblastine secretion from cell lines overexpressing multidrug resistance protein (P-glycoprotein) and multidrug resistance-associated proteins (MRP1 and MRP2). Pharmacology. 2002;64(3):126–34.
53. Izumi S, Nozaki Y, Maeda K, Komori T, Takenaka O, Kusuhara H, *et al.* Investigation of the impact of substrate selection on *in vitro* organic anion transporting polypeptide 1B1 inhibition profiles for the prediction of drug-drug interactions. Drug Metab Dispos. 2015;43(2):235–47.
54. Landersdorfer C, Kirkpatrick C, Kinzig M, Bulitta J, Holzgrabe U, Jaehde U, *et al.* Competitive inhibition of renal tubular secretion of ciprofloxacin and metabolite by probenecid. Br J Clin Pharmacol. 2010;69(2):167–78.
55. Emanuelsson B, Beermann B, Paalzow L. Non-linear elimination and protein binding of probenecid. Eur J Clin Pharmacol. 1987;32(4):395–401.
56. Branch R, Roberts C, Homeida M, Levine D. Determinants of response to frusemide in normal subjects. Br J Clin Pharmacol. 1977;4(2):121–7.
57. U.S. Food and Drug Administration. Clinical Pharmacology and Biopharmaceutics Review - NDA: 21–913 - part 2. 2006. p. 163–362.
58. Waller E, Crismon M, Smith R, Bauza M, Doluisio J. Comparative bioavailability of furosemide from solution and 40 mg tablets with different dissolution characteristics following oral administration in normal men. Biopharm Drug Dispos. 1988;9(2):211–8.
59. Smith D, Gee W, Brater D, Lin E, Benet L. Preliminary evaluation of furosemide–probenecid interaction in humans. J Pharm Sci. 1980;69(5):571–5.
60. Kenwright S, Levi AJ. Impairment of hepatic uptake of rifamycin antibiotics by probenecid, and its therapeutic implications. Lancet (London, England). 1973;2(7843):1401–5.
61. Guest E, Aarons L, Houston J, Rostami-Hodjegan A, Galetin A. Critique of the two-fold measure of prediction success for ratios: application for the assessment of drug-drug interactions. Drug Metab Dispos. 2011;39(2):170–3.
62. Homeida M, Roberts C, Branch R. Influence of probenecid and spironolactone on furosemide kinetics and dynamics in man. Clin Pharmacol Ther. 1977;22(4):402–9.
63. Shen H, Holenarsipur V, Mariappan T, Drexler D, Cantone J, Rajanna P, *et al.* Evidence for the validity of pyridoxic acid (PDA) as a plasma-based endogenous probe for OAT1 and OAT3 function in healthy subjects. J Pharmacol Exp Ther. 2019;368(1):136–45.
64. Vree T, van den Biggelaar-Martea M, Verwey-van WC. Probenecid inhibits the renal clearance of frusemide and its acyl glucuronide. Br J Clin Pharmacol. 1995;39(6):692–5.

5

DISCUSSION, FUTURE DIRECTIONS AND CONCLUSION

5.1 DISCUSSION

Pharmacometrics and PBPK modeling, in particular, play a crucial role during drug development. The number of drug regulatory submissions including PBPK modeling has increased over the last years both at the FDA and the EMA (see figure 5.1) [59, 61].

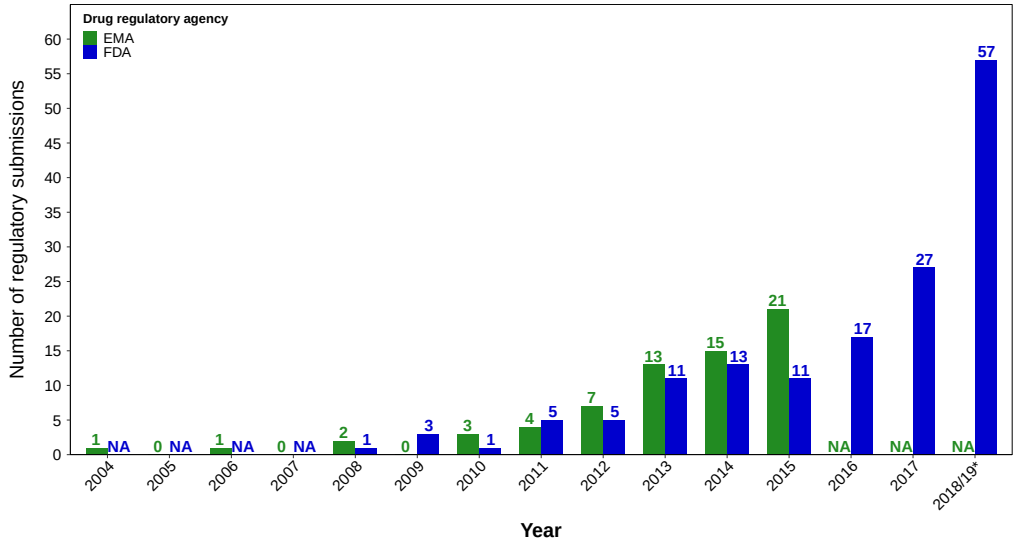

Figure 5.1: PBPK models in drug regulatory submissions. Number of drug regulatory submissions including PBPK analyses for the EMA (2004–2015) and FDA (2008–2019) [59–61]. *The data on submissions for the years 2018 and 2019 are available as a combined total, with no separate breakdown for each year. EMA: European Medicines Agency, FDA: U.S. Food and Drug Administration, NA: not available

The PBPK model submissions reflect its different application areas. The purpose of the PBPK analyses in these submissions includes the description of PK parameters in general and in the presence of organ insufficiencies (kidney or liver) or genetic polymorphisms. Furthermore, PBPK analyses for special populations (e.g. pediatrics) and for the prediction of metabolizing enzyme- or transporter-based DDIs have been submitted to the drug regulatory agencies [59–61]. The importance of PBPK modeling for the investigation of DDIs is evident in the investigational new drugs and new drug applications submissions to the FDA in the years 2018 and 2019. A total of 56% of these submissions included PBPK analyses to investigate metabolizing enzyme- and transporter-mediated DDIs [60].

5.1.1 *PBPK model development and evaluation*

In the context of DDI modeling, selecting a PBPK modeling platform and model type that ensures a high degree of interoperability is essential. This requires the use of a model that captures the required physiological and pharmacokinetic characteristics across various scenarios. Whole-body PBPK models are a suitable choice. These models provide a comprehensive representation of physiological parameters, including blood flow, enzyme and transporter distribution and their expression in different organs. This detailed representation facilitates more accurate predictions of drug distribution, metabolism and potential DDIs. Compared to minimal PBPK models or other pharmacometric approaches, whole-body PBPK models provide a framework to account for inter-individual variability, including factors like age, sex and genetics, thereby enhancing the predictive power.
For projects I-III, a PBPK modeling platform was selected that allows the development of flexible and expandable whole-body PBPK models. Additionally, the developed PBPK models were made freely accessible to the PBPK modeling community after successful evaluation and application for PBPK DDI modeling. Hence, the modeling platform Open Systems Pharmacology (OSP)-Suite® was used. The OSP-Suite® is an open-source platform providing a versatile model structure for predicting PK across various species and administration routes [102, 104]. In addition, the platform meets the predictive capability requirements set by regulatory agencies for the intended application of the models in predicting DDIs [62, 63, 105]. Whole-body PBPK models that have already been developed in the OSP framework are made publicly accessible in the OSP PBPK model library [66]. These models have been evaluated for their good predictive performance during their development. Furthermore, the continued applicability of these models despite changes in software versions is enabled by the existing framework for (re-)qualification [105]. This continuous evaluation of the PBPK models is essential in the development of PBPK DDI networks to ensure model compatibility across software versions. By integrating new data, refining parameters and incorporating technological advances, PBPK models can adequately predict drug PK, thus enhancing drug development.
When building the individual PBPK models, the quality of published *in vitro* and *in vivo* studies employed for the selection of system- and drug-dependent parameters is of importance [106]. Clinical trial data are almost exclusively published as mean concentration-time profiles and mean PK parameters and are often exclusively used for PBPK model building and evaluation [107]. However, individual concentration-time profiles and PK parameters are rarely reported in clinical study reports. The incorporation of individual data enables a more precise characterization and understanding of drug distribution, metabolism and elimination and their impacts on drug PK. Nevertheless, the use of individual data can increase complexity and introduce greater uncertainty, especially when data points are limited. Using mean concentration-time profiles and PK parameters can obscure between-subject variability and introduce potential bias, particularly from extreme values, such as very high or low measurements, which can skew the mean and affect the accuracy of the analysis. To use the available concentration-time profiles for PBPK model development, conversion to numerical values using data digitization software is required. In projects I-III, data digitization software

was used, which has been evaluated and provides data with high precision and accuracy, thereby enabling a robust representation of the available data [103]. Following careful data curation, these digitized datasets can be incorporated into the modeling platform for use as either training or test dataset. A sensitivity analysis integrated into the model evaluation should assess the potential impact of possible biases and determine the robustness of the PBPK model [58, 108].

5.1.2 *PBPK DDI modeling*

In the development of individual PBPK models, accurate representation of drug properties, including physicochemical characteristics and metabolic pathways, is essential. Additionally, the incorporation of inter-individual variability, such as age and sex, enhances the predictive power of PBPK models. Metabolism and excretion processes of a drug of interest can be implemented in PBPK models with generic unspecific processes that may be sufficient to describe drug PK [33]. However, DDIs are generally mediated by specific metabolizing enzymes or transporters involved in the ADME processes of drugs. Hence, generic implementation of these processes in PBPK models is typically inadequate to describe or predict DDIs [19]. Metabolizing enzymes and transporters that play a pivotal role in the ADME processes of a drug should be considered in the PBPK model and adequately represented in the different organs according to protein expression data from the literature [33, 109–120].
The flexibility and quality of the developed whole-body PBPK models are showcased by the rifampicin model presented in this thesis. The rifampicin PBPK model was initially developed to examine the impact of CYP3A4 and Pgp induction and inhibition on the PK of CYP3A4 and Pgp substrates [121]. Moreover, rifampicin itself is a Pgp substrate, as well as an inducer and inhibitor of numerous other enzymes and transporters [122–133]. To investigate additional DDIs, the rifampicin PBPK model was used to evaluate a newly developed theophylline PBPK model. This involved incorporating interaction parameters for CYP1A2 and CYP2E1 induction into the rifampicin PBPK model to predict the rifampicin-theophylline DDI in this thesis [134]. Subsequent investigations included the incorporation of CYP2B6, CYP2C8, CYP2C19, UGT2B7, OATP1B1, OATP1B3 induction and CYP2B6, CYP2C8, UGT2B7, OATP1B1, OATP1B3 inhibition parameters in the whole-body PBPK model of rifampicin. Consequently, rifampicin-theophylline, rifampicin-caffeine, rifampicin-efavirenz, rifampicin-bupropion, rifampicin-pioglitazone, rifampicin-repaglinide, rifampicin-clopidogrel and rifampicin-quinidine DDIs could be adequately described and predicted [134–139].
It is imperative for PBPK DDI modeling to either develop or have access to PBPK models of relevant victim and perpetrator drugs as proposed by the FDA or EMA [40, 43, 44]. Access to the public OSP PBPK model library allows the prediction of DDIs, the development of new PBPK DDI networks or the extension of established PBPK DDI networks by using newly developed and library PBPK models. These networks are essential for evaluating complex scenarios involving multiple drugs and their combined effects on various physiological processes. The study conducted by Wendl et al. underscores the significance of whole-body PBPK DDI modeling in drug development [140]. Specifically, their investigation focused

on finerenone, a substrate of CYP3A4. While various clinical studies had been conducted assessing the effect of moderate CYP3A4 perpetrator drugs, there was a notable lack of studies assessing the effect of strong and weak CYP3A4 inhibitors and inducers on the PK of finerenone [140]. To address this gap, Wendl et al. developed and validated a whole-body PBPK model of finerenone to predict CYP3A4 mediated-DDIs with the perpetrator drugs included in the existing CYP3A4-DDI compound network [105, 121, 134, 137, 140]. This comprehensive PBPK DDI modeling approach can be considered as a substitute for costly and time-consuming clinical DDI studies with finerenone as a CYP3A4 victim drug, as it not only provides additional insights into the drug interactions of finerenone with CYP3A4 perpetrator drugs, but also supports drug labeling by predicting the expected extent of CYP3A4 interactions on the PK of finerenone.

5.1.3 *PBPK modeling in special populations*

Clinical PK studies typically include young, healthy individuals, predominantly male individuals and often lack participants with co-morbidities. This may result in an inadequate representation of post-marketing conditions. In contrast, post-marketing patient cohorts are generally characterized by greater heterogeneity and often include individuals of all ages, genders, those with multiple diseases, polypharmacy, organ dysfunction or ethnicity. Clinical studies including special populations, such as children, chronic kidney disease (CKD) patients, pregnant women and the elderly, present unique challenges. Vulnerable populations, particularly the elderly or patients with CKD, are at higher risk of ADRs due to polypharmacy and physiological changes. Conducting studies with these populations is often ethically questionable due to potential risks to participants. As a result, these studies are often costly, requiring specialized protocols and patient monitoring to ensure participant safety and data integrity. To address this limitation, M&S techniques can be applied and are encouraged by the FDA and EMA [45, 47, 64, 141, 142]. Especially PBPK modeling provides a comprehensive and mechanistic approach to understand drug disposition and allows for the inclusion of various physiological factors that may influence drug disposition.
CKD is characterized by kidney damage or an estimated glomerular filtration rate (eGFR) < 60 ml/min/1.73 m² for at least 3 months, regardless of the cause [143]. CKD can be classified into six groups based on eGFR with G1 as normal kidney function (eGFR > 90 ml/min/1.73 m²) and G5 as kidney failure (eGFR < 15 ml/min/1.73 m²). The stage G3 is further divided into G3a and G3b [143]. Kidney damage involves diverse and heterogeneous pathophysiological changes within the kidney that lead to irreversible alterations in the function and structure of the kidneys [144, 145]. CKD has multiple effects on the PK of drugs [146]. Primarily, key PK parameters such as clearance and volume of distribution are altered [146]. Impaired renal function significantly affects drug elimination, especially for drugs that are renally cleared [147]. Changes in the activity of metabolizing enzymes and transporters in patients with CKD, especially those involved in drug metabolism and transport, result in altered drug metabolism and excretion [148–150].
During drug development, it is advisable to include patients across all stages

of CKD in clinical PK studies to gain a comprehensive understanding of renal function and drug disposition, because the impact on drug PK varies across CKD stages [64, 151]. Since CKD patients often take multiple drugs per day, conducting PK studies without patients with polypharmacy can be challenging [152, 153]. In these cases, PBPK modeling can provide significant support for understanding drug disposition or proposing dosing regimens. When developing PBPK models, the physiological changes must be carefully considered for each CKD stage, emphasizing the necessity for separate models to accurately capture the different effects in each stage [154–156]. Starting from a whole-body PBPK model initially evaluated for healthy individuals, various important physiological factors that influence drug disposition, such as the altered glomerular filtration rate, should be included [154].
Furosemide undergoes renal elimination by both active and passive processes [157]. Furosemide is glomerularly filtered, actively taken up into renal cells via OAT and actively secreted into urine via multidrug resistance-associated protein 4 (MRP4) [35, 96, 158]. In CKD patients, the secretory clearance of OAT substrates varies at different stages of the disease [159]. It is hypothesized that not only this reduction but also the additional decline in GFR and non-renal clearance processes lead to reduced drug clearance [160]. The study by Dubinsky et al. used PBPK modeling to determine the reduction of OAT transport at different stages of CKD [161]. The PBPK models of furosemide and probenecid developed in this thesis were used. The study introduces a parameterization for the relative activity of OAT transporters at different stages of renal impairment. This parameterization is based on a novel approach using PBPK DDI modeling with probenecid as the OAT perpetrator drug to estimate the proportion of OAT-mediated secretion of the investigated drugs [161]. This innovative approach using DDI modeling contributes to the understanding of drug disposition in CKD and has implications for drug development by aiding dose selection and clinical trial design. In addition, PBPK CKD models can be used to estimate potential DDI in patients with CKD.

5.1.4 *PBPK drug-gene interaction modeling*

The use of PBPK modeling to assess the impact of DGIs on the PK of drugs represents a significant advancement in pharmacology. DGIs may arise when a patient's genetic profile, specifically concerning metabolizing enzymes or transporters, impacts their capability to metabolize or clear a drug [14]. These variations in pharmacogenes can result in different phenotypes compared to the typical wild-type, as they may alter protein expression, enzyme or transporter activity or inducibility [69, 162].
PBPK modeling enables the integration of genetic information into drug disposition models, allowing for the assessment of how specific genetic variants affect drug ADME parameters. By incorporating data on drug-metabolizing enzymes, transporters and the respective genetic polymorphisms, PBPK models can predict drug concentrations and exposure profiles in individuals with different genetic alterations. These DGI-dependent parameters can be derived from either *in vitro* or *in vivo* studies [106]. *In vitro* parameters, such as K_M, v_{max} or protein expression data, are used within a mechanistic approach and provide a detailed representa-

tion of drug metabolism and transport processes in the PBPK models. Conversely, *in vivo* parameters, such as enzyme activity scores or hepatic clearance, are used within an empirical approach, that relies on observed clinical data to inform model parameters in a PBPK model.
The whole-body PBPK model development of fluvoxamine was supported by PopPK modeling to determine the effect of CYP2D6 phenotype on fluvoxamine clearance [134]. However, most of the studies used for fluvoxamine PBPK model development lacked information on the CYP2D6 phenotype. Consequently, the influence of the CYP2D6 phenotype was considered by incorporating a decrease in enzyme activity (empirical approach). Both the PopPK model and the whole-body PBPK model successfully predicted the impact of the CYP2D6 phenotypes on fluvoxamine clearance [134]. When the corresponding genotypes of the metabolizing enzyme or transporter are available for the development of PBPK DGI models, the effect can be predicted more accurately, as studies by Tuerk et al. and Ruedesheim et al. demonstrate by using a mechanistic approach [137, 163].
The study by Tuerk et al. takes it a step further and utilizes the created PBPK DGI and PBPK DDI models to predict drug-drug-gene interactions (DDGIs) [137]. DDGIs can lead to additional alterations in the PK or PD of the affected drug compared to a DGI or DDI alone. There are three types of DDGIs: a perpetrator drug inhibits or induces the same metabolizing enzyme or transporter affected by a genetic variant; a perpetrator drug affects a different metabolizing enzyme or transporter from that affected by a genetic variant; a genetic variant in an enzyme or transporter gene indirectly affects the PK or PD of a victim drug, leading to a more or less pronounced interaction effect [106]. Using PBPK models, Tuerk et al. were able to predict doses of repaglinide and pioglitazone in complex DDGIs that matched the control AUC without polymorphism and DDI and presented a safe therapeutic dose [137]. This approach demonstrates the versatility of PBPK modeling. By integrating genetic information into drug disposition models, PBPK modeling enables the prediction of drug response based on individual genetic profiles. This approach has significant implications for optimizing drug therapy and reducing adverse events. Ongoing research will further enhance the application of PBPK modeling in medicine and therapeutic decision-making.

5.2 FUTURE DIRECTIONS

The integration of PBPK modeling into the drug development process, especially in model-informed drug discovery and development, represents a promising approach for future research. The process of continuous model evaluation within the OSP platform allows for the incorporation of new data and technological advances to improve model accuracy and precision over time. The availability of the developed PBPK models in this thesis within the OSP PBPK model library enables their utilization for predicting DDIs involving new potential substrates, inhibitors or inducers of CYP3A4, CYP1A2, OAT and Pgp. These models, when integrated into PBPK DDI networks, play a pivotal role in evaluating complex scenarios involving multiple drugs and their combined effects on various physiological processes. Moreover, beyond demonstrating their predictive performance in DDI prediction, these models exhibit further clinical relevance by incorporating DGIs

or considering the impact of CKD. Future directions in PBPK modeling involve these models to predict PK in special populations such as pediatric patients or individuals with comorbidities, thereby expanding their utility in clinical practice. Furthermore, PBPK models offer potential clinical benefits through dose adjustment predictions, enabling customized dosing regimens for specific scenarios such as DDIs, DGIs or vulnerable patient groups. Additionally, the combination of vulnerable populations and DDIs presents another research opportunity that demonstrates the versatility of PBPK modeling in addressing complex clinical scenarios. Through continuous refinement and extension, PBPK modeling holds tremendous potential to advance drug discovery, development and clinical practice and ultimately improve patient outcomes.

5.3 CONCLUSION

A key area of investigation in drug development is the examination of metabolizing enzymes and transporters involved in the ADME processes of drugs. At an early stage of drug development, these investigations contribute to the identification and exploration of potential factors that influence both PK and PD. MIDD, particularly PBPK modeling, plays a crucial role in the investigation of ADME processes of a drug. PBPK modeling provides a valuable tool for improving the understanding of ADME processes of a drug and its potential DDIs. Additionally, it offers the capability to simulate more realistic and complex DDI scenarios, especially in the context of PBPK DDI networks. In the context of this thesis, whole-body PBPK models for representative clinical index metabolizing enzyme and transporter substrates, inhibitors and inducers were developed. In addition, metabolizing enzymes (CYP3A4 and CYP1A2) and transporters (Pgp and OAT) involved in ADME processes of multiple therapeutic drugs were selected. The developed PBPK models have been successfully evaluated for describing plasma concentrations following various administration routes and doses and for predicting different DDIs. The open accessibility of these models in the OSP PBPK model library supports the investigation of new drug candidates within the drug development process [66]. Furthermore, these models facilitate dose-finding studies, particularly for DDIs, DDGIs or organ impairment. This increases the safety of drug therapy for patients.

BIBLIOGRAPHY

1. Brand, A., Allen, L., Altman, M., Hlava, M. & Scott, J. Beyond authorship: Attribution, contribution, collaboration, and credit. *Learned Publishing* **28,** 151–155 (2015).
2. Wissenschaftliches Institut der AOK (WIdO). *Der GKV-Arzneimittelmarkt: Klassifikation, Methodik und Ergebnisse 2022* tech. rep. (2022), 1–120.
3. Puth, M.-T., Weckbecker, K., Schmid, M. & Münster, E. Prevalence of multimorbidity in Germany: Impact of age and educational level in a cross-sectional study on 19,294 adults. *BMC Public Health* **17,** 826 (2017).
4. Van den Bussche, H. & Scherer, M. Das Verbundvorhaben „Komorbidität und Multimorbidität in der hausärztlichen Versorgung" (MultiCare). *Zeitschrift für Gerontologie und Geriatrie* **44,** 73–100 (2011).
5. Bjerrum, L., Gonzalez Lopez-Valcarcel, B. & Petersen, G. Risk factors for potential drug interactions in general practice. *European Journal of General Practice* **14,** 23–29 (2008).
6. Rasool, M. F. *et al.* Assessment of risk factors associated with potential drug-drug interactions among patients suffering from chronic disorders. *PLOS ONE* **18,** e0276277 (2023).
7. Aronson, J. K. & Ferner, R. E. Clarification of terminology in drug safety. *Drug Safety* **28,** 851–870 (2005).
8. Ellison, D. H. & Loffing, J. Thiazide effects and adverse effects. *Hypertension* **54,** 196–202 (2009).
9. Sperber, A. D. Toxic interaction between fluvoxamine and sustained release theophylline in an 11-year-old boy. *Drug Safety* **6,** 460–462 (1991).
10. Stangier, J., Rathgen, K., Stähle, H. & Mazur, D. Influence of renal impairment on the pharmacokinetics and pharmacodynamics of oral dabigatran etexilate: An open-label, parallel-group, single-centre study. *Clinical Pharmacokinetics* **49,** 259–268 (2010).
11. Schurig, A. M. *et al.* Adverse drug reactions and emergencies - the prevalence of suspected ADR in four emergency departments in Germany. *Dtsch Arztebl Int* **115,** 251–8 (2018).
12. Rottenkolber, D. *et al.* Adverse drug reactions in Germany: Direct costs of internal medicine hospitalizations. *Pharmacoepidemiology and Drug Safety* **20,** 626–634 (2011).
13. Robertson, S. & Penzak, S. in *Principles of Clinical Pharmacology* (eds Atkinson, A. J., Abernethy, D. R., Daniels, C. E., Dedrick, R. L. & Markey, S. P.) Second Edi, 229–247 (Elsevier, Burlington, 2007).
14. Verbeurgt, P., Mamiya, T. & Oesterheld, J. How common are drug and gene interactions? Prevalence in a sample of 1143 patients with CYP2C9 , CYP2C19 and CYP2D6 genotyping. *Pharmacogenomics* **15,** 655–665 (2014).

15. Magro, L., Moretti, U. & Leone, R. Epidemiology and characteristics of adverse drug reactions caused by drug–drug interactions. *Expert Opinion on Drug Safety* **11,** 83–94 (2012).

16. Johnell, K. & Klarin, I. The relationship between number of drugs and potential drug-drug interactions in the elderly: A study of over 600,000 elderly patients from the Swedish Prescribed Drug Register. *Drug Safety* **30,** 911–918 (2007).

17. Palleria, C. *et al.* Pharmacokinetic drug-drug interaction and their implication in clinical management. *Journal of research in medical sciences : the official journal of Isfahan University of Medical Sciences* **18,** 601–10 (2013).

18. Corrie, K. & Hardman, J. G. Mechanisms of drug interactions: Pharmacodynamics and pharmacokinetics. *Anaesthesia & Intensive Care Medicine* **18,** 331–334 (2017).

19. Cascorbi, I. Drug interactions - Principles, examples and clinical consequences. *Dtsch Arztebl Int* **109,** 546–556 (2012).

20. Niu, J., Straubinger, R. M. & Mager, D. E. Pharmacodynamic drug-drug interactions. *Clinical Pharmacology & Therapeutics* **105,** 1395–1406 (2019).

21. Knijff-Dutmer, E. A., Schut, G. A. & van de Laar, M. A. Concomitant coumarin-NSAID therapy and risk for bleeding. *Annals of Pharmacotherapy* **37,** 12–16 (2003).

22. Centanni, M. *et al.* Thyroxine in goiter, Helicobacter pylori infection, and chronic gastritis. *New England Journal of Medicine* **354,** 1787–1795 (2006).

23. Sachmechi, I. *et al.* Effect of proton pump inhibitors on serum thyroid-stimulating hormone level in euthyroid patients treated with levothyroxine for hypothyroidism. *Endocrine Practice* **13,** 345–349 (2007).

24. Prakash, C. *et al.* Nuclear receptors in drug metabolism, drug response and drug interactions. *Nuclear Receptor Research* **2** (2015).

25. Jaakkola, T., Backman, J., Neuvonen, M. & Neuvonen, P. Effects of gemfibrozil, itraconazole, and their combination on the pharmacokinetics of pioglitazone. *Clinical Pharmacology & Therapeutics* **77,** 404–414 (2005).

26. Liang, Y., Li, S. & Chen, L. The physiological role of drug transporters. *Protein & Cell* **6,** 334–350 (2015).

27. Giacomini, K. M. *et al.* Membrane transporters in drug development. *Nature Reviews Drug Discovery* **9,** 215–236 (2010).

28. Gurley, B. J., Swain, A., Williams, D. K., Barone, G. & Battu, S. K. Gauging the clinical significance of P-glycoprotein-mediated herb-drug interactions: Comparative effects of St. John's wort, Echinacea, clarithromycin, and rifampin on digoxin pharmacokinetics. *Molecular Nutrition & Food Research* **52,** 772–779 (2008).

29. Bünning, P. in *Drug Discovery and Evaluation: Safety and Pharmacokinetic Assays* (eds Hock, F. J. & Pugsley, M. K.) 975–987 (Springer Berlin Heidelberg, Berlin, Heidelberg, 2013).

30. Ring, B., Wrighton, S. A. & Mohutsky, M. in *Enzyme Kinetics in Drug Metabolism: Fundamentals and Applications* (eds Nagar, S., Argikar, U. A. & Tweedie, D.) 29–50 (Springer US, New York, NY, 2021).

31. Zhao, M. *et al.* Cytochrome P450 enzymes and drug metabolism in humans. *International Journal of Molecular Sciences* **22,** 12808 (2021).

32. Strelow, J. *et al.* in *Assay Guidance Manual* (Eli Lilly & Company and the National Center for Advancing Translational Sciences, Bethesda (MD), 2012).

33. Open Systems Pharmacology Community. *Open Systems Pharmacology Suite Manual* 2023. https://docs.open-systems-pharmacology.org/ (2024).

34. Tsuruya, Y. *et al.* Investigation of endogenous compounds applicable to drug-drug interaction studies involving the renal organic anion transporters, OAT1 and OAT3, in humans. *Drug Metabolism and Disposition* **44,** 1825–1933 (2016).

35. Britz, H. *et al.* Physiologically based pharmacokinetic models of probenecid and furosemide to predict transporter mediated drug-drug interactions. *Pharmaceutical Research* **37,** 250 (2020).

36. Deodhar, M. *et al.* Mechanisms of CYP450 inhibition: Understanding drug-drug interactions due to mechanism-based inhibition in clinical practice. *Pharmaceutics* **12,** 846 (2020).

37. Ito, K., Ogihara, K., Kanamitsu, S.-i. & Itoh, T. Prediction of the in vivo interaction between midazolam and macrolides based on in vitro studies using human liver microsomes. *Drug Metabolism and Disposition* **31,** 945–954 (2003).

38. U.S. Food and Drug Administration. *Clinical pharmacology section of labeling for human biological products - prescription drug and content and format. Guidance for Industry* (2016).

39. European Medicines Agency. *Pharmacokinetic studies in man - Scientific guideline* (2015).

40. European Medicines Agency. *Guideline on the investigation of drug interactions* (2012).

41. U.S. Food and Drug Administration. *In vitro drug interaction studies - Cytochrome P450 enzyme- and transporter-mediated drug interactions. Guidance for Industry* (2020).

42. U.S. Food and Drug Administration. *Clinical drug interaction studies - Cytochrome P450 enzyme- and transporter-mediated drug interactions. Guidance for Industry* (2020).

43. U.S. Food and Drug Administration. Drug development and drug interactions: table of substrates, inhibitors and inducers. https://www.fda.gov/Drugs/DevelopmentApprovalProcess/DevelopmentResources/DrugInteractionsLabeling/ucm093664.htm (2023).

44. U.S. Food and Drug Administration. FDA's examples of drugs that interact with CYP enzymes and transporter systems. https://www.fda.gov/drugs/drug-interactions-labeling/healthcare-professionals-fdas-examples-drugs-interact-cyp-enzymes-and-transporter-systems (2023).

45. Madabushi, R., Seo, P., Zhao, L., Tegenge, M. & Zhu, H. Review: Role of model-informed drug development approaches in the lifecycle of drug development and regulatory decision-making. *Pharmaceutical Research* **39,** 1669–1680 (2022).

46. U.S. Food and Drug Administration. *Innovation or stagnation: Challenge and opportunity on the critical path to new medical products* (2004).

47. Kim, T. H., Shin, S. & Shin, B. S. Model-based drug development: Application of modeling and simulation in drug development. *Journal of Pharmaceutical Investigation* **48,** 431–441 (2018).

48. Manolis, E. *et al.* The role of modeling and simulation in development and registration of medicinal products: Output from the EFPIA/EMA modeling and simulation workshop. *CPT: Pharmacometrics & Systems Pharmacology* **2,** 31 (2013).

49. Williams, P. J., Desai, A. & Ette, E. I. in *Cardiac Drug Development Guide. Methods in Pharmacology and Toxicology.* (ed Pugsley, M. K.) 365–388 (Humana Press, Totowa, NJ, 2003).

50. Usman, M. & Rasheed, H. in *Encyclopedia of Pharmacy Practice and Clinical Pharmacy* (ed Zaheer-Ud-Din Babar) 3B, 227–238 (Elsevier, 2019).

51. Williams, P. J. & Ette, E. I. in *Pharmacometrics: The Science of Quantitative Pharmacology* (eds Ette, E. I. & Williams, P. J.) 1–21 (John Wiley & Sons, Inc., Hoboken, New Jersey, 2007).

52. Mould, D. & Upton, R. Basic concepts in population modeling, simulation, and model-based drug development. *CPT: Pharmacometrics & Systems Pharmacology* **1,** 6 (2012).

53. Peters, S. A. *Physiologically-based pharmacokinetic (PBPK) modeling and simulations: Principles, methods, and applications in the pharmaceutical industry* (John Wiley & Sons, Inc., Hoboken, New Jersey, 2012).

54. Jamei, M., Dickinson, G. L. & Rostami-Hodjegan, A. A framework for assessing inter-individual variability in pharmacokinetics using virtual human populations and integrating general knowledge of physical chemistry, biology, anatomy, physiology and genetics: A tale of 'bottom-up' vs 'top-down' recognition. *Drug Metabolism and Pharmacokinetics* **24,** 53–75 (2009).

55. Mould, D. & Upton, R. Basic concepts in population modeling, simulation, and model-based drug development-part 2: Introduction to pharmacokinetic modeling methods. *CPT: Pharmacometrics & Systems Pharmacology* **2,** 38 (2013).

56. Jones, H. & Rowland-Yeo, K. Basic concepts in physiologically based pharmacokinetic modeling in drug discovery and development. *CPT: Pharmacometrics & Systems Pharmacology* **2,** 1–12 (2013).

57. Rowland, M., Peck, C. & Tucker, G. Physiologically-based pharmacokinetics in drug development and regulatory science. *Annual Review of Pharmacology and Toxicology* **51,** 45–73 (2011).

58. Kuepfer, L. *et al.* Applied concepts in PBPK modeling: How to build a PBPK/PD Model. *CPT: Pharmacometrics & Systems Pharmacology* **5,** 516–531 (2016).

59. Grimstein, M. *et al.* Physiologically based pharmacokinetic modeling in regulatory science: An update from the U.S. Food and Drug Administration's Office of Clinical Pharmacology. *Journal of Pharmaceutical Sciences* **108,** 21–25 (2019).

60. Zhang, X. *et al.* Application of PBPK modeling and simulation for regulatory decision making and its impact on US prescribing information: An update on the 2018-2019 submissions to the US FDA's Office of Clinical Pharmacology. *The Journal of Clinical Pharmacology* **60,** S160–S178 (2020).

61. Luzon, E. *et al.* Physiologically based pharmacokinetic modeling in regulatory decision-making at the European Medicines Agency. *Clinical Pharmacology & Therapeutics* **102,** 98–105 (2017).

62. U.S. Food and Drug Administration. *Physiologically based pharmacokinetic analyses - Format and content. Guidance for Industry* (2018).

63. European Medicines Agency. *Guideline on the reporting of physiologically based pharmacokinetic (PBPK) modelling and simulation* (2018).

64. U.S. Food and Drug Administration. *Guidance for Industry. Pharmacokinetics in patients with impaired renal function: Study design, data analysis, and impact on dosing* (2020).

65. U.S. Food and Drug Administration. *The use of physiologically based pharmacokinetic analyses - Biopharmaceutics applications for oral drug product development , manufacturing changes, and controls. Guidance for Industry* (2020).

66. Open Systems Pharmacology. *OSP repositories* https://github.com/orgs/Open-Systems-Pharmacology/repositories (2024).

67. Shimada, T., Yamazaki, H., Mimura, M., Inui, Y. & Guengerich, F. P. Interindividual variations in human liver cytochrome P-450 enzymes involved in the oxidation of drugs, carcinogens and toxic chemicals: Studies with liver microsomes of 30 Japanese and 30 Caucasians. *The Journal of pharmacology and experimental therapeutics* **270,** 414–23 (1994).

68. Zhou, S.-F., Yang, L.-P., Zhou, Z.-W., Liu, Y.-H. & Chan, E. Insights into the substrate specificity, inhibitors, regulation, and polymorphisms and the clinical impact of human cytochrome P450 1A2. *The AAPS Journal* **11,** 481–494 (2009).

69. Zanger, U. M. & Schwab, M. Cytochrome P450 enzymes in drug metabolism: Regulation of gene expression, enzyme activities, and impact of genetic variation. *Pharmacology & Therapeutics* **138,** 103–141 (2013).

70. Lee, S.-C., Arya, V., Yang, X., Volpe, D. A. & Zhang, L. Evaluation of transporters in drug development: Current status and contemporary issues. *Advanced Drug Delivery Reviews* **116,** 100–118 (2017).

71. Motohashi, H. *et al.* Gene expression levels and immunolocalization of organic ion transporters in the human kidney. *Journal of the American Society of Nephrology* **13,** 866–874 (2002).

72. Mathialagan, S. *et al.* Quantitative prediction of human renal clearance and drug-drug interactions of organic anion transporter substrates using in vitro transport data: A relative activity factor approach. *Drug Metabolism and Disposition* **45,** 409–417 (2017).

73. Patki, K. C., von Moltke, L. L. & Greenblatt, D. J. In vitro metabolism of midazolam, triazolam, nifedipine, and testosterone by human liver microsomes and recombinant cytochromes p450: Role of CYP3A4 and CYP3A5. *Drug Metabolism and Disposition* **31,** 938–944 (2003).

74. Piramal Critical Care Deutschland GmbH. *Fachinformation - RAPIFEN 0,5 mg / ml Injektionslösung* 2022.

75. Kharasch, E. D., Walker, A., Hoffer, C. & Sheffels, P. Intravenous and oral alfentanil as in vivo probes for hepatic and first-pass cytochrome P450 3A activity: Noninvasive assessment by use of pupillary miosis. *Clinical Pharmacology & Therapeutics* **76,** 452–466 (2004).

76. Nordt, S. P. & Clark, R. F. Midazolam: A review of therapeutic uses and toxicity. *The Journal of Emergency Medicine* **15,** 357–365 (1997).

77. Desitin Arzneimittel GmbH. *Fachinformation - Midazolam Desitin® Lösung zur Anwendung in der Mundhöhle* 2023.

78. Heizmann, P., Eckert, M. & Ziegler, W. Pharmacokinetics and bioavailability of midazolam in man. *British Journal of Clinical Pharmacology* **16** (1983).

79. Viatris Healthcare GmbH. *Fachinformation - Klacid® Filmtabletten, 250 mg* 2023.

80. Rodrigues, A. D., Roberts, E. M., Mulford, D. J., Yao, Y. & Ouellet, D. Oxidative metabolism of clarithromycin in the presence of human liver microsomes. Major role for the cytochrome P4503A (CYP3A) subfamily. *Drug metabolism and disposition: the biological fate of chemicals* **25,** 623–30 (1997).

81. JANSSEN-CILAG GmbH. *Fachinformation - SEMPERA® Kapseln* 2023.

82. Janssen Pharmaceutical Companies. *Label - SPORANOX® (itraconazole) Capsules* 2018.

83. Concordia Pharmaceuticals Inc. *Full prescribing information - LANOXIN® (digoxin) tablets, for oral use* 2015.

84. Greiner, B. *et al.* The role of intestinal P-glycoprotein in the interaction of digoxin and rifampin. *Journal of Clinical Investigation* **104,** 147–153 (1999).

85. Aspen Pharma Trading Limited. *Fachinformation - Lenoxin® Tabletten* 2023.

86. Esteve Pharmaceuticals GmbH. *Fachinformation - EREMFAT® 600 mg* 2023.

87. Glenwood GmbH. *Fachinformation - Bronchoretard® 500 forte* 2018.

88. Zhang, Z.-y. & Kaminsky, L. S. Characterization of human cytochromes P450 involved in theophylline 8-hydroxylation. *Biochemical Pharmacology* **50,** 205–211 (1995).

89. Lu, P. *et al.* Mechanism-based inhibition of human liver microsomal cytochrome P450 1A2 by zileuton, a 5-lipoxygenase inhibitor. *Drug Metabolism and Disposition* **31,** 1352–1360 (2003).

90. Karjalainen, M. J., Neuvonen, P. J. & Backman, J. T. Rofecoxib is a potent, metabolism-dependent inhibitor of CYP1A2: Implications for in vitro prediction of drug interactions. *Drug Metabolism and Disposition* **34,** 2091–2096 (2006).

91. neuraxpharm Arzneimittel GmbH. *Fachinformation - Fluvoxamin-neuraxpharm® Filmtabletten* 2020.

92. Miura, M. & Ohkubo, T. Identification of human cytochrome P450 enzymes involved in the major metabolic pathway of fluvoxamine. *Xenobiotica; the fate of foreign compounds in biological systems* **37,** 169–79 (2007).

93. Spigset, O., Axelsson, S., Norström, Å., Hägg, S. & Dahlqvist, R. The major fluvoxamine metabolite in urine is formed by CYP2D6. *European Journal of Clinical Pharmacology* **57,** 653–658 (2001).

94. Spigset, O., Granberg, K., Hägg, S., Norström, Å. & Dahlqvist, R. Relationship between fluvoxamine pharmacokinetics and CYP2D6/CYP2C19 phenotype polymorphisms. *European Journal of Clinical Pharmacology* **52,** 129–133 (1997).

95. Spigset, O., Carleborg, L., Hedenmalm, K. & Dahlqvist, R. Effect of cigarette smoking on fluvoxamine pharmacokinetics in humans. *Clinical Pharmacology & Therapeutics* **58,** 399–403 (1995).

96. Ebner, T., Ishiguro, N. & Taub, M. The use of transporter probe drug cocktails for the assessment of transporter-based drug–drug interactions in a clinical setting - Proposal of a four component transporter cocktail. *Journal of Pharmaceutical Sciences* **104,** 3220–3228 (2015).

97. Sanofi-Aventis Deutschland GmbH. *Fachinformation - Lasix® 40 mg Tabletten Lasix® 500 mg Tabs* 2022.

98. Kerdpin, O., Knights, K. M., Elliot, D. J. & Miners, J. O. In vitro characterisation of human renal and hepatic frusemide glucuronidation and identification of the UDP-glucuronosyltransferase enzymes involved in this pathway. *Biochemical Pharmacology* **76,** 249–257 (2008).

99. Biokanol® Pharma GmbH. *Fachinformation - Probenecid Weimer®* 2010.

100. Ito, Y., Fukami, T., Yokoi, T. & Nakajima, M. An orphan esterase ABHD10 modulates probenecid acyl glucuronidation in human liver. *Drug Metabolism and Disposition* **42,** 2109–2116 (2014).

101. Vree, T. B., Van Ewijk-Beneken Kolmer, E. W. J., Wuis, E. W. & Hekster, Y. A. Capacity-limited renal glucuronidation of probenecid by humans. *Pharmaceutisch Weekblad* **14,** 325–331 (1992).

102. Open Systems Pharmacology. *Open Systems Pharmacology Suite* https://github.com/Open-Systems-Pharmacology (2024).

103. Wojtyniak, J.-G., Britz, H., Selzer, D., Schwab, M. & Lehr, T. Data digitizing: Accurate and precise data extraction for quantitative systems pharmacology and physiologically-based pharmacokinetic modeling. *CPT: Pharmacometrics & Systems Pharmacology* **9,** 322–331 (2020).

104. Hack, C. *et al.* in *Physiologically Based Pharmacokinetic (PBPK) Modeling* (eds Fisher, J. W., Gearhart, J. M. & Lin, Z.) 81–126 (Elsevier, 2020).

105. Frechen, S. *et al.* A generic framework for the physiologically-based pharmacokinetic platform qualification of PK-Sim and its application to predicting cytochrome P450 3A4–mediated drug–drug interactions. *CPT: Pharmacometrics & Systems Pharmacology* **10,** 633–644 (2021).

106. Türk, D. *et al.* Novel models for the prediction of drug-gene interactions. *Expert Opinion on Drug Metabolism & Toxicology* **17,** 1293–1310 (2021).

107. Fossler, M. J. Some thoughts about the mean concentration-versus-time plot. *Clinical Pharmacology in Drug Development* **6,** 220–223 (2017).

108. Frechen, S. & Rostami-Hodjegan, A. Quality assurance of PBPK modeling platforms and guidance on building, evaluating, verifying and applying PBPK models prudently under the umbrella of qualification: Why, when, what, how and by whom? *Pharmaceutical Research* **39,** 1733–1748 (2022).

109. Nishimura, M., Yagutti, H., Yoshitsugu, H., Naito, S. & Satoh, T. Tissue distribution of mRNA expression of human cytochrome P450 isoforms assessed by high-sensitivity real-time reverse transcription PCR. *Yakugaku zasshi* **123,** 369–375 (2003).

110. Meyer, M., Schneckener, S., Ludewig, B., Kuepfer, L. & Lippert, J. Using expression data for quantification of active processes in physiologically based pharmacokinetic modeling. *Drug Metabolism and Disposition* **40,** 892–901 (2012).

111. Nishimura, M. & Naito, S. Tissue-specific mRNA expression profiles of human phase I metabolizing enzymes except for cytochrome P450 and phase II metabolizing enzymes. *Drug Metabolism and Pharmacokinetics* **21,** 357–374 (2006).

112. Greenblatt, D. Time course of recovery of cytochrome p450 3A function after single doses of grapefruit juice. *Clinical Pharmacology & Therapeutics* **74,** 121–129 (2003).

113. Prasad, B. *et al.* Interindividual variability in hepatic organic anion-transporting polypeptides and P-glycoprotein (ABCB1) protein expression: Quantification by liquid chromatography tandem mass spectroscopy and influence of genotype, age, and sex. *Drug Metabolism and Disposition* **42,** 78–88 (2014).

114. Nishimura, M. & Naito, S. Tissue-specific mRNA expression profiles of human ATP-binding cassette and solute carrier transporter superfamilies. *Drug Metabolism and Pharmacokinetics* **20,** 452–477 (2005).

115. Scotcher, D. *et al.* Microsomal and cytosolic scaling factors in dog and human kidney cortex and application for in vitro-in vivo extrapolation of renal metabolic clearance. *Drug Metabolism and Disposition* **45,** 556–568 (2017).

116. Margaillan, G. *et al.* Quantitative profiling of human renal UDP-glucuronosyltransferases and glucuronidation activity: A comparison of normal and tumoral kidney tissues. *Drug Metabolism and Disposition* **43,** 611–619 (2015).

117. Open Systems Pharmacology Community. *PK-Sim® Ontogeny Database Documentation, Version 7.3* 2018.

118. Rodrigues, A. D. Integrated cytochrome P450 reaction phenotyping: Attempting to bridge the gap between cDNA-expressed cytochromes P450 and native human liver microsomes. *Biochemical Pharmacology* **57,** 465–480 (1999).

119. Rowland Yeo, K., Walsky, R., Jamei, M., Rostami-Hodjegan, A. & Tucker, G. Prediction of time-dependent CYP3A4 drug-drug interactions by physiologically based pharmacokinetic modelling: Impact of inactivation parameters and enzyme turnover. *European Journal of Pharmaceutical Sciences* **43,** 160–173 (2011).

120. Prasad, B. *et al.* Abundance of drug transporters in the human kidney cortex as quantified by quantitative targeted proteomics. *Drug Metabolism and Disposition* **44,** 1920–1924 (2016).

121. Hanke, N. *et al.* PBPK models for CYP3A4 and P-gp DDI prediction: A modeling network of rifampicin, itraconazole, clarithromycin, midazolam, alfentanil, and digoxin. *CPT: Pharmacometrics & Systems Pharmacology* **7,** 647–659 (2018).

122. Collett, A., Tanianis-Hughes, J., Hallifax, D. & Warhurst, G. Predicting P-glycoprotein effects on oral absorption: Correlation of transport in Caco-2 with drug pharmacokinetics in wild-type and mdr1a(-/-) mice in vivo. *Pharmaceutical Research* **21,** 819–826 (2004).

123. Ramamoorthy, A. *et al.* Regulation of microRNA expression by rifampin in human hepatocytes. *Drug metabolism and disposition: the biological fate of chemicals* **41,** 1763–8 (2013).

124. Zhang, H. *et al.* Polymorphic variants of cytochrome P450 2B6 (CYP2B6.4-CYP2B6.9) exhibit altered rates of metabolism for bupropion and efavirenz: A charge-reversal mutation in the K139E variant (CYP2B6.8) impairs formation of a functional cytochrome p450-reductase complex. *The Journal of pharmacology and experimental therapeutics* **338,** 803–9 (2011).

125. Soars, M. G., Petullo, D. M., Eckstein, J. A., Kasper, S. C. & Wrighton, S. A. An assessment of udp-glucuronosyltransferase induction using primary human hepatocytes. *Drug metabolism and disposition: the biological fate of chemicals* **32,** 140–8 (2004).

126. Shimokawa, Y. *et al.* Inhibitory potential of twenty five anti-tuberculosis drugs on CYP activities in human liver microsomes. *Biological & Pharmaceutical Bulletin* **38,** 1425–1429 (2015).

127. Rajaonarison, J. F., Lacarelle, B., Catalin, J., Placidi, M. & Rahmani, R. 3'-azido-3'-deoxythymidine drug interactions. Screening for inhibitors in human liver microsomes. *Drug metabolism and disposition: the biological fate of chemicals* **20,** 578–84 (1992).

128. Kajosaari, L. I., Laitila, J., Neuvonen, P. J. & Backman, J. T. Metabolism of repaglinide by CYP2C8 and CYP3A4 in vitro: Effect of fibrates and rifampicin. *Basic Clin Pharmacol Toxicol* **97,** 249–256 (2005).

129. Buckley, D. B., Wiegand, C. M., Prentiss, P. L. & Fahmi, O. A. *Time-course of cytochrome P450 (CYP450) induction in cultured human hepatocytes: Evaluation of activity and mRNA expression profiles for six inducible CYP450 enzymes* 2013. https://www.xenotech.com/wp-content/uploads/2020/05/CYP-Induction-Time-Course-Buckley.pdf.

130. Annaert, P., Ye, Z., Stieger, B. & Augustijns, P. Interaction of HIV protease inhibitors with OATP1B1, 1B3, and 2B1. *Xenobiotica* **40,** 163–176 (2010).

131. Chen, Y., Liu, L., Laille, E., Kumar, G. & Surapaneni, S. In vitro assessment of cytochrome P450 inhibition and induction potential of azacitidine. *Cancer Chemotherapy and Pharmacology* **65,** 995–1000 (2010).

132. Rae, J. M., Johnson, M. D., Lippman, M. E. & Flockhart, D. A. Rifampin is a selective, pleiotropic inducer of drug metabolism genes in human hepatocytes: Studies with cDNA and oligonucleotide expression arrays. *The Journal of pharmacology and experimental therapeutics* **299,** 849–57 (2001).

133. Hirano, M., Maeda, K., Shitara, Y. & Sugiyama, Y. Drug-drug interaction between pitavastatin and various drugs via OATP1B1. *Drug Metabolism and Disposition* **34,** 1229–1236 (2006).

134. Britz, H. *et al.* Physiologically-based pharmacokinetic models for CYP1A2 drug-drug interaction prediction: A modeling network of fluvoxamine, theophylline, caffeine, rifampicin, and midazolam. *CPT: Pharmacometrics & Systems Pharmacology* **8,** 296–307 (2019).

135. Fuhr, L. M., Marok, F. Z., Hanke, N., Selzer, D. & Lehr, T. Pharmacokinetics of the CYP3A4 and CYP2B6 inducer carbamazepine and its drug–drug interaction potential: A physiologically based pharmacokinetic modeling approach. *Pharmaceutics* **13,** 270 (2021).

136. Marok, F. Z., Fuhr, L. M., Hanke, N., Selzer, D. & Lehr, T. Physiologically based pharmacokinetic modeling of bupropion and its metabolites in a CYP2B6 drug-drug-gene interaction network. *Pharmaceutics* **13,** 331 (2021).

137. Türk, D. *et al.* Physiologically based pharmacokinetic models for prediction of complex CYP2C8 and OATP1B1 (SLCO1B1) drug–drug–gene interactions: A modeling network of gemfibrozil, repaglinide, pioglitazone, rifampicin, clarithromycin and itraconazole. *Clinical Pharmacokinetics* **58,** 1595–1607 (2019).

138. Loer, H. L. H., Türk, D., Gómez-Mantilla, J. D., Selzer, D. & Lehr, T. Physiologically based pharmacokinetic (PBPK) modeling of clopidogrel and its four relevant metabolites for CYP2B6, CYP2C8, CYP2C19, and CYP3A4 drug–drug–gene interaction predictions. *Pharmaceutics* **14,** 915 (2022).

139. Feick, D. *et al.* Physiologically-based pharmacokinetic modeling of quinidine to establish a CYP3A4, P-gp, and CYP2D6 drug-drug-gene interaction network. *CPT: Pharmacometrics & Systems Pharmacology* **12,** 1143–1156 (2023).

140. Wendl, T., Frechen, S., Gerisch, M., Heinig, R. & Eissing, T. Physiologically-based pharmacokinetic modeling to predict CYP3A4-mediated drug-drug interactions of finerenone. *CPT: Pharmacometrics & Systems Pharmacology* **11,** 199–211 (2022).

141. U.S. Food and Drug Administration. *General clinical pharmacology - General considerations for pediatric pharmacokinetic studies of drugs, including biological products. Guidance for Industry* (2022).

142. European Medicines Agency. *Guideline on the evaluation of the pharmacokinetics of medicinal products in patients with impaired hepatic function* (2005).

143. Levey, A. S. *et al.* The definition, classification, and prognosis of chronic kidney disease: A KDIGO Controversies Conference report. *Kidney International* **80,** 17–28 (2011).

144. Matovinović, M. S. 1. Pathophysiology and classification of kidney diseases. *EJIFCC* **20,** 2–11 (2009).

145. Webster, A. C., Nagler, E. V., Morton, R. L. & Masson, P. Chronic kidney disease. *The Lancet* **389,** 1238–1252 (2017).

146. Lea-Henry, T. N., Carland, J. E., Stocker, S. L., Sevastos, J. & Roberts, D. M. Clinical pharmacokinetics in kidney disease. *Clinical Journal of the American Society of Nephrology* **13,** 1085–1095 (2018).

147. Nolin, T. D. A synopsis of clinical pharmacokinetic alterations in advanced CKD. *Seminars in Dialysis* **28,** 325–329 (2015).

148. Yoshida, K. *et al.* Systematic and quantitative assessment of the effect of chronic kidney disease on CYP2D6 and CYP3A4/5. *Clinical Pharmacology & Therapeutics* **100,** 75–87 (2016).

149. Joy, M. S. *et al.* In vivo alterations in drug metabolism and transport pathways in patients with chronic kidney diseases. *Pharmacotherapy: The Journal of Human Pharmacology and Drug Therapy* **34,** 114–122 (2014).

150. Sun, H., Frassetto, L. & Benet, L. Z. Effects of renal failure on drug transport and metabolism. *Pharmacology & Therapeutics* **109,** 1–11 (2006).

151. Lalau, J.-D. *et al.* Metformin treatment in patients with type 2 diabetes and chronic kidney disease stages 3A, 3B, or 4. *Diabetes Care* **41,** 547–553 (2018).

152. Schmidt, I. M. *et al.* Patterns of medication use and the burden of polypharmacy in patients with chronic kidney disease: The German Chronic Kidney Disease study. *Clinical Kidney Journal* **12,** 663–672 (2019).

153. Laville, S. M. *et al.* Evaluation of the adequacy of drug prescriptions in patients with chronic kidney disease: Results from the CKD-REIN cohort. *British Journal of Clinical Pharmacology* **84,** 2811–2823 (2018).

154. Hanke, N. *et al.* A comprehensive whole-body physiologically based pharmacokinetic drug–drug–gene interaction model of metformin and cimetidine in healthy adults and renally impaired individuals. *Clinical Pharmacokinetics* **59,** 1419–1431 (2020).

155. Malik, P. R. *et al.* A physiological approach to pharmacokinetics in chronic kidney disease. *The Journal of Clinical Pharmacology* **60** (2020).

156. Deng, G. *et al.* Physiologically based pharmacokinetic-pharmacodynamic evaluation of meropenem in CKD and hemodialysis individuals. *Frontiers in Pharmacology* **14** (2023).

157. Ponto, L. L. B. & Schoenwald, R. D. Furosemide (Frusemide) - A pharmacokinetic/pharmacodynamic review (part I). *Clinical Pharmacokinetics* **18,** 381–408 (1990).

158. Hasegawa, M. *et al.* Multidrug resistance-associated protein 4 is involved in the urinary excretion of hydrochlorothiazide and furosemide. *Journal of the American Society of Nephrology* **18,** 37–45 (2007).

159. Hsueh, C.-H. *et al.* Identification and quantitative assessment of uremic solutes as inhibitors of renal organic anion transporters, OAT1 and OAT3. *Molecular Pharmaceutics* **13,** 3130–3140 (2016).

160. Hsueh, C.-H. *et al.* PBPK modeling of the effect of reduced kidney function on the pharmacokinetics of drugs excreted renally by organic anion transporters. *Clinical Pharmacology & Therapeutics* **103,** 485–492 (2018).

161. Dubinsky, S., Malik, P., Hajducek, D. M. & Edginton, A. Determining the effects of chronic kidney disease on organic anion transporter 1/3 activity through physiologically based pharmacokinetic modeling. *Clinical Pharmacokinetics* **61,** 997–1012 (2022).

162. Yee, S. W. *et al.* Influence of transporter polymorphisms on drug disposition and response: A perspective from the International Transporter Consortium. *Clinical Pharmacology & Therapeutics* **104,** 803–817 (2018).

163. Ruedesheim, S. *et al.* Physiologically based pharmacokinetic modeling of metoprolol enantiomers and α-hydroxymetoprolol to describe CYP2D6 drug-gene interactions. *Pharmaceutics* **12,** 1200 (2020).

A

PUBLICATIONS

A.1 ORIGINAL ARTICLES

Hannah Britz, Nina Hanke, Mitchell E Taub, Ting Wang, Bhagwat Prasad, Éric Fernandez, Peter Stopfer, Valerie Nock, Thorsten Lehr. Physiologically based pharmacokinetic models of probenecid and furosemide to predict transporter mediated drug-drug interactions. Pharm Res. 2020;37(12):250. doi: 10.1007/s11095-020-02964-z

Jan-Georg Wojtyniak, **Hannah Britz**, Dominik Selzer, Matthias Schwab, Thorsten Lehr. Data digitizing: Accurate and precise data extraction for quantitative systems pharmacology and physiologically-based pharmacokinetic modeling. CPT Pharmacometrics Syst Pharmacol. 2020;9(6):322-331. doi: 10.1002/psp4.12511

Lukas Kovar, Dominik Selzer, **Hannah Britz**, Neal Benowitz, Gideon St. Helen, Yvonne Kohl, Robert Bals, Thorsten Lehr. Comprehensive parent-metabolite PBPK/PD modeling insights into nicotine replacement therapy strategies. Clin Pharmacokinet. 2020;59(9):1119-1134. doi: 10.1007/s40262-020-00880-4

Hannah Britz, Nina Hanke, Anke-Katrin Volz, Olav Spigset, Matthias Schwab, Thomas Eissing, Thomas Wendl, Sebastian Frechen, Thorsten Lehr. Physiologically-based pharmacokinetic models for CYP1A2 drug-drug interaction prediction: A modeling network of fluvoxamine, theophylline, caffeine, rifampicin, and midazolam. CPT Pharmacometrics Syst Pharmacol. 2019;8(5):296-307. doi: 10.1002/psp4.12397

Nina Hanke, Sebastian Frechen, Daniel Moj, **Hannah Britz**, Thomas Eissing, Thomas Wendl, Thorsten Lehr. PBPK Models for CYP3A4 and P-gp DDI prediction: A modeling network of rifampicin, itraconazole, clarithromycin, midazolam, alfentanil, and digoxin. CPT Pharmacometrics Syst Pharmacol. 2018;7(10):647-659. doi: 10.1002/psp4.12343

Nina Hanke, Michael Teifel, Daniel Moj, Jan-Georg Wojtyniak, **Hannah Britz**, Babette Aicher, Herbert Sindermann, Nicola Ammer, Thorsten Lehr. A physiologically based pharmacokinetic (PBPK) parent-metabolite model of the chemotherapeutic zoptarelin doxorubicin-integration of in vitro results, Phase I and Phase II data and model application for drug-drug interaction potential analysis. Cancer Chemother Pharmacol. 2018;81(2):291-304. doi: 10.1007/s00280-017-3495-2

Daniel Moj, **Hannah Britz**, Jürgen Burhenne, Clinton F Stewart, Gerlinde Egerer, Walter E Haefeli, Thorsten Lehr. A physiologically based pharmacokinetic and pharmacodynamic (PBPK/PD) model of the histone deacetylase (HDAC) inhibitor vorinostat for pediatric and adult patients and its application for dose speci-

fication. Cancer Chemother Pharmacol. 2017;80(5):1013-1026. doi: 10.1007/s00280-017-3447-x

Daniel Moj, Nina Hanke, **Hannah Britz**, Sebastian Frechen, Tobias Kanacher, Thomas Wendl, Walter E Haefeli, Thorsten Lehr. Clarithromycin, midazolam, and digoxin: Application of PBPK modeling to gain new insights into drug-drug interactions and co-medication regimens. AAPS J. 2017;19(1):298-312. doi: 10.1208/s12248-016-0009-9

A.2 CONFERENCE ABSTRACTS

Lukas Kovar, **Hannah Britz**, Dominik Selzer, Neal L Benowitz, Yvonne Lydia Kohl, Robert Bals, Thorsten Lehr. A physiologically based pharmacokinetic/pharmacodynamic (PBPK/PD) parent-metabolite model of nicotine including its chronotropic effect and CYP2A6/CYP2B6 metabolism. Annual Meeting of the German Pharmaceutical Society (DPhG), September 2019, Heidelberg, Germany

Hannah Britz, Nina Hanke, Thorsten Lehr. A physiologically based pharmacokinetic model of the CYP1A2 substrate theophylline and its application for the prediction of drug-drug interactions with fluvoxamine, rifampicin and smoking. Annual Meeting of the German Pharmaceutical Society (DPhG), September 2019, Heidelberg, Germany

Lukas Kovar, **Hannah Britz**, Yvonne Lydia Kohl, Robert Bals, Thorsten Lehr. Physiologically-based pharmacokinetic (PBPK) modelling of nicotine and its main metabolite cotinine in healthy volunteers and smokers. 28th Population Approach Group Europe (PAGE) meeting, June 2019, Stockholm, Sweden

Jan-Georg Wojtyniak, **Hannah Britz**, Fatima Zahra Marok, Denise Turk, Laura Fuhr, Lukas Kovar, Nina Hanke, Matthias Schwab, Thorsten Lehr. Physiologically-based pharmacokinetic (PBPK) modelling of a CYP3A4/P-gp DDI network with ketoconazole, midazolam, alfentanil, repaglinide and digoxin. International PhD Student & Postdoc Meeting of the German Pharmaceutical Society (DPhG) 2019, March 2019, Darmstadt, Germany

Hannah Britz, Nina Hanke, Thorsten Lehr. Physiologically-based pharmacokinetic (PBPK) modeling of the strong CYP1A2 inhibitor fluvoxamine. 27th Population Approach Group Europe (PAGE) meeting, May 2018, Montreux, Switzerland

Daniel Moj, **Hannah Britz**, Gerlinde Egerer, Walter E Haefeli, Thorsten Lehr. Application of a physiologically-based pharmacokinetic and pharmacodynamic (PBPK/PD) model of the histone deacetylase (HDAC) inhibitor vorinostat to improve dosing regimens in adults. 26th Population Approach Group Europe (PAGE) meeting, June 2017, Budapest, Hungary

Hannah Britz, Nina Hanke, Thorsten Lehr. Physiologically-based pharmacokinetic (PBPK) modeling of dronedarone and its main metabolite N-debutyldronedarone. Annual meeting of the German Pharmaceutical Society (DPhG), September 2017, Saarbrücken, Germany

Hannah Britz, Daniel Moj, Nina Hanke, Thorsten Lehr. Physiologically-based pharmacokinetic (PBPK) modeling of the dronedarone drug-drug interaction with digoxin. 25th Population Approach Group Europe (PAGE) meeting, June 2016, Lisbon, Portugal

Nina Hanke, Sebastian Frechen, **Hannah Britz**, Daniel Moj, Tobias Kanacher, Thomas Eissing, Thomas Wendl, Thorsten Lehr. Physiologically-based pharmacokinetic modeling of rifampicin drug-drug interactions with midazolam and digoxin. 25th Population Approach Group Europe (PAGE) meeting, June 2016, Lisbon, Portugal

COLOPHON

This document was typeset using the typographical look-and-feel `classicthesis` developed by André Miede and Ivo Pletikosić. The style was inspired by Robert Bringhurst's seminal book on typography "*The Elements of Typographic Style*". `classicthesis` is available for both LaTeX and LyX:

https://bitbucket.org/amiede/classicthesis/

Happy users of `classicthesis` usually send a real postcard to the author, a collection of postcards received so far is featured here:

http://postcards.miede.de/

Thank you very much for your feedback and contribution.